DEVELOPMENT OF DYE-HCRBPII BASED NOVEL PHOTOSWITCHABLE FLUORESCENT PROTEINS

By

Soham Maity

A DISSERTATION

Submitted to
Michigan State University
in partial fulfillment of the requirements
for the degree of

Chemistry – Doctor of Philosophy

2022

ABSTRACT

Modern fluorescence imaging technologies such as super-resolution microscopies require novel fluorescent labeling tags possessing nonconventional optical features, including light controlled turn-on/off of the fluorescence. Our previous reports have demonstrated the ability to engineer hCRBPII to bind a myriad of fluorescent dyes and tune their optical properties. Based on these earlier reports, the goal of this PhD research was to find novel photo-controlled pathways for fluorescence activation of hCRBPII bound fluorophore.

In the past two decades, tremendous effort has been invested in the optimization and derivatization of GFP-like fluorescent proteins (FPs). This includes the discovery of photoactivable fluorescent protein (PAFP) variants that becomes fluorescent or change color when they are triggered with light. In contrast to the conventional fluorescent protein, which is permanently fluorescent, photoactive proteins becomes fluorescent only at the site of interest. In this context, fusion protein which uses synthetic dyes for its optical phenomena provide a broader chemical space for tailoring desired optic features including spectral wavelengths, brightness, stability, and many more photophysical and/or photochemical functionalities.

To achieve light controlled fluorescence activation, two different strategies have been applied here- 1) a cysteine residue containing a sulfur was engineered inside hCRBPII, which can participate in a reversible addition with the fluorophore. Utilizing spectroscopic analyses along with X-ray crystallographic studies, we demonstrated that conjugation via Michael addition of a cysteine with a coumarin analog that creates a non-fluorescent complex. UV illumination reverses the conjugation, yielding a fluorescent species, presumably through a *retro*-Michael process. This series of events can be repeated between a bound and non-bound form of the cysteine reversibly, resulting in the ON-OFF control of fluorescence. The details of the mechanism of photoswitching

were illuminated by recapitulation of the process in light irradiated single crystals, confirming the mechanism at atomic resolution. (2) a light induced double proton transfer that results in switching between two spectrally different states of the hCRBPII bound fluorophore. Through spectroscopic and high-resolution structural data, we showed that the protein can be engineered to support selective protonation of the chromophore's aryl amine instead of its imine even at low pH. However, the UV absorbing ammonium ion can be reversibly deprotonated, yielding a highly redshifted fluorophore upon exposure to UV light. Structural data before and after UV irradiation shows that the light triggered event alters the protein's interaction with the fluorophore, correlating with the spectral change.

The last major endeavor was to develop fluorene based fluorescent dyes with improved optical properties. We have previously reported two fluorene-based dyes, **FR0** and **FR1V**, for fluorescence imaging of the live cells. In this study, effort was made to engineer the dye skeleton to minimize different non-radiating pathways based on literature studies. Spectral data of the new derivatives were collected in different solvents and compared with the previous dyes. We have also been able to demonstrate members of the dyes with red-shifted absorption and emission, high fluorescence QY and improved water solubility.



ACKNOWLEDGEMENTS

Firstly, I am thankful to my PhD advisor, Professor Babak Borhan for his continuous support and encouragement. I am exceedingly grateful to him for instilling me with an independent and resilient research attitude. As spotlighted by his three distinct research areas that span widely from total synthesis and synthetic methodologies to bioorganic chemistry and CD spectroscopies, his well-rounded research expertise always inspires me to grow into the same type of multifaceted researcher. Nourished by his open mindedness, I was able to explore and experiment into different chemistry disciplines for the fulfillment of my PhD. I also greatly appreciate the freedom he allows in choosing and starting new projects, as well as the assistance provided in learning new techniques.

There are many other group members I need to express gratitude to. For this, I would like to first thank Dr. Setare Nick for her guidance in experimental techniques and analyze results in bio-oriented projects in the group. She is also a good friend who paid heartful attention to my well-being inside the group, especially in the first few years. For the aforementioned, I would also like to thank Dr. Chrysoula Vasileiou. She was more than helpful anytime I have needed assistance. I would like to thank Dr. Wei Sheng for many helpful discussions and letting me continue some his projects. Shared more common feelings than other lab folks, grad school buddies Dr. Debarshi Chakraborty, Dr. Saeedeh Torabi Kohlbouni and Dr. Aliakbar Mohammadlou made my life in lab much smoother and connected. The list should also include other current and past lab members and can go miles on. I am also grateful to many other dear friends in the department including Dr. Shafaat Al Mehdi and Dr. Prakash K. Shee for their mutual supports.

I want to extend my appreciation to my committee members Professor Xuefei Huang, Professor James Geiger, Professor Rob Maleczka help in the graduate courses and useful comments on my research projects. Especially, I am grateful to Professor James Geiger for the intense collaboration with his research group on my research projects. Being more specifically, I am thankful to Dr. Nona Ehyaei and Courtney Bingham for the structural data which is essential in many of these projects. I have also grateful to Professor Jessica Fortin for the fruitful collaboration on developing pharmacologically important molecules. The collaboration with Professor Jens Schmidt and Professor Wenjing Wang widely expanded my research scope and capability. I have obtained many instructions from different people on operations of essential instrumentation that facilitated my research work. Thanks to Dr. Tony Schilmiller for the training of high-resolution mass spectrometer, and Dr. Dan Holmes for NMR, Dr. Melinda Frame for the help with fluorescence microscopes.

Research is not the sole part of the graduate life. Chasing a dream of research and becoming a graduate student on the other side of earth can be extremely challenging. I have unfound gratitude to my late grandfather who dreamt me to grow as a scientist. The endless love, understanding, and support from my grandmother, parents, uncles, aunts and fiancé will never be paid back. My final acknowledgement to my East Lansing friends who are bonded as a family while we are thousands of miles away from home.

TABLE OF CONTENTS

LIST C	OF ABBREVIATIONS	viii
Chante	er I: Methods employed for fluorescent labelling of protein of interest: A	
_	verview	1
I.1	Fluorescent protein in the area of bioimaging	1
I.2	Photoactivable fluorescent proteins (PAFPs)	4
I.3	Site-specific chemical labelling.	9
1.3 I.4	1	
	Preliminary work towards the hCRBPII-based fluorescent tag	13
KEFEK	ENCES	16
_	er II: Light Controlled Reversible Michael Addition of Cysteine: A New Tool	
•	namic Site-Specific Labeling of Proteins	28
II.1	Choice of fluorophore for photochemical reversibility of C-S bond	30
II.2	Modification of the dye to improve the optical properties	35
II.3	Conclusion and outlook	49
II.4	Experimental Section	50
REFER	ENCES	60
Chanta	or III. Designating the Machanism of NID Emitting hCDDDII/ED1V Deced	
	er III: Deciphering the Mechanism of NIR Emitting hCRBPII/FR1V Based witchable Protein	64
III.1	Preliminary work towards hCRBPII based photoswitchable proteins	66
	•	
III.2	Discovery of a new optical state of M1/FR1V at pH 2.8	75
III.3	Conclusions and outlook.	83
III.4	Experimental Section.	84
REFER	ENCES	89
Chapte	er IV: Rational Design of Fluorene Dyes: Synthesis and Structure-	
_	hysical Relationship.	93
_	Current approaches to minimize the non-radiating decay pathways	94
IV.2	Structural modification of fluorene dyes to improve QY	100
IV.2	Synthesis of fluorene dyes 4-9	102
IV.3 IV.4	Optical properties.	102
IV.4 IV.5	Aldehyde as an electron withdrawing unit	103
IV.5 IV.6	·	
	Conclusion and Future Scope.	113
IV.7	Experimental Section.	114
IV.8	NMR Spectrum	124
KEFER	ENCES	134

LIST OF ABBREVIATIONS

A alanine, Ala

C cysteine, Cys

D aspartic acid, Asp

E glutamic acid, Glu

F phenylalanine, Phe

G glycine, Gly

H histidine, His

K lysine, Lys

L leucine, Leu

M methionine, Met

N asparagine, Asn

P proline, Pro

Q glutamine, Gln

R arginine, Arg

S serine, Ser

T threonine, Thr

V valine, Val

W tryptophan, Trp

Y tyrosine, Tyr

Å angstrom, 10⁻¹⁰ meter

cm centimeter

μ**m** micrometer

nm nanometer

Da dalton

g gram

mg milligram

μ**g** microgram

M molar

μM micromolar

nM nanomolar

mol mole

mmol millimole

xs excess

h hour

min minute

sec second

t time

t1/2 half-life, maturation half-time

 ε molar extinction coefficient

φ quantum yield

T temperature

°C degree Celsius

K kelvin

mW milliwatt

h Planck's constant

ν frequency

Hz hertz

cm-1 wavenumber

aq. Aqueous

FL fluorescence

UV ultraviolet

Vis visible

IR infrared

NIR near-infrared

Abs λ absorbance, absorption wavelength maximum

Em λem emission wavelength maximum

SS Stokes shift

QY quantum yield

BP bandpass (filter)

LP longpass (filter)

FP fluorescent protein

GFP green fluorescent protein

EGFP enhanced green fluorescent protein

BFP blue fluorescent protein

YFP yellow fluorescent protein

RFP red fluorescent protein

PA-FP photoactivatable fluorescent protein

PS-FP photoswitchable fluorescent protein

RSFP reversibly photoswitchable fluorescent protein

PYP photoactive yellow protein

Y-FAST Yellow Fluorescence-Activating and absorption-Shifting Tag

ESPT excited state proton transfer

ICT intramolecular charge transfer

PLICT planarized intramolecular charge transfer

TICT twisted intramolecular charge transfer

PeT photoinduced electron transfer

IC internal conversion

ISC intersystem crossing

RESOLFT reversible saturable optical fluorescence transition

PALM photo-activated localization microscopy

STORM stochastic optical reconstruction microscopy

SB Schiff base

PSB protonated Schiff base

EDG electron donating group

EWG electron withdrawing group

HOMO highest occupied molecular orbital

LUMO lowest unoccupied molecular orbital

MS molecular sieve

nBA n-butylamine

IPTG isopropyl β -D-1-thiogalactopyranoside

p-HBI 4-(p-Hydroxy-benzylidene)-5-imidazolinone

BODIPY boron dipyrromethene

CuAAC copper-catalyzed alkyne-azide cycloaddition

SPAAC strain-promoted alkyne-azide cycloaddition

DIBAL diisobutylaluminium hydride

PDB protein data bank

PCR polymerase chain reaction

PBS phosphate buffered saline

LB Luria broth

equiv equivalent

DMSO dimethyl sulfoxide

Chapter I: Methods employed for fluorescent labelling of protein of interest: A brief overview

I.1 Fluorescent protein in the area of bioimaging

Florescence imaging is an indispensable tool in biological discovery. 1-11 The field was greatly enriched from the discovery of green fluorescence protein (GFP) from jellyfish Aequorea *Victoria* and subsequent use as an *in vivo* tag for labelling biological samples. ^{12,13} In the last three decades since GFP was cloned in 1992, the biological research community has witnessed a tremendous success, which was recognized by the Nobel Prize in Chemistry in 2008, jointly awarded to Osamu Shimomura, Martin Chalfie, and Roger Y. Tsien. GFP can be genetically encoded to allow for visualization of a protein of interest (POI), and thus has become extremely important in the field of cell biology. The discovery has resulted in the development of other fluorescent proteins (FPs) with a wide array of colors. Most of these FPs share a common structure, containing a 11-stranded β -barrel with a single α -helix at the center of the barrel. ¹⁴⁻¹⁹ The chromophore 4-(p-hydroxy-benzylidene)-5-imidazolinone (p-HBI) forms inside this hydrophobic core via the cyclization of Ser65-Tyr66-Gly67. ^{20,21} The most widely accepted mechanism involves -1) initial attack of the Gly67 amide nitrogen to the carbonyl carbon of Ser65, 2) dehydration of hemiaminal to form a imidazolin-5-one intermediate and 3) dehydrogenation of the C_{α} - C_{β} bond of Tyr66 by molecular oxygen, yielding the fully conjugated ring structure. It is important to note that upon denaturation, GFP becomes nonfluorescent, but upon refolding it regains its fluorescence (**Figure 1**).²²⁻²⁵

Other than *Aequorea Victoria*, there are FPs from other animal species including jellyfishes, coral polyps, comb jellies, crustaceans and lancelets with colors covering the entire visible

spectrum.²⁶⁻³¹ FPs are generally categorized based on excitation and emission wavelengths, UV FPs ($\lambda_{ex} < 380$ nm, $\lambda_{em} < 450$ nm, e.g., Sirius),³² Blue FPs ($\lambda_{ex} : 380 \sim 400$ nm, $\lambda_{em} \sim 450$ nm, e.g., Azurite, EBFP2, TagBFP, etc.),³³⁻³⁵ Cyan FPs ($\lambda_{ex} \sim 430$ nm, $\lambda_{em} : 470 \sim 490$ nm, e.g., ECFP, mTurquoise, Cerulean, etc.);^{22,36-38} Green FPs ($\lambda_{ex} : 480 \sim 510$ nm, $\lambda_{em} : 500 \sim 520$ nm, e.g., EGFP, mEmerald, TagGFP2, TurboGFP, etc.),^{35,39-41} Yellow FPs ($\lambda_{ex} : 510 \sim 530$ nm, $\lambda_{em} \sim 540$ nm, e.g., EYFP, Venus, mPapaya1, etc.),^{20,42-44} Orange FPs ($\lambda_{ex} : 550$ nm, $\lambda_{em} \sim 560$ nm, e.g., mOrange, mKO, etc.),^{45,46} Red FPs ($\lambda_{ex} : 550 \sim 580$ nm, $\lambda_{em} = 580 \sim 610$ nm, e.g., TagRFP, mRuby, mCherry, mScarlet, etc.);⁴⁷⁻⁴⁹ Far-red FPs ($\lambda_{ex} : 590 \sim 610$ nm, $\lambda_{em} : 630 \sim 670$ nm, e.g., mKate2, mRaspberry, mNeptune, NirFP, etc.);⁵⁰ and Near-infrared (NIR) FPs ($\lambda_{ex} : 680 \sim 700$ nm, $\lambda_{em} > 680$ nm, e.g. iFP2.0, iRFP720, GAF-FP, etc.).^{51,52}

The optical property of each FP depends on two predominant factors including a) structural modification of the chromophore and b) specific interaction with the surrounding residues

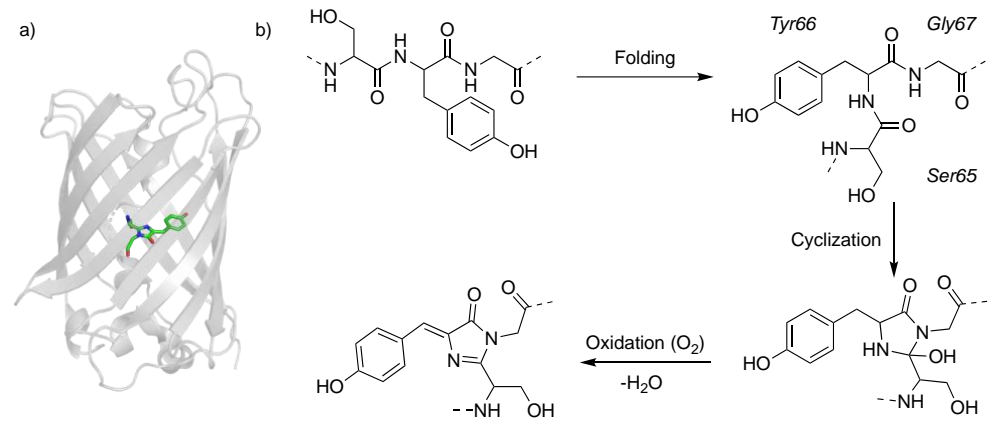


Figure 1. a) The β -barrel structure of GFP, containing the chromophore, embedded in the hydrophobic pocket. b) The proposed pathway of maturation of GFP chromophore involving folding of the protein, followed by cyclization and oxidation.

enclosing the chromophore. Example of the first type is the spectrally red-shifted FP, DsRed which involves an extra oxidation step to form the chromophore. 53,54 A neutral blue-emitting intermediate from cyclization and dehydration of the tripeptide can be oxidized by molecular oxygen at the C α -N bond of residue 65 thus extending the conjugation of the five-membered imidazolinone ring to

an acylimine group instead of the phenolic Tyr66 (**Figure 2**). The role of the protein environment can be observed in the wild type GFP, where the chromophore *p*-HBI can experience two ionization states based on the interaction with the nearby amino acid residues. In its neutral state, the Tyr66 of the chromophore remains as the protonated form that maximally absorbs at 396 nm

Figure 2. The structural variation in the chromophore backbone results in the difference in the optical properties. Elongation of conjugation results in red-shifted absorption in DsRed than GFP.

(**Figure 3**). On the other hand, the same hydroxyl group can undergo a proton transfer to form the corresponding phenolate upon photoexcitation, with a red-shifted absorption (475 nm). 18,19 The pK_a of the hydroxyl group reduces upon photoexcitation which enables proton transfer via a buried water and Ser205 and Glu222 while the charge on the phenolate is stabilized by the Thr203. This process is refereed as excited state proton transfer (ESPT) as it requires photoexcitation of the protein at 400 nm. $^{55-57}$ As FPs can be genetically attached to the protein of interest (POI), they have found tremendous applications in molecular and cell biology. For example, FPs can be used for labelling nucleic acids (i.e., DNA and RNAs), organelles, cells and even whole organism for whole body imaging. $^{2,5,18,58-61}$ With the wide choice of colors, multicolor labelling can be achievable with spectrally resolved excitation and emission wavelengths. 62 Such imaging tools are

invaluable to study subcellular localization, visualizing the protein-protein interactions and monitor gene expression. Out of all the FPs, red variants are of particular importance as the

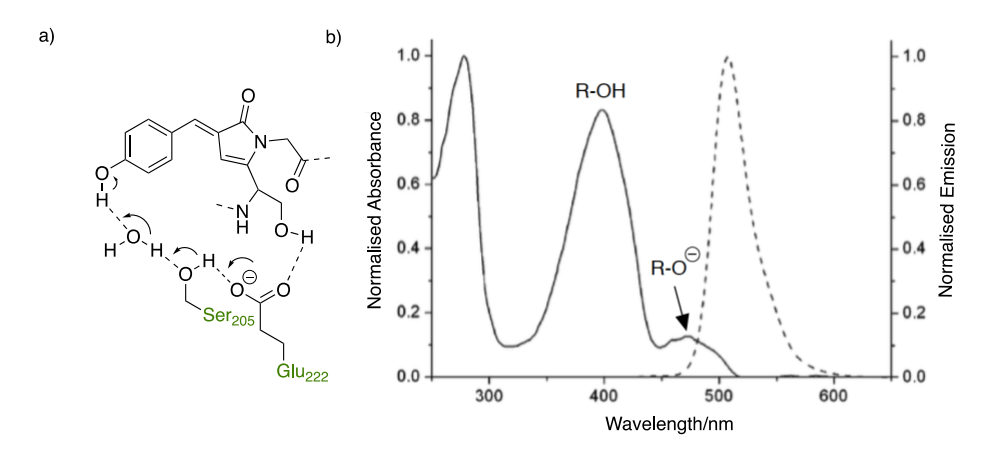


Figure 3. a) Proton shuttle in GFP depicting the role of protein environment surrounding the chromophore b) Absorbance spectra of protonated and deprotonated species which has same emission spectra due to excited state proton transfer (ESPT).

emission channel has lower signal from the cellular autofluorescence. 16,45,61,63-67 In addition, longer wavelengths allow greater tissue penetrability and less damage to protein and DNA components.

While naturally found FPs like GFP and its analogues have been used for plethora of applications, they have their limitation. As discussed earlier, maturation of the chromophores in these proteins requires molecular oxygen, thus they are not useful for anaerobic conditions.²⁷ In addition to that, some FPs have a tendency to aggregate, forming dimers, tetramers or other oligomers. Although extensive efforts have led the development of monomeric FPs, their large size and intrinsic oligomerizing nature has affected the function and distribution of POI.⁶⁸ Recently, Landgraf *et al.* observed that fused FPs will also cause the mislocalization of POIs.⁶⁹

I.2 Photoactivable fluorescent proteins (PAFPs)

In line with developing several variants of FPs, photoactivable fluorescent proteins (PAFP) have become popular as they can be activated to fluoresce only at the site of interest. In contrast to conventional FPs, which permanently fluorescent, photoactive proteins becomes fluorescent or

change color when they are triggered with light. 70,71 These systems have found utility in superresolution microscopy techniques such as reversibly saturable optical fluorescence transition (RESOLFT) imaging, photoactivated localization microscopy (PALM) and stochastic optical reconstruction microscopy (STORM).72-76 With these advanced techniques, the limit of fluorescence microscopy has reached 200 nm to as small as 30-40 nm. Over twenty different varieties of PAFPs have so far been discovered. These include irreversibly photoconvertible proteins that undergo an irreversible photoconversion from the nonfluorescent (OFF) to a fluorescent state (ON) or from one fluorescent color to another.⁶¹ In addition to these, there are several reversibly photoswitchable FPs that can be repeatedly photoswitched between ON and OFF states.⁶¹ Within these classes, individual PAFPs can be further differentiated based on particular optical and biochemical characteristics (**Table 1**). These include their brightness level, oligomeric state, contrast ratio, rate of spontaneous conversion into an activated state and rate of photobleaching. The specific combination of these characteristics exhibited by a particular PAFP makes it more or less suitable for various types of applications in diffraction-limited and superresolution imaging.

The brightness of a PAFP after it has been photoactivated is the product of the activated chromophore's extinction coefficient (ε , M⁻¹cm⁻¹) and quantum yield (Φ). In general, the brightest PAFP is most useful for all applications because brighter molecules emit more photons and thereby are easier to image. Additionally, contrast ratio of a PAFP is the ratio of its fluorescence before and after photoactivation. Variability in contrast ratios among PAFPs is largely due to differences in their spontaneous photoconversion in the absence of controlled activation, which increases the background fluorescence during imaging. For this reason, a PAFP with high contrast ratio is best

for most imaging purposes. Photoactivated PAFPs undergo photobleaching during imaging, which limits how long their signals can be observed. In most diffraction-limited imaging applications the

Table 1. Different photoactivable proteins with their ON state properties, adapted from reference⁷⁷

Proteins	$\lambda_{\rm ex}/{\rm nm}$	λ_{em}/nm	brightness	Oligomeric state	Contrast			
Photoconvertible, OFF to ON								
PAGFP	504	517	13,750	monomer	70			
PAmCherry1	564	595	8,280	monomer	4000			
Photoconvertible, wavelength shift								
PS-CFP2	490	511	10,810	monomer	>2000			
Kaede	572	582	19,900	tetramer	2000			
KikGR	583	593	21,200	tetramer	>2000			
mKikGR	580	591	17,650	monomer	NR			
Dendra2	553	573	19,250	tetramer	300			
EsoFP	571	581	22,600	monomer	NR			
mEos2	573	584	30,300	tetramer	NR			
Photoswitchable								
Dronpa	503	518	80,800	monomer	NR			
rsFastime	496	518	30,100	monomer	70			
Padron	396	522	27,500	monomer	140			
KFP1	580	600	4,100	tetramer	>30			
rsCherry	572	610	1,600	monomer	7			
rsCherryRev	572	608	420	monomer	20			

less photobleaching the better. By contrast, in single molecule super-resolution imaging, because localized molecules must be bleached before others can be photoactivated, a balance between rate of photobleaching and photoactivation is desirable.

I.2.1 Photoconvertible proteins

PAFPs in this class photoconvert from one fluorescence emission bandwidth to another. Proteins in this class include EosFP, Kaede, KikGR and Dendra2 are derived from stony corals, and contain a chromophore that initially emits green fluorescence.⁷⁸⁻⁸¹ Irradiation with UV light causes irreversible peptide cleavage near the chromophore, leading to the extension of the electron conjugation system that results in a new red-shifted emission (**Figure 4a**).^{82,83} One of the best overall performers among the green to red PAFP is EosFP.⁸⁰ It has high brightness, good contrast

ratio and has been engineered into a monomeric form suitable for live cell imaging (e.g. mEosFP,dEosFP and tdEosFP). EosFP has the highest photon output of all known

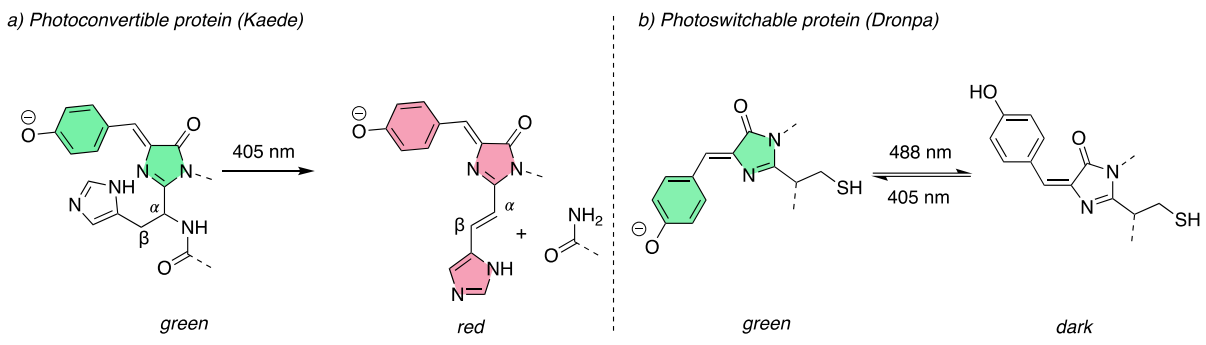


Figure 4. Representative of photoactivable fluorescent proteins a) Kaede, a photoconvertible protein, changes color from green to red upon activation with blue light b) Dronpa, photoswitchable protein, switches between a fluorescent state and a dark state with activation of blue and green light.

photoconvertible FPs, confirmed by its frequent use in single molecule super-resolution imaging.^{84,85} The simultaneous decrease of green fluorescence and increase of red emission upon photoactivation of EosFP can be further exploited in a ratiometric analysis using two-channel detection. Two-color, diffraction-limited imaging with EosFP is also possible by co-expressing it with a fusion protein containing EGFP.⁸⁶ After Eos-FP is photoconverted to red, each protein is visibly distinct and can be imaged over time.

Kaede is another green-to-red PAFP, which is brightest in its green state, roughly equivalent to the originally published EosFP variants.⁷⁸ KikGR was engineered from a non-photoactivatable FP based on the Kaede structure, but like Kaede is tetrameric and is unsuitable for fusion protein studies because of the possibility of mistargeting/aggregation.⁷⁹ Fortunately, a monomeric version of KikGR has been recently developed and successfully used in both diffraction-limited and superresolution imaging.⁸⁷ Dendra2, another green fluorescent variant, is monomeric and gives a 4500-fold increase in the red-to-green ratio after photoconversion.⁸¹ PS-CFP2 is a photoswitchable cyan FP that photoconverts from cyan to green upon irradiation at 405

nm.⁸⁸ The cyan fluorescence observed before photoconversion makes it easy to find regions for selective illumination. The green-to-cyan ratio after activation is >2000-fold, producing good contrast that is similar to other photoconversion proteins. In addition, PS-CFP2 is monomeric so it is useful as a fusion protein tag. PS-CFP2 has been used in two-color, super-resolution experiments with EosFP because of its higher photon output than PA-GFP.⁸⁹

I.2.2 Reversibly switchable fluorescent proteins

The other class of PAFPs are reversibly photoswitchable fluorescent proteins with ON/OFF switching which include FP595, Dronpa and its variants, red reversible PA-Cherry molecules (rsCherry and rsCherryRev), Kindling-FP, Iris-FP, DsRed timer and monomeric blueto-red timers. 78,90-97 These PAFPs are characterized by their ability to be repeatedly photoswitched between two states using light of two distinct wavelengths. Dronpa, one of the best known PAFPs, initially fluoresces green.98 Prolonged or intense irradiation with 470-510 nm light causes switching to a non-fluorescent state. On the other hand, it can be reversibly activated back to its green, fluorescent form by irradiation at 400 nm light. This activation/ quenching cycle can be repeated many times in a single cell expressing this protein (**Figure 4b**). Dronpa's large extinction coefficient and quantum yield make it the brightest of any PAFP. 77 A variant of Dronpa, called Padron, displays the opposite photoswitching as it remains OFF in the resting state and can be activated with blue light.⁹⁹ The rsCherry and rsCherryRev, monomeric variant of mCherry, have relatively high background fluorescence. 93,100 However, with high single molecule brightness and red emitting ON state they are good potential partners with the green PAFPs for two-color imaging. In the case of Kindling-FP, low intensity green or yellow light results in transient red fluorescence, termed kindling, which slowly decays back to a non-fluorescent state. 94 Intense blue light can be used to immediately quench the red fluorescence, whereas high intensity green illumination results

in irreversible photoconversion to the red state. The ON/OFF switching capability of the reversibly photoswitchable fluorescent proteins has been utilized in a variety of ways for spatiotemporal tracking of molecules within cell.

I.3 Site-specific chemical labelling

Due to limitations of naturally occurring FPs and their variants, a great deal of research has been devoted to developing alternatives. A major effort has focused on site-specific chemical labelling where extrinsically non-fluorescent protein becomes fluorescent upon addition of a ligand. This can be used as a fluorescent tag for visualization and understanding the function of POI. The biggest advantage in comparison to naturally occurring FPs is the flexibility of choosing fluorophores with desired optical properties. 101-103 The idea of labelling proteins spurred from the fact that cell uses protein post-translational modification to expand structural and functional diversity. 104 In this context, several self-labelling enzymes have been developed to bind with substrates. 105-109 Representative self-labelling enzyme tags are SNAP-tag, CLIP-tag, Halo Tag and tetra-cysteine tags (Figure 5).

SNAP-tag is a self-labelling protein tag that is engineered from the human suicide protein O⁶-alkylguanine-DNA alkyl-transferase (hAGT) which can specially bind with O⁶-benzylguanine (BG) derivatives. ¹¹⁰⁻¹¹⁴ Similar to SNAP, a CLIP-tag reacts irreversibly with a O²-benzylcytosine (BC) derivatives. In combination with SNAP-tag, CLIP-tag is used for simultaneous labelling of POI with different fluorescent probes. ^{110,115-117} In addition to this, 2,4-diamino-5-(3,4,5-trimethoxybenzyl) pyrimidine (trimethoprim or TMP) tag is popularly used, which involves an engineered *E. Coli* dihydrofolate reductase (eDHFR) and trimethoprim-fused fluorophores. ^{118,119} The probes are reported to show fast kinetics with high binding affinity (in nM). ¹¹⁹⁻¹²¹

HALO-tag is a bacterial *haloalkane dehalogenase* enzyme and is a suicidal covalent ligand-binding protein similar to SNAP and CLIP-tags. As shown in **Figure 5**, the enzyme is equipped with a nucleophilic Asp106 residue which undergoes esterification with fluorophore

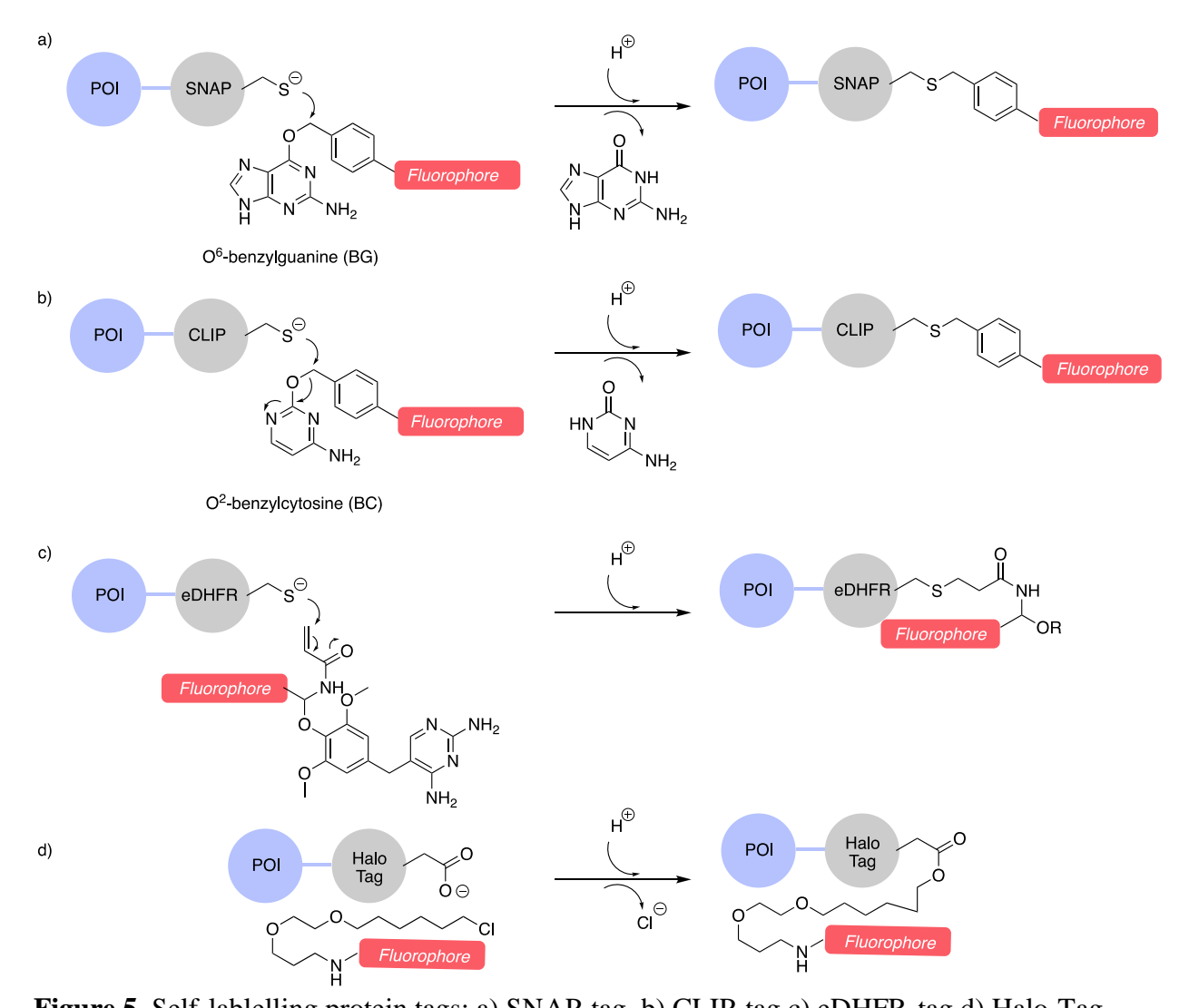


Figure 5. Self-lablelling protein tags: a) SNAP-tag. b) CLIP-tag c) eDHFR-tag d) Halo-Tag. conjugated alkyl-halide ligand. The hydrolysis of the ester and subsequent release of the enzyme in the wild-type protein is prevented by incorporation of H272P mutation. As opposed to the enzymatic labelling as discussed before, short peptide sequences are also developed for covalent binding with fluorescent probes. The sequences are genetically introduced to the target protein and

generally contains cysteine residues such as Cys-Cys-Xaa-Cys-Cys where Xaa is the amino acids other than cysteine. ^{124,125} Example of probes include fluorescein arsenical hairpin binder (FlAsH)

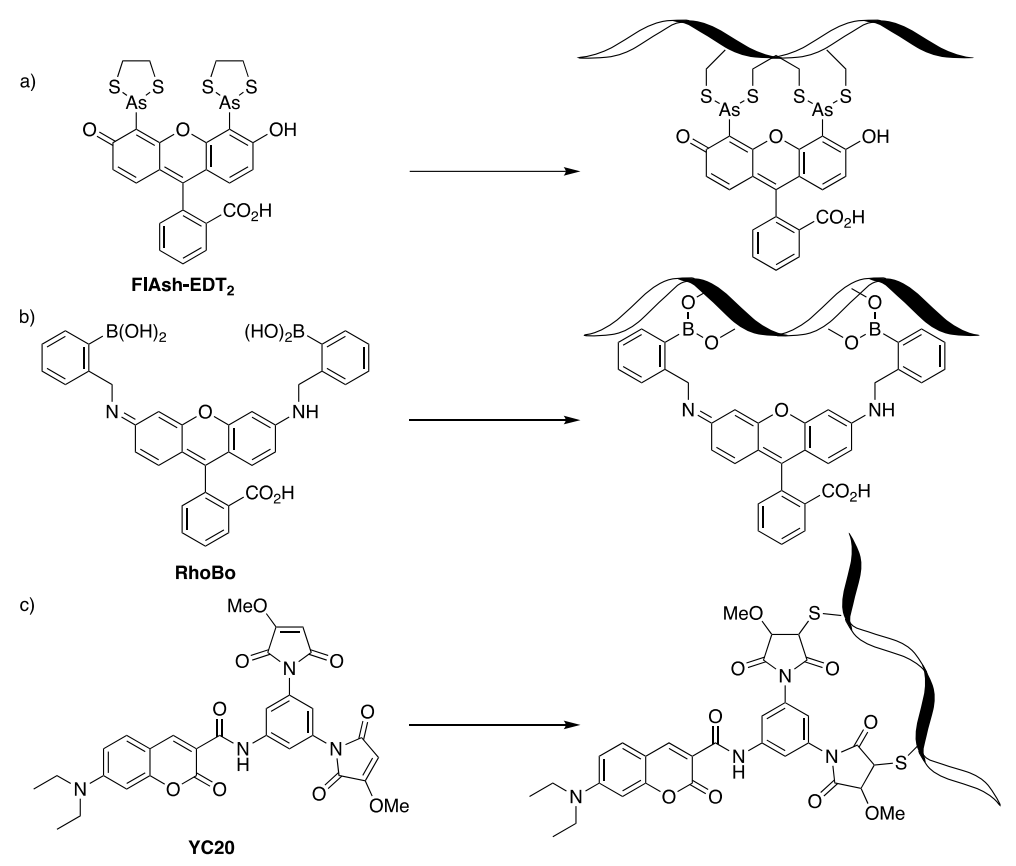


Figure 6. Labelling approaches with short peptides a) FlAsh with tetra-cysteine b) bis-boronic acid RhoBo with tetra-serine and c) bismaleimide coumarin YC20 with vicinal di-cysteine motif. and the more red-shifted analog resofurin arsenical hairpin binder (ReAsH). These probes carry a biarsenical binding motif for selective covalent labelling with the short peptide in the live cell as described by Tsein and coworkers. 124,126

Covalent labelling methods discussed above represent a powerful approach for labelling proteins and the study of cellular processes. Major limitation of these approaches is the drawback associated with the addition of external fluorescent ligand. As these can be fluorescent in both non-bound and in the non-specific bonded form, the addition of the ligand result in excessive background emission. Thus, in most cases a stringent washing step is required to enhance signal

to noise ratio. In addition to the complexity of the process, this increases the time for data acquisition and hampers real time monitoring of fluorescence signal.

I.3.1 Fluorogenic probes

Fluorogens are fluorescence generating dyes that are dark until constrained, bound or activated, ensuring that unreacted dye produces a minimal background signal. Fluorescence is produced only when the dye is bound or modified by the target, providing temporal control of the signal based on addition of the dye. Spatial control of the signal is achieved by fusing the activating protein to a specific protein or peptide that targets an organelle. Two well-known examples of fluorogens are thiazole orange and malachite green (**Figure 7a**). These dyes are essentially nonfluorescent in solution, as a result of the free rotations of aromatic rings, which lead to nonradiative decay of the excited states. The rotation around the single bond is constrained upon binding with the target and thus fluorescence is "activated."

In pioneering studies conducted by Waggoner and coworkers, human single-chain antibodies (scFvs) were developed as a fluorogenic activating protein (FAP) through yeast surface display. scFVs bind with thiazole orange with nanomolar affinity and provide a report of protein location and abundance with both temporal and spatial control. Additionally, FAPs derived from malachite green are highly fluorogenic and emit in the far-red spectral region and display low nonspecific labeling in living cells. 127

Another well-known example of FAP is the photoactive yellow protein (PYP)-tag, developed by Kikuchi and co-workers (**Figure 7**). PYP is a 14-kDa, water-soluble protein derived from purple bacteria, which naturally binds to the CoA thioester of 4-hydroxycinnamic acid through trans-thioesterification with Cys69. The natural ligand can be modified to a structural analog, 4-hydroxycoumarin or 4-aminocoumarin with high binding affinity. Free ligand can

associate in polar environment resulting in the quenching of fluorescence. Fluorescence is turned ON after trans-thioesterification with the PYP protein that breaks the association. Alternatively, the PYP ligand can simultaneously be linked to a quencher and an emitter to realize the same

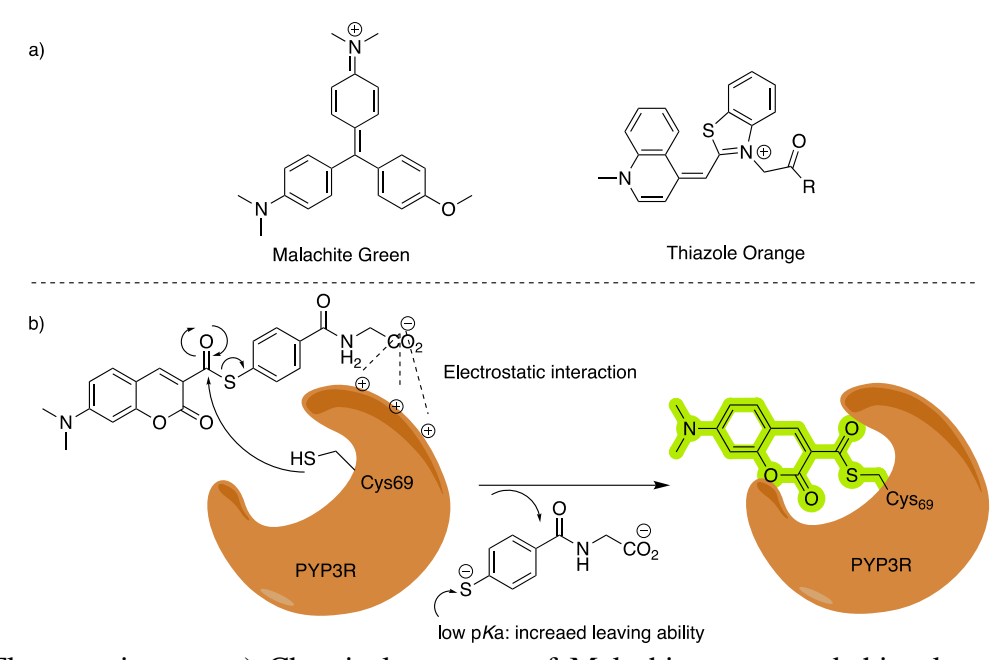


Figure 7. Fluorogenic tags: a) Chemical structure of Malachite green and thiazole orange b) schematic showing the reaction between PYP tag and the aminocoumarin dye.

function. $^{128-130}$ p K_a modulation of the thioester leaving group together with charge optimization surrounding the binding cavity has further improved the kinetics of conjugation. 131,132

I.4 Preliminary work towards the hCRBPII-based fluorescent tag

Our group has previously reported on the wavelength regulation of all-trans-retinal when bound to type II human cellular retinoid binding protein (hCRBPII). All trans retinal, containing an aldehyde group is complexed with hCRBPII through imine formation with lysine 108. The complex can be protonated under physiological pH to form an iminium protonated Schiff base, PSB. Interestingly, the absorption wavelength of this retinylidene PSB can be tuned from 425 nm to 644 nm by mutating key residues in the binding pocket, shown in **Figure 8**. The ligand-protein interactions that result in spanning of the absorption are attributed to the collective effect of

electrostatic perturbation and steric restraints. The tight binding pocket also provides highly ordered water molecules to facilitate specific hydrogen-bonding networks that further manipulate

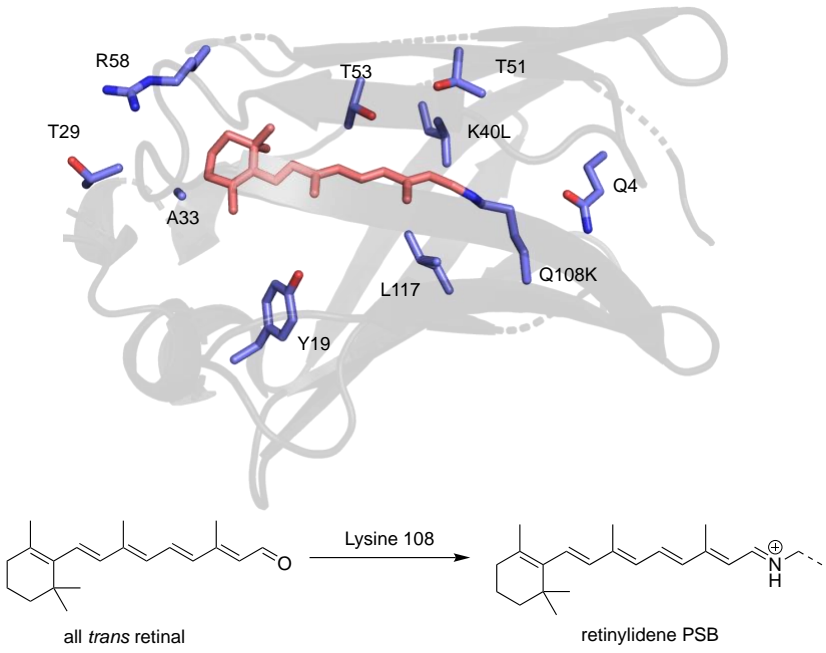


Figure 8. X-Ray crystal structure of all trans retinal bound hCRBPII.¹³³ The aldehyde functionality of the retinal reacts with the lysine 108 to form iminium. Highlighted residues were mutated to tune the absorption spectra of the bound chromophore.

the ligand-protein interaction. Additionally, hCRBPII has high tolerance for mutations without sacrificing its shape or folding.¹³⁴ Hence, hCRBPII can serve as a robust platform to design novel fluorescent complexes by replacing all-*trans*-retinal with different synthetic dyes. hCRBPII has certain advantages over FPs and previously discussed protein-based tags. It is a relatively small protein with 133 amino acids (15 KDa). As synthetic fluorescent ligand will be used, it would not be oxygen dependent unlike GFP and its analogous. In addition, as shown in the case of retinal, optical properties of the hCRBPII/fluorophore can also be tuned through engineering the binding cavity of the protein.

As a proof of concept, the merocyanine based aldehydic dye **MCRA** was synthesized and conjugated with hCRBPII.¹³⁵ Structurally, **MCRA** is a donor-acceptor (D-A) based fluorescent

dye with a polyene chain, much like all-trans retinal (**Figure 9**). **MCRA** binds to selective hCRBPII mutants through formation of an iminium/PSB. Hence this can be considered as an insitu formation of a cyanine dye (like Cy5) as it contains two nitrogen atoms connected through a

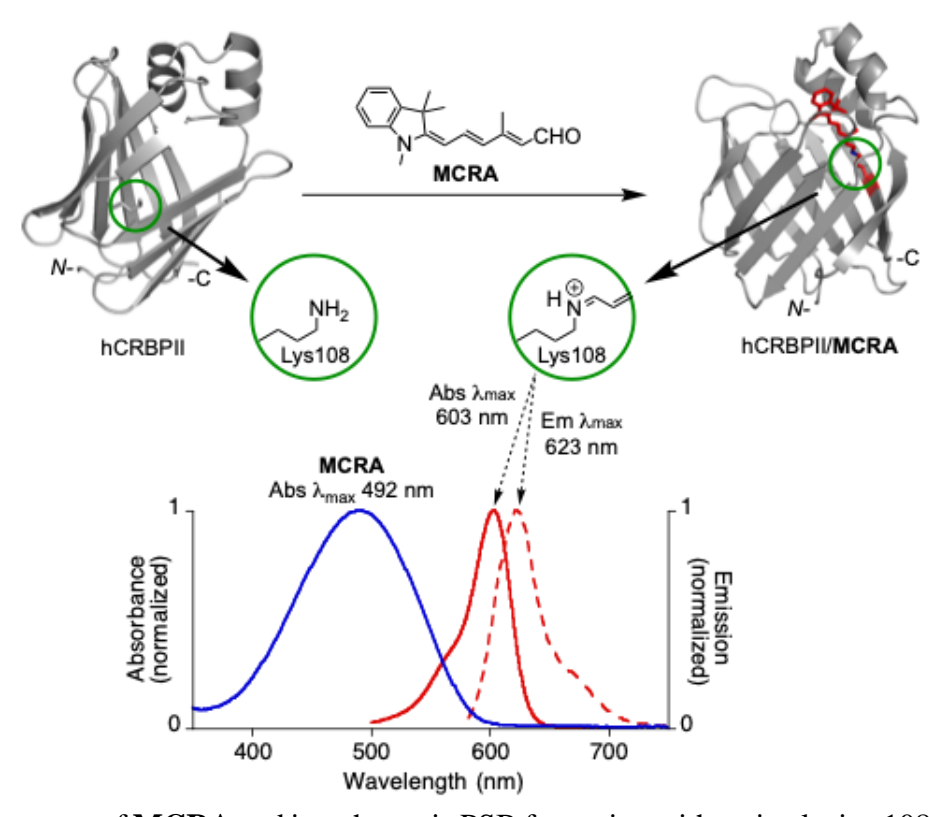


Figure 9. Structure of **MCRA** and its schematic PSB formation with active lysine 108 of hCRBPII. The absorption and emission spectra of hCRBPII complexed with **MCRA**. Picture is copied from reference.¹³⁵

penta-methyne chain. The use of these complexes as potential fluorescent imaging tags was demonstrated by fluorescence imaging with both E. coli and mammalian cells. With extensive protein engineering, the binding time of **MCRA** to hCRBPII mutants can be shortened to less than 1 minute. Imaging of subcellular compartments such as nuclei and cytosol have been realized by targeting the hCRBPII mutant with signaling peptides such as the nucleus-localizing sequence (NES) and the nucleus- exclusion sequence (NES). It was also observed that the binding rate and pK_a can be manipulated by rational mutagenesis of hCRBPII. 136

REFERENCES

- (1) Dean, K. M.; Palmer, A. E. Advances in fluorescence labeling strategies for dynamic cellular imaging. *Nat. Chem. Biol.* **2014**, *10* (7), 512.
- (2) Specht, E. A.; Braselmann, E.; Palmer, A. E. A Critical and Comparative Review of Fluorescent Tools for Live-Cell Imaging. *Annu. Rev. Physiol.* **2017**, *79* (1), 93.
- (3) Kowada, T.; Maeda, H.; Kikuchi, K. BODIPY-based probes for the fluorescence imaging of biomolecules in living cells. *Chem. Soc. Rev.* **2015**, *44* (14), 4953.
- (4) Yuan, L.; Lin, W.; Zheng, K.; He, L.; Huang, W. Far-red to near infrared analyte-responsive fluorescent probes based on organic fluorophore platforms for fluorescence imaging. *Chem. Soc. Rev.* **2013**, *42* (2), 622.
- (5) Nienhaus, K.; Nienhaus, G. U. Fluorescent proteins for live-cell imaging with super-resolution. *Chem. Soc. Rev.* **2014**, *43* (4), 1088.
- (6) Yang, Z.; Cao, J.; He, Y.; Yang, J. H.; Kim, T.; Peng, X.; Kim, J. S. Macro-/micro-environment-sensitive chemosensing and biological imaging. *Chem. Soc. Rev.* **2014**, *43* (13), 4563.
- (7) Hilderbrand, S. A.; Weissleder, R. Near-infrared fluorescence: application to in vivo molecular imaging. *Curr. Opin. Chem. Biol.* **2010**, *14* (1), 71.
- (8) Guo, Z.; Park, S.; Yoon, J.; Shin, I. Recent progress in the development of near-infrared fluorescent probes for bioimaging applications. *Chem. Soc. Rev.* **2014**, *43* (1), 16.
- (9) Luo, S.; Zhang, E.; Su, Y.; Cheng, T.; Shi, C. A review of NIR dyes in cancer targeting and imaging. *Biomaterials* **2011**, *32* (29), 7127.
- (10) Lee, M. H.; Kim, J. S.; Sessler, J. L. Small molecule-based ratiometric fluorescence probes for cations, anions, and biomolecules. *Chem. Soc. Rev.* **2015**, *44* (13), 4185.
- (11) Sevick-Muraca, E. M. Translation of near-infrared fluorescence imaging technologies: emerging clinical applications. *Annu. Rev. Med.* **2012**, *63* (1), 217.
- (12) Prasher, D. C.; Eckenrode, V. K.; Ward, W. W.; Prendergast, F. G.; Cormier, M. J. Primary structure of the Aequorea victoria green-fluorescent protein. *Gene* **1992**, *111* (2), 229.
- (13) Chalfie, M.; Tu, Y.; Euskirchen, G.; Ward, W. W.; Prasher, D. C. Green fluorescent protein as a marker for gene expression. *Science* **1994**, *263* (5148), 802.
- (14) Sample, V.; Newman, R. H.; Zhang, J. The structure and function of fluorescent proteins. *Chem. Soc. Rev.* **2009**, *38* (10), 2852.

- (15) Stepanenko, O. V.; Stepanenko, O. V.; Kuznetsova, I. M.; Verkhusha, V. V.; Turoverov, K. K. In *Int. Rev. Cell Mol. Biol.*; Jeon, K. W., Ed.; Academic Press, 2013; Vol. 302.
- (16) Subach, F. V.; Verkhusha, V. V. Chromophore transformations in red fluorescent proteins. *Chem. Rev.* **2012**, *112* (7), 4308.
- (17) Remington, S. J. Fluorescent proteins: maturation, photochemistry and photophysics. *Curr. Opin. Struct. Biol.* **2006**, *16* (6), 714.
- (18) Zimmer, M. GFP: from jellyfish to the Nobel prize and beyond. *Chem. Soc. Rev.* **2009**, *38* (10), 2823.
- (19) Tsien, R. Y. The green fluorescent protein. Annu. Rev. Biochem 1998, 67 (1), 509.
- (20) Ormo, M.; Cubitt, A. B.; Kallio, K.; Gross, L. A.; Tsien, R. Y.; Remington, S. J. Crystal structure of the Aequorea victoria green fluorescent protein. *Science* **1996**, *273* (5280), 1392.
- (21) Yang, F.; Moss, L. G.; Phillips, G. N., Jr. The molecular structure of green fluorescent protein. *Nat. Biotechnol.* **1996**, *14* (10), 1246.
- (22) Heim, R.; Prasher, D. C.; Tsien, R. Y. Wavelength mutations and posttranslational autoxidation of green fluorescent protein. *Proc. Natl. Acad. Sci. U. S. A.* **1994,** *91* (26), 12501.
- (23) Cubitt, A. B.; Heim, R.; Adams, S. R.; Boyd, A. E.; Gross, L. A.; Tsien, R. Y. Understanding, improving and using green fluorescent proteins. *Trends Biochem. Sci* **1995**, 20 (11), 448.
- (24) Reid, B. G.; Flynn, G. C. Chromophore formation in green fluorescent protein. *Biochemistry* **1997**, *36* (22), 6786.
- (25) Bokman, S. H.; Ward, W. W. Renaturation of Aequorea green-fluorescent protein. *Biochem. Biophys. Res. Commun.* **1981,** *101* (4), 1372.
- (26) Baird, G. S.; Zacharias, D. A.; Tsien, R. Y. Biochemistry, mutagenesis, and oligomerization of DsRed, a red fluorescent protein from coral. *Proc. Natl. Acad. Sci. U. S. A.* **2000**, *97* (22), 11984.
- (27) Matz, M. V.; Fradkov, A. F.; Labas, Y. A.; Savitsky, A. P.; Zaraisky, A. G.; Markelov, M. L.; Lukyanov, S. A. Fluorescent proteins from nonbioluminescent Anthozoa species. *Nat. Biotechnol.* **1999**, *17* (10), 969.
- (28) Verkhusha, V. V.; Lukyanov, K. A. The molecular properties and applications of Anthozoa fluorescent proteins and chromoproteins. *Nat. Biotechnol.* **2004**, 22 (3), 289.

- (29) Gross, L. A.; Baird, G. S.; Hoffman, R. C.; Baldridge, K. K.; Tsien, R. Y. The structure of the chromophore within DsRed, a red fluorescent protein from coral. *Proc. Natl. Acad. Sci. U. S. A.* **2000**, *97* (22), 11990.
- (30) Haddock, S. H.; Mastroianni, N.; Christianson, L. M. A photoactivatable green-fluorescent protein from the phylum Ctenophora. *Proc. Biol. Sci.* **2010**, *277* (1685), 1155.
- (31) Deheyn, D. D.; Kubokawa, K.; McCarthy, J. K.; Murakami, A.; Porrachia, M.; Rouse, G. W.; Holland, N. D. Endogenous green fluorescent protein (GFP) in amphioxus. *Biol. Bull.* **2007**, *213* (2), 95.
- (32) Tomosugi, W.; Matsuda, T.; Tani, T.; Nemoto, T.; Kotera, I.; Saito, K.; Horikawa, K.; Nagai, T. An ultramarine fluorescent protein with increased photostability and pH insensitivity. *Nat. Methods* **2009**, *6* (5), 351.
- (33) Mena, M. A.; Treynor, T. P.; Mayo, S. L.; Daugherty, P. S. Blue fluorescent proteins with enhanced brightness and photostability from a structurally targeted library. *Nat. Biotechnol.* **2006**, *24* (12), 1569.
- (34) Ai, H. W.; Shaner, N. C.; Cheng, Z.; Tsien, R. Y.; Campbell, R. E. Exploration of new chromophore structures leads to the identification of improved blue fluorescent proteins. *Biochemistry* **2007**, *46* (20), 5904.
- (35) Subach, O. M.; Gundorov, I. S.; Yoshimura, M.; Subach, F. V.; Zhang, J.; Gruenwald, D.; Souslova, E. A.; Chudakov, D. M.; Verkhusha, V. V. Conversion of red fluorescent protein into a bright blue probe. *Chem. Biol.* **2008**, *15* (10), 1116.
- (36) Rizzo, M. A.; Springer, G. H.; Granada, B.; Piston, D. W. An improved cyan fluorescent protein variant useful for FRET. *Nat. Biotechnol.* **2004**, *22* (4), 445.
- (37) Goedhart, J.; van Weeren, L.; Hink, M. A.; Vischer, N. O.; Jalink, K.; Gadella, T. W., Jr. Bright cyan fluorescent protein variants identified by fluorescence lifetime screening. *Nat. Methods* **2010**, *7* (2), 137.
- (38) Markwardt, M. L.; Kremers, G. J.; Kraft, C. A.; Ray, K.; Cranfill, P. J.; Wilson, K. A.; Day, R. N.; Wachter, R. M.; Davidson, M. W.; Rizzo, M. A. An improved cerulean fluorescent protein with enhanced brightness and reduced reversible photoswitching. *PLoS One* **2011**, *6* (3), e17896.
- (39) Yang, T. T.; Cheng, L.; Kain, S. R. Optimized codon usage and chromophore mutations provide enhanced sensitivity with the green fluorescent protein. *Nucleic Acids Res.* **1996**, 24 (22), 4592.
- (40) Evdokimov, A. G.; Pokross, M. E.; Egorov, N. S.; Zaraisky, A. G.; Yampolsky, I. V.; Merzlyak, E. M.; Shkoporov, A. N.; Sander, I.; Lukyanov, K. A.; Chudakov, D. M.

- Structural basis for the fast maturation of Arthropoda green fluorescent protein. *EMBO Rep.* **2006,** 7 (10), 1006.
- (41) Sarkisyan, K. S.; Goryashchenko, A. S.; Lidsky, P. V.; Gorbachev, D. A.; Bozhanova, N. G.; Gorokhovatsky, A. Y.; Pereverzeva, A. R.; Ryumina, A. P.; Zherdeva, V. V.; Savitsky, A. P.et al. Green fluorescent protein with anionic tryptophan-based chromophore and long fluorescence lifetime. *Biophys. J.* **2015**, *109* (2), 380.
- (42) Nagai, T.; Ibata, K.; Park, E. S.; Kubota, M.; Mikoshiba, K.; Miyawaki, A. A variant of yellow fluorescent protein with fast and efficient maturation for cell-biological applications. *Nat. Biotechnol.* **2002**, *20* (1), 87.
- (43) Kremers, G. J.; Goedhart, J.; van Munster, E. B.; Gadella, T. W., Jr. Cyan and yellow super fluorescent proteins with improved brightness, protein folding, and FRET Forster radius. *Biochemistry* **2006**, *45* (21), 6570.
- (44) Hoi, H.; Howe, E. S.; Ding, Y.; Zhang, W.; Baird, M. A.; Sell, B. R.; Allen, J. R.; Davidson, M. W.; Campbell, R. E. An engineered monomeric Zoanthus sp. yellow fluorescent protein. *Chem. Biol.* **2013**, *20* (10), 1296.
- (45) Shaner, N. C.; Campbell, R. E.; Steinbach, P. A.; Giepmans, B. N.; Palmer, A. E.; Tsien, R. Y. Improved monomeric red, orange and yellow fluorescent proteins derived from Discosoma sp. red fluorescent protein. *Nat. Biotechnol.* **2004**, *22* (12), 1567.
- (46) Karasawa, S.; Araki, T.; Nagai, T.; Mizuno, H.; Miyawaki, A. Cyan-emitting and orange-emitting fluorescent proteins as a donor/acceptor pair for fluorescence resonance energy transfer. *Biochem. J* **2004**, *381* (Pt 1), 307.
- (47) Merzlyak, E. M.; Goedhart, J.; Shcherbo, D.; Bulina, M. E.; Shcheglov, A. S.; Fradkov, A. F.; Gaintzeva, A.; Lukyanov, K. A.; Lukyanov, S.; Gadella, T. W.et al. Bright monomeric red fluorescent protein with an extended fluorescence lifetime. *Nat. Methods* **2007**, *4* (7), 555.
- (48) Kredel, S.; Oswald, F.; Nienhaus, K.; Deuschle, K.; Rocker, C.; Wolff, M.; Heilker, R.; Nienhaus, G. U.; Wiedenmann, J. mRuby, a bright monomeric red fluorescent protein for labeling of subcellular structures. *PLoS One* **2009**, *4* (2), e4391.
- (49) Bindels, D. S.; Haarbosch, L.; van Weeren, L.; Postma, M.; Wiese, K. E.; Mastop, M.; Aumonier, S.; Gotthard, G.; Royant, A.; Hink, M. A.et al. mScarlet: a bright monomeric red fluorescent protein for cellular imaging. *Nat. Methods* **2017**, *14* (1), 53.
- (50) Shcherbo, D.; Murphy, C. S.; Ermakova, G. V.; Solovieva, E. A.; Chepurnykh, T. V.; Shcheglov, A. S.; Verkhusha, V. V.; Pletnev, V. Z.; Hazelwood, K. L.; Roche, P. M.et al. Far-red fluorescent tags for protein imaging in living tissues. *Biochem. J* **2009**, *418* (3), 567.

- (51) Shcherbakova, D. M.; Verkhusha, V. V. Near-infrared fluorescent proteins for multicolor in vivo imaging. *Nat. Methods* **2013**, *10* (8), 751.
- (52) Yu, D.; Gustafson, W. C.; Han, C.; Lafaye, C.; Noirclerc-Savoye, M.; Ge, W. P.; Thayer, D. A.; Huang, H.; Kornberg, T. B.; Royant, A.et al. An improved monomeric infrared fluorescent protein for neuronal and tumour brain imaging. *Nat. Commun.* **2014**, *5* (1), 3626.
- (53) Strack, R. L.; Strongin, D. E.; Mets, L.; Glick, B. S.; Keenan, R. J. Chromophore formation in DsRed occurs by a branched pathway. *J. Am. Chem. Soc.* **2010**, *132* (24), 8496.
- (54) Subach, O. M.; Malashkevich, V. N.; Zencheck, W. D.; Morozova, K. S.; Piatkevich, K. D.; Almo, S. C.; Verkhusha, V. V. Structural characterization of acylimine-containing blue and red chromophores in mTagBFP and TagRFP fluorescent proteins. *Chem. Biol.* **2010**, *17* (4), 333.
- (55) Chattoraj, M.; King, B. A.; Bublitz, G. U.; Boxer, S. G. Ultra-fast excited state dynamics in green fluorescent protein: multiple states and proton transfer. *Proc. Natl. Acad. Sci. U. S. A.* **1996,** *93* (16), 8362.
- (56) Lossau, H.; Kummer, A.; Heinecke, R.; Pöllinger-Dammer, F.; Kompa, C.; Bieser, G.; Jonsson, T.; Silva, C. M.; Yang, M. M.; Youvan, D. C.et al. Time-resolved spectroscopy of wild-type and mutant Green Fluorescent Proteins reveals excited state deprotonation consistent with fluorophore-protein interactions. *Chem. Phys.* **1996**, *213* (1-3), 1.
- (57) Jung, G.; Wiehler, J.; Zumbusch, A. The photophysics of green fluorescent protein: influence of the key amino acids at positions 65, 203, and 222. *Biophys. J.* **2005**, 88 (3), 1932.
- (58) Zhang, J.; Campbell, R. E.; Ting, A. Y.; Tsien, R. Y. Creating new fluorescent probes for cell biology. *Nat. Rev. Mol. Cell. Biol.* **2002**, *3* (12), 906.
- (59) Day, R. N.; Davidson, M. W. The fluorescent protein palette: tools for cellular imaging. *Chem. Soc. Rev.* **2009**, *38* (10), 2887.
- (60) Mishin, A. S.; Belousov, V. V.; Solntsev, K. M.; Lukyanov, K. A. Novel uses of fluorescent proteins. *Curr. Opin. Chem. Biol.* **2015**, *27*, 1.
- (61) Piatkevich, K. D.; Verkhusha, V. V. Advances in engineering of fluorescent proteins and photoactivatable proteins with red emission. *Curr. Opin. Chem. Biol.* **2010**, *14* (1), 23.
- (62) Kogure, T.; Karasawa, S.; Araki, T.; Saito, K.; Kinjo, M.; Miyawaki, A. A fluorescent variant of a protein from the stony coral Montipora facilitates dual-color single-laser fluorescence cross-correlation spectroscopy. *Nat. Biotechnol.* **2006**, *24* (5), 577.

- (63) Piatkevich, K. D.; Efremenko, E. N.; Verkhusha, V. V.; Varfolomeev, S. D. Red fluorescent proteins and their properties. *Russ. Chem. Rev.* **2010**, *79* (3), 243.
- (64) Shcherbakova, D. M.; Subach, O. M.; Verkhusha, V. V. Red fluorescent proteins: advanced imaging applications and future design. *Angew. Chem. Int. Ed. Engl.* **2012**, *51* (43), 10724.
- (65) Campbell, R. E.; Tour, O.; Palmer, A. E.; Steinbach, P. A.; Baird, G. S.; Zacharias, D. A.; Tsien, R. Y. A monomeric red fluorescent protein. *Proc. Natl. Acad. Sci. U. S. A.* **2002**, *99* (12), 7877.
- (66) Subach, F. V.; Piatkevich, K. D.; Verkhusha, V. V. Directed molecular evolution to design advanced red fluorescent proteins. *Nat. Methods* **2011**, *8* (12), 1019.
- (67) Shcherbakova, D. M.; Baloban, M.; Emelyanov, A. V.; Brenowitz, M.; Guo, P.; Verkhusha, V. V. Bright monomeric near-infrared fluorescent proteins as tags and biosensors for multiscale imaging. *Nat. Commun* **2016**, *7* (1), 12405.
- (68) Newman, R. H.; Fosbrink, M. D.; Zhang, J. Genetically encodable fluorescent biosensors for tracking signaling dynamics in living cells. *Chem. Rev.* **2011**, *111* (5), 3614.
- (69) Subach, O. M.; Cranfill, P. J.; Davidson, M. W.; Verkhusha, V. V. An enhanced monomeric blue fluorescent protein with the high chemical stability of the chromophore. *PLoS One* **2011**, *6* (12), e28674.
- (70) Hell, S. W.; Sahl, S. J.; Bates, M.; Zhuang, X.; Heintzmann, R.; Booth, M. J.; Bewersdorf, J.; Shtengel, G.; Hess, H.; Tinnefeld, P.et al. The 2015 super-resolution microscopy roadmap. *J. Phys. D: Appl. Phys.* **2015**, *48* (44), 443001.
- (71) Shcherbakova, D. M.; Sengupta, P.; Lippincott-Schwartz, J.; Verkhusha, V. V. Photocontrollable fluorescent proteins for superresolution imaging. *Annu. Rev. Biophys.* **2014**, *43* (1), 303.
- (72) Hell, S. W.; Wichmann, J. Breaking the diffraction resolution limit by stimulated emission: stimulated-emission-depletion fluorescence microscopy. *Opt. Lett.* **1994,** *19* (11), 780.
- (73) Gustafsson, M. G. Nonlinear structured-illumination microscopy: wide-field fluorescence imaging with theoretically unlimited resolution. *Proc. Natl. Acad. Sci. U. S. A.* **2005,** *102* (37), 13081.
- (74) Rust, M. J.; Bates, M.; Zhuang, X. Sub-diffraction-limit imaging by stochastic optical reconstruction microscopy (STORM). *Nat. Methods* **2006**, *3* (10), 793.
- (75) Betzig, E.; Patterson, G. H.; Sougrat, R.; Lindwasser, O. W.; Olenych, S.; Bonifacino, J. S.; Davidson, M. W.; Lippincott-Schwartz, J.; Hess, H. F. Imaging Intracellular Fluorescent Proteins at Nanometer Resolution. *Science* **2006**, *313* (5793), 1642.

- (76) Hess, S. T.; Girirajan, T. P.; Mason, M. D. Ultra-high resolution imaging by fluorescence photoactivation localization microscopy. *Biophys. J.* **2006**, *91* (11), 4258.
- (77) Lippincott-Schwartz, J.; Patterson, G. H. Photoactivatable fluorescent proteins for diffraction-limited and super-resolution imaging. *Trends Cell Biol.* **2009**, *19* (11), 555.
- (78) Ando, R.; Hama, H.; Yamamoto-Hino, M.; Mizuno, H.; Miyawaki, A. An optical marker based on the UV-induced green-to-red photoconversion of a fluorescent protein. *Proc. Natl. Acad. Sci. U. S. A.* **2002**, *99* (20), 12651.
- (79) Tsutsui, H.; Karasawa, S.; Shimizu, H.; Nukina, N.; Miyawaki, A. Semi-rational engineering of a coral fluorescent protein into an efficient highlighter. *EMBO Rep.* **2005**, 6 (3), 233.
- (80) Wiedenmann, J.; Ivanchenko, S.; Oswald, F.; Schmitt, F.; Rocker, C.; Salih, A.; Spindler, K. D.; Nienhaus, G. U. EosFP, a fluorescent marker protein with UV-inducible green-to-red fluorescence conversion. *Proc. Natl. Acad. Sci. U. S. A.* 2004, 101 (45), 15905.
- (81) Gurskaya, N. G.; Verkhusha, V. V.; Shcheglov, A. S.; Staroverov, D. B.; Chepurnykh, T. V.; Fradkov, A. F.; Lukyanov, S.; Lukyanov, K. A. Engineering of a monomeric green-to-red photoactivatable fluorescent protein induced by blue light. *Nat. Biotechnol.* **2006**, 24 (4), 461.
- (82) Mizuno, H.; Mal, T. K.; Tong, K. I.; Ando, R.; Furuta, T.; Ikura, M.; Miyawaki, A. Photo-induced peptide cleavage in the green-to-red conversion of a fluorescent protein. *Mol. Cell.* **2003**, *12* (4), 1051.
- (83) Nienhaus, K.; Nienhaus, G. U.; Wiedenmann, J.; Nar, H. Structural basis for photo-induced protein cleavage and green-to-red conversion of fluorescent protein EosFP. *Proc. Natl. Acad. Sci. U. S. A.* **2005**, *102* (26), 9156.
- (84) Habuchi, S.; Ando, R.; Dedecker, P.; Verheijen, W.; Mizuno, H.; Miyawaki, A.; Hofkens, J. Reversible single-molecule photoswitching in the GFP-like fluorescent protein Dronpa. *Proc. Natl. Acad. Sci. U. S. A.* **2005**, *102* (27), 9511.
- (85) Betzig, E.; Patterson, G. H.; Sougrat, R.; Lindwasser, O. W.; Olenych, S.; Bonifacino, J. S.; Davidson, M. W.; Lippincott-Schwartz, J.; Hess, H. F. Imaging intracellular fluorescent proteins at nanometer resolution. *Science* **2006**, *313* (5793), 1642.
- (86) Wiedenmann, J.; Nienhaus, G. U. Live-cell imaging with EosFP and other photoactivatable marker proteins of the GFP family. *Expert Rev. Proteomics* **2006**, *3* (3), 361.
- (87) Habuchi, S.; Tsutsui, H.; Kochaniak, A. B.; Miyawaki, A.; van Oijen, A. M. mKikGR, a monomeric photoswitchable fluorescent protein. *PLoS One* **2008**, *3* (12), e3944.

- (88) Chudakov, D. M.; Verkhusha, V. V.; Staroverov, D. B.; Souslova, E. A.; Lukyanov, S.; Lukyanov, K. A. Photoswitchable cyan fluorescent protein for protein tracking. *Nat. Biotechnol.* **2004**, *22* (11), 1435.
- (89) Shroff, H.; Galbraith, C. G.; Galbraith, J. A.; White, H.; Gillette, J.; Olenych, S.; Davidson, M. W.; Betzig, E. Dual-color superresolution imaging of genetically expressed probes within individual adhesion complexes. *Proc. Natl. Acad. Sci. U. S. A.* **2007**, *104* (51), 20308.
- (90) Lukyanov, K. A.; Fradkov, A. F.; Gurskaya, N. G.; Matz, M. V.; Labas, Y. A.; Savitsky, A. P.; Markelov, M. L.; Zaraisky, A. G.; Zhao, X.; Fang, Y. et al. Natural animal coloration can Be determined by a nonfluorescent green fluorescent protein homolog. *J. Biol. Chem.* **2000**, *275* (34), 25879.
- (91) Stiel, A. C.; Trowitzsch, S.; Weber, G.; Andresen, M.; Eggeling, C.; Hell, S. W.; Jakobs, S.; Wahl, M. C. 1.8 A bright-state structure of the reversibly switchable fluorescent protein Dronpa guides the generation of fast switching variants. *Biochem. J* **2007**, *402* (1), 35.
- (92) Andresen, M.; Stiel, A. C.; Folling, J.; Wenzel, D.; Schonle, A.; Egner, A.; Eggeling, C.; Hell, S. W.; Jakobs, S. Photoswitchable fluorescent proteins enable monochromatic multilabel imaging and dual color fluorescence nanoscopy. *Nat. Biotechnol.* **2008**, *26* (9), 1035.
- (93) Stiel, A. C.; Andresen, M.; Bock, H.; Hilbert, M.; Schilde, J.; Schönle, A.; Eggeling, C.; Egner, A.; Hell, S. W.; Jakobs, S. Generation of Monomeric Reversibly Switchable Red Fluorescent Proteins for Far-Field Fluorescence Nanoscopy. *Biophys. J.* **2008**, *95* (6), 2989.
- (94) Chudakov, D. M.; Belousov, V. V.; Zaraisky, A. G.; Novoselov, V. V.; Staroverov, D. B.; Zorov, D. B.; Lukyanov, S.; Lukyanov, K. A. Kindling fluorescent proteins for precise in vivo photolabeling. *Nat. Biotechnol.* **2003**, *21* (2), 191.
- (95) Adam, V.; Lelimousin, M.; Boehme, S.; Desfonds, G.; Nienhaus, K.; Field, M. J.; Wiedenmann, J.; McSweeney, S.; Nienhaus, G. U.; Bourgeois, D. Structural characterization of IrisFP, an optical highlighter undergoing multiple photo-induced transformations. *Proc. Natl. Acad. Sci. U. S. A.* **2008**, *105* (47), 18343.
- (96) Terskikh, A.; Fradkov, A.; Ermakova, G.; Zaraisky, A.; Tan, P.; Kajava, A. V.; Zhao, X.; Lukyanov, S.; Matz, M.; Kim, S.et al. "Fluorescent timer": protein that changes color with time. *Science* **2000**, *290* (5496), 1585.
- (97) Subach, F. V.; Subach, O. M.; Gundorov, I. S.; Morozova, K. S.; Piatkevich, K. D.; Cuervo, A. M.; Verkhusha, V. V. Monomeric fluorescent timers that change color from blue to red report on cellular trafficking. *Nat. Chem. Biol.* **2009**, *5* (2), 118.
- (98) Ando, R.; Mizuno, H.; Miyawaki, A. Regulated fast nucleocytoplasmic shuttling observed by reversible protein highlighting. *Science* **2004**, *306* (5700), 1370.

- (99) Andresen, M.; Stiel, A. C.; Fölling, J.; Wenzel, D.; Schönle, A.; Egner, A.; Eggeling, C.; Hell, S. W.; Jakobs, S. Photoswitchable fluorescent proteins enable monochromatic multilabel imaging and dual color fluorescence nanoscopy. *Nat. Biotechnol.* **2008**, *26* (9), 1035.
- (100) Stiel, A. C.; Andresen, M.; Bock, H.; Hilbert, M.; Schilde, J.; Schonle, A.; Eggeling, C.; Egner, A.; Hell, S. W.; Jakobs, S. Generation of monomeric reversibly switchable red fluorescent proteins for far-field fluorescence nanoscopy. *Biophys. J.* **2008**, *95* (6), 2989.
- (101) Grimm, J. B.; English, B. P.; Chen, J.; Slaughter, J. P.; Zhang, Z.; Revyakin, A.; Patel, R.; Macklin, J. J.; Normanno, D.; Singer, R. H.et al. A general method to improve fluorophores for live-cell and single-molecule microscopy. *Nat. Methods* **2015**, *12* (3), 244.
- (102) Cheng, Y.; Li, G.; Liu, Y.; Shi, Y.; Gao, G.; Wu, D.; Lan, J.; You, J. Unparalleled Ease of Access to a Library of Biheteroaryl Fluorophores via Oxidative Cross-Coupling Reactions: Discovery of Photostable NIR Probe for Mitochondria. *J. Am. Chem. Soc.* **2016**, *138* (14), 4730.
- (103) Grimm, J. B.; Muthusamy, A. K.; Liang, Y.; Brown, T. A.; Lemon, W. C.; Patel, R.; Lu, R.; Macklin, J. J.; Keller, P. J.; Ji, N.et al. A general method to fine-tune fluorophores for live-cell and in vivo imaging. *Nat. Methods* **2017**, *14* (10), 987.
- (104) Rashidian, M.; Dozier, J. K.; Distefano, M. D. Enzymatic labeling of proteins: techniques and approaches. *Bioconjug. Chem.* **2013**, *24* (8), 1277.
- (105) Gong, Y.; Pan, L. Recent advances in bioorthogonal reactions for site-specific protein labeling and engineering. *Tetrahedron Lett.* **2015**, *56* (17), 2123.
- (106) Lang, K.; Chin, J. W. Bioorthogonal reactions for labeling proteins. *ACS Chem Biol* **2014**, 9 (1), 16.
- (107) Li, J.; Chen, P. R. Development and application of bond cleavage reactions in bioorthogonal chemistry. *Nat. Chem. Biol.* **2016**, *12* (3), 129.
- (108) Lim, R. K.; Lin, Q. Photoinducible bioorthogonal chemistry: a spatiotemporally controllable tool to visualize and perturb proteins in live cells. *Acc. Chem. Res.* **2011**, *44* (9), 828.
- (109) Shieh, P.; Bertozzi, C. R. Design strategies for bioorthogonal smart probes. *Org. Biomol. Chem.* **2014**, *12* (46), 9307.
- (110) Gautier, A.; Juillerat, A.; Heinis, C.; Correa, I. R., Jr.; Kindermann, M.; Beaufils, F.; Johnsson, K. An engineered protein tag for multiprotein labeling in living cells. *Chem. Biol.* **2008**, *15* (2), 128.

- (111) Keppler, A.; Gendreizig, S.; Gronemeyer, T.; Pick, H.; Vogel, H.; Johnsson, K. A general method for the covalent labeling of fusion proteins with small molecules in vivo. *Nat. Biotechnol.* **2003**, *21* (1), 86.
- (112) Keppler, A.; Pick, H.; Arrivoli, C.; Vogel, H.; Johnsson, K. Labeling of fusion proteins with synthetic fluorophores in live cells. *Proc. Natl. Acad. Sci. U. S. A.* **2004,** *101* (27), 9955.
- (113) Lukinavicius, G.; Umezawa, K.; Olivier, N.; Honigmann, A.; Yang, G.; Plass, T.; Mueller, V.; Reymond, L.; Correa, I. R., Jr.; Luo, Z. G.et al. A near-infrared fluorophore for live-cell super-resolution microscopy of cellular proteins. *Nat. Chem.* **2013**, *5* (2), 132.
- (114) Sun, X.; Zhang, A.; Baker, B.; Sun, L.; Howard, A.; Buswell, J.; Maurel, D.; Masharina, A.; Johnsson, K.; Noren, C. J.et al. Development of SNAP-tag fluorogenic probes for wash-free fluorescence imaging. *Chembiochem* **2011**, *12* (14), 2217.
- (115) Hoehnel, S.; Lutolf, M. P. Capturing Cell-Cell Interactions via SNAP-tag and CLIP-tag Technology. *Bioconjug. Chem.* **2015**, *26* (8), 1678.
- (116) Maurel, D.; Comps-Agrar, L.; Brock, C.; Rives, M. L.; Bourrier, E.; Ayoub, M. A.; Bazin, H.; Tinel, N.; Durroux, T.; Prezeau, L.et al. Cell-surface protein-protein interaction analysis with time-resolved FRET and snap-tag technologies: application to GPCR oligomerization. *Nat. Methods* **2008**, *5* (6), 561.
- (117) Jones, S. A.; Shim, S. H.; He, J.; Zhuang, X. Fast, three-dimensional super-resolution imaging of live cells. *Nat. Methods* **2011**, *8* (6), 499.
- (118) Calloway, N. T.; Choob, M.; Sanz, A.; Sheetz, M. P.; Miller, L. W.; Cornish, V. W. Optimized fluorescent trimethoprim derivatives for in vivo protein labeling. *Chembiochem* **2007**, *8* (7), 767.
- (119) Miller, L. W.; Cai, Y.; Sheetz, M. P.; Cornish, V. W. In vivo protein labeling with trimethoprim conjugates: a flexible chemical tag. *Nat. Methods* **2005**, *2* (4), 255.
- (120) Liu, W.; Li, F.; Chen, X.; Hou, J.; Yi, L.; Wu, Y. W. A rapid and fluorogenic TMP-AcBOPDIPY probe for covalent labeling of proteins in live cells. *J. Am. Chem. Soc.* **2014**, *136* (12), 4468.
- (121) Jing, C.; Cornish, V. W. A fluorogenic TMP-tag for high signal-to-background intracellular live cell imaging. *ACS Chem. Biol.* **2013**, 8 (8), 1704.
- (122) Los, G. V.; Encell, L. P.; McDougall, M. G.; Hartzell, D. D.; Karassina, N.; Zimprich, C.; Wood, M. G.; Learish, R.; Ohana, R. F.; Urh, M.et al. HaloTag: a novel protein labeling technology for cell imaging and protein analysis. *ACS Chem. Biol.* **2008**, *3* (6), 373.

- (123) Pries, F.; Kingma, J.; Krooshof, G. H.; Jeronimus-Stratingh, C. M.; Bruins, A. P.; Janssen, D. B. Histidine 289 Is Essential for Hydrolysis of the Alkyl-enzyme Intermediate of Haloalkane Dehalogenase *. J. Biol. Chem. 1995, 270 (18), 10405.
- (124) Griffin, B. A.; Adams, S. R.; Tsien, R. Y. Specific covalent labeling of recombinant protein molecules inside live cells. *Science* **1998**, *281* (5374), 269.
- (125) Albert Griffin, B.; Adams, S. R.; Jones, J.; Tsien, R. Y. In *Applications of Chimeric Genes and Hybrid Proteins Part B: Cell Biology and Physiology*; Thorner, J.;Emr, S. D.;Abelson, J. N., Eds.; Academic Press, 2000; Vol. 327.
- (126) Adams, S. R.; Campbell, R. E.; Gross, L. A.; Martin, B. R.; Walkup, G. K.; Yao, Y.; Llopis, J.; Tsien, R. Y. New biarsenical ligands and tetracysteine motifs for protein labeling in vitro and in vivo: synthesis and biological applications. *J. Am. Chem. Soc.* **2002**, *124* (21), 6063.
- (127) Szent-Gyorgyi, C.; Schmidt, B. F.; Creeger, Y.; Fisher, G. W.; Zakel, K. L.; Adler, S.; Fitzpatrick, J. A.; Woolford, C. A.; Yan, Q.; Vasilev, K. V.et al. Fluorogen-activating single-chain antibodies for imaging cell surface proteins. *Nat. Biotechnol.* **2008**, *26* (2), 235.
- (128) Hori, Y.; Kikuchi, K. Protein labeling with fluorogenic probes for no-wash live-cell imaging of proteins. *Curr. Opin. Chem. Biol.* **2013**, *17* (4), 644.
- (129) Hori, Y.; Ueno, H.; Mizukami, S.; Kikuchi, K. Photoactive yellow protein-based protein labeling system with turn-on fluorescence intensity. *J. Am. Chem. Soc.* **2009**, *131* (46), 16610.
- (130) Hori, Y.; Norinobu, T.; Sato, M.; Arita, K.; Shirakawa, M.; Kikuchi, K. Development of fluorogenic probes for quick no-wash live-cell imaging of intracellular proteins. *J. Am. Chem. Soc.* **2013**, *135* (33), 12360.
- (131) Hori, Y.; Hirayama, S.; Sato, M.; Kikuchi, K. Redesign of a Fluorogenic Labeling System To Improve Surface Charge, Brightness, and Binding Kinetics for Imaging the Functional Localization of Bromodomains. *Angew. Chem. Int. Ed. Engl.* **2015**, *54* (48), 14368.
- (132) Kamikawa, Y.; Hori, Y.; Yamashita, K.; Jin, L.; Hirayama, S.; Standley, D. M.; Kikuchi, K. Design of a protein tag and fluorogenic probe with modular structure for live-cell imaging of intracellular proteins. *Chem Sci* **2016**, *7* (1), 308.
- (133) Wang, W.; Nossoni, Z.; Berbasova, T.; Watson, C. T.; Yapici, I.; Lee, K. S.; Vasileiou, C.; Geiger, J. H.; Borhan, B. Tuning the electronic absorption of protein-embedded all-transretinal. *Science* **2012**, *338* (6112), 1340.

- (134) Gunasekaran, K.; Hagler, A. T.; Gierasch, L. M. Sequence and structural analysis of cellular retinoic acid-binding proteins reveals a network of conserved hydrophobic interactions. *Proteins* **2004**, *54* (2), 179.
- (135) Santos, E. M.; Berbasova, T.; Wang, W.; Salmani, R. E.; Sheng, W.; Vasileiou, C.; Geiger, J. H.; Borhan, B. Engineering of a Red Fluorogenic Protein/Merocyanine Complex for Live-Cell Imaging. *Chembiochem* **2020**, *21* (5), 723.
- (136) Vasileiou, C.; Wang, W.; Jia, X.; Lee, K. S.; Watson, C. T.; Geiger, J. H.; Borhan, B. Elucidating the exact role of engineered CRABPII residues for the formation of a retinal protonated Schiff base. *Proteins* **2009**, *77* (4), 812.

Chapter II: Light Controlled Reversible Michael Addition of Cysteine: A New Tool for Dynamic Site-Specific Labeling of Proteins

In chapter I, I have described the broad scope of available FPs including photoactivable FPs (PAFPs), which becomes fluorescent or change color when triggered with light. These become useful in several super-resolution microscopy techniques, which has changed the limit of fluorescence imaging from 200 nm to as small as 30-40 nm. Despite the success of these FPs, they are inherently limited in their spectral window of emission as the fluorophore is innately formed. In addition to that, the requirement of molecular oxygen in fluorophore maturation limits their use in anaerobic experimental settings as discussed in **Section I.1**. Alternative approaches to FPs is site-specific chemical labelling where a tag is developed by conjugating a non-fluorescent protein with a fluorescent ligand. Use of self-labelling enzymes and engineered short peptides have enabled covalent conjugation of a broad array of fluorescent dyes with desired optical properties. Among different modalities, cysteine-based thiol conjugation has been widely used for labelling due to its relatively high nucleophilicity and its relatively low natural occurrence in protein sequences.² Commonly used approaches for the derivatization of cysteines are trans thioesterification (e.g. PYP), S-alkylation (e.g. SNAP, CLIP), and Michael addition (e.g. TMPacrylamide, maleimide containing dyes).³⁻⁸ Utilizing these chemical approaches, fluorescent molecules such as, BODIPY,³ fluorescein,⁴ cyanine,⁵ and coumarin⁶⁻⁸ based dyes have been conjugated with protein targets. Most systems, however, exhibit irreversible binding, where the fluorescent probes permanently bind with the protein tag. A more versatile system would toggle on-demand between non-fluorescent (OFF) and fluorescent (ON) states using an external stimulus. In this context, stimuli responsive probes offer enhanced spatial and temporal resolution, and hence

provide an additional level of control for the system of interest. 9-17 Light offers several advantages over other forms of stimuli since it can be delivered with high spatiotemporal precision through control of wavelength, intensity, and irradiation time. 18,19 In particular, photoswitchable synthetic dyes provide a unique opportunity to achieve selective ON/OFF of fluorescence. One such example is the photoswitchability of carbocyanine dyes (Cy5) with thiols, which can be toggled between a fluorescent (ON) and a dark (OFF) state (**Figure 0**). 20,21 These systems can be

Figure 10. Light controlled reversible Michael addition of thiols with a Cy5 photoswitch.

cycled hundreds of times, yielding thousands of detected photons per switching cycle.²⁰ Dempsey *et. al.* unveiled that under illumination of red light, Cy5 reacts covalently with the externally added thiol via Michael addition to form a non-fluorescent adduct (OFF state). This was reversed by illuminating the conjugated sample with ultraviolet light. The latter observation piqued our interest to investigate the potential light controlled reversible covalent chemistry between a fluorescent dye and a judiciously placed cysteine residue in a protein host. Recent studies have highlighted the value for a reversibly photoswitchable fluorescent system that can transit between two optical states for live cell super-resolution microscopies (e.g., RESOLFT, psSIM, STORM, PALM), information storage, and optical control of protein activity.^{22,23} Thus, a probe that can reversibly label a protein target and can switch between a fluorescent OFF and ON state could have important implications in bioconjugation.

II.1 Choice of fluorophore for photochemical reversibility of C-S bond

As discussed in **Section I.4**, our group has developed a synthetic fluorescent protein using the intracellular lipid binding family of proteins (iLBP), namely human cellular retinol binding protein II (hCRBPII) and fluorescent ligand **MCRA**.²⁴ This protein was engineered to have an active site lysine residue that can react with an aldehydic dye to form protonated (PSB) or neutral (SB) Schiff base. One such example is **FR1V**, a fluorene-based dye, developed by Dr. Wei Sheng from our group (**Figure**).²⁴ **FR1V**, a bright fluorescent dye, possess an aldehyde functional

Figure 11. The reaction of *n*-butylamine with of **FR1V** and **FR1V**-cyano in ethanol.

group that can be used for binding with the hCRBPII. Additionally, the dye possesses a vinyl group for red shift of the absorption and emission. We speculated that incorporation of an electron withdrawing group (like -CN) at the α -carbon can make the β -carbon sufficiently electron deficient for a possible center of nucleophilic addition. An additional nucleophilic amino acid such as cysteine can be used for the secondary addition with the vinyl group. Such addition will disrupt the conjugation of the fluorophore resulting large change in optical properties. Further, like Cy5 dye, we hoped photoactivation of the complex will drive the reverse reaction though disruption of the bond.

To study the effect of a strong electron withdrawing group at the α -carbon with respect to the aldehyde, I synthesized **FR1V**-cyano and its reactivity was compared with previously

developed **FR1V**. First, we used n-butylamine which can act as a surrogate for the engineered lysine residue of hCRBPII. As previously observed, with addition of excess n-butylamine in ethanolic solution of **FR1V**, the corresponding imine or SB was formed via 1,2 addition. However, with **FR1V**-cyano, an imine corresponding to the aldehyde was not observed, rather product **FR0**-SB was formed with the loss of a three carbon fragment. We believe the reaction passes through intermediate 1, which is the result of both 1,2- and 1,4 additions (Michael addition) of n-butylamine with **FR1V**-cyano. The resulting intermediate undergoes retro-Knoevenagel type reaction to form **FR0**-SB. The difference in nature of the product between **FR1V**-cyano and **FR1V** indicates incorporation of a strong electron withdrawing group like nitrile results a Michael addition with the β -carbon in addition to the nucleophilic addition with the aldehyde.

II.1.1 Formation of cysteine linkage in hCRBPII/FR1V-cyano

With the solution results in hand, we proceeded to study the binding of **FR1V**-cyano with an engineered protein. For this purpose, we used hCRBPII, which has been extensively studied by our research group for various ligands including the previously mentioned **FR1V**. ^{24,25} From our efforts in engineering hCRBPII, we recognized the 108 position is ideally suited for the active site lysine residue (Q108K), while K40E, T53A, R58L, Q38F, and Q4F mutations were either required to facilitate the formation of requisite SB/PSB or protein expression. Upon incubation of the mutant **M1**(Q108K:K40E:T53A:R58L:Q38F:Q4F) with **FR1V**-cyano the absorption maximum corresponding to the free ligand (540 nm) disappears with the concomitant formation of SB with blue shifted peak for the product (445 nm) (**Figure12a**). This result indicates even though **FR1V**-**M2** cyano shows both 1,2 and 1,4 addition with *n*-butylamine in organic solvent, it is limited to just 1,2-addition with a protein carrying Q108K as the nucleophile. This opens the scope to further engineering of the protein to incorporate an additional nucleophilic site for secondary addition

with **FR1V**-cyano. We screened several hCRBPII mutants separately containing cysteine such as T51C, T53C, L119C, L117C of which T51C exhibits the fastest rate of reaction with ligand.

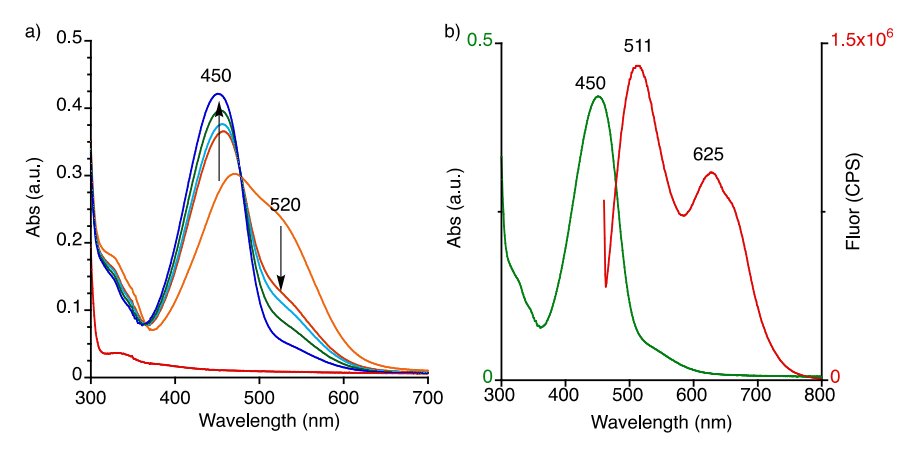


Figure 12. a) Formation of imine between **M1**(Q108K:K40E:T53A:R58L:Q38F:Q4F) and **FR1V**-cyano (scanned after every 10 minutes after addition) b) absorption and emission spectra of the product.

Additionally, T53S mutation was instrumental to increase the rate of reaction with the protein. Resulting mutant (Q108K:K40E:T51C:T53S:R58L:Q38F:Q4F) binds with **FR1V**-cyano yielding two different products based on the absence/presence of ambient light (**Figure**). In the absence

Figure 13. a) Formation of PS^{450} (via 1,2 addition) and PS^{330} (via both 1,2 and 1,4-additon) for M2/FR1V-cyano in dark and presence of daylight respectively.

of light, the yellow-colored complex absorbs at 450 nm much like M1/FR1V-cyano and is referred to as PS⁴⁵⁰ for further discussion. The spectroscopic properties of PS⁴⁵⁰ are similar with that of M1/FR1V-cyano, indicates possible formation of a SB (Figure and Figure). In contrast, under ambient light, the ligand binds with M2 to form a different species with absorption and emission

maxima at 330 and 380 nm, respectively (**Figure**). This complex is referred as PS^{330} as it displays absorption maxima at 330 nm. Intuitively, this large blue shift of absorption and emission (PS^{330} compared to PS^{450}) indicates possible disruption of conjugation within the

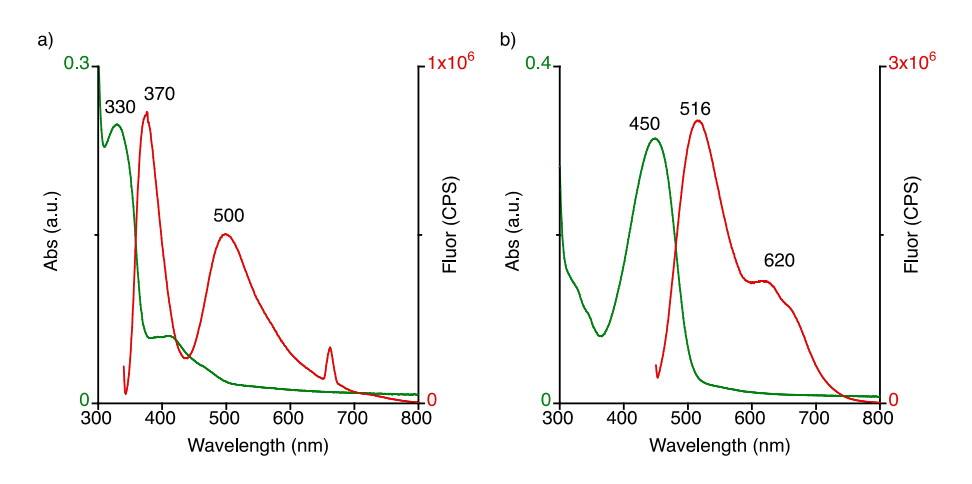


Figure 14. Comparison of absorption and emission spectra of a) PS^{330} and b) PS^{450} of M2/FR1V-cyano.

chromophore. This is presumably the consequence of cysteine addition with the chromophore, possibly through Michael addition with the β -carbon with respect to the imine. To verify, we compared the spectral data of the **PS**³³⁰ with model compounds and N-alkyl-**FR**-bromo and **FR1V**-cyano-acetal (**Figure**). Michael addition of cysteine with the β -carbon of the ligand would lead to the optical properties similar to N-alkyl-**FR**-bromo and 1,2-addition would lead to optical properties similar to **FR1V**-cyano-acetal as they have similar degree of undisrupted conjugation. Comparison of absorption between **PS**³³⁰ with those of the model compounds illustrates that it is possibly a mixture of both 1,2 and 1,4 cysteine addition product. We hypothesized a highly electron withdrawing nitrile group not only increased the reactivity of the β -carbon but also the aldehyde group in **FR1V**-cyano. This increased reactivity resulted in the formation of a mixture of products.

II.1.2 Photoswitchability between PS³³⁰ and PS⁴⁵⁰

Next, we examined if PS^{330} and PS^{450} are interconvertible through reversibility of the cysteine linkage. Gratifyingly, Illumination of visible light (LP 400 nm) for 4 min partially transfer the PS^{450} state to PS^{330} . In addition, illumination of UV light (BP 300-400) for 20 s leads to the

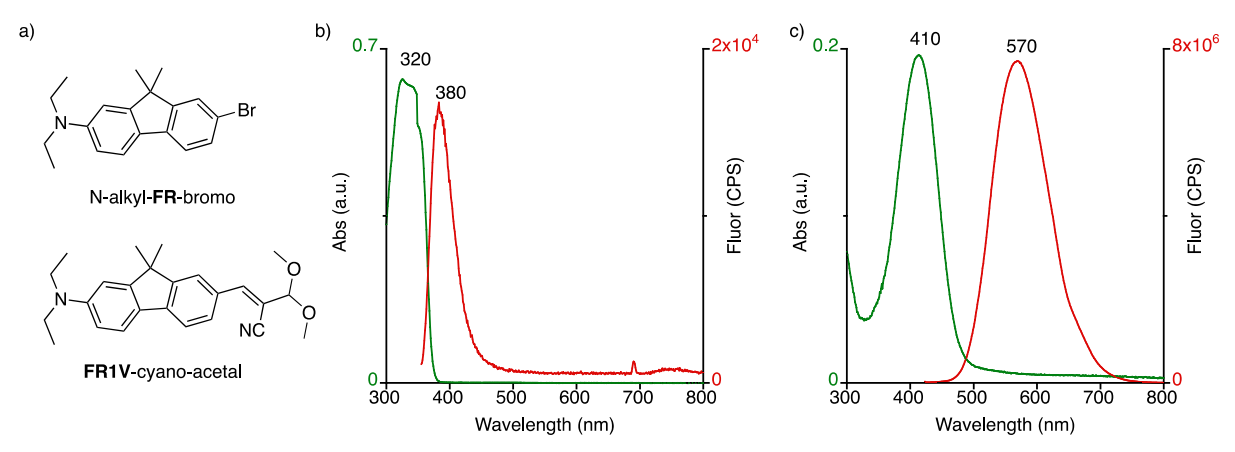


Figure 15. a) Structure of N-alkyl-**FR**-bromo and **FR1V**-cyano-acetal. Absorption and emission spectrum of b) N-alkyl-**FR**-bromo and c) **FR1V**-cyano-acetal.

restoration of **PS**⁴⁵⁰, as evident from the change in absorption and emission spectrum. We believe this is caused by the *retro*-Michael addition of the C-S linkage which results in the restoration of the conjugation. This set of results is interesting as it indicates reversibility of the cysteine linkage. Dr. Nona Ehyaei from Professor James H. Geiger's lab has repeatedly attempted to obtain the crystal structure of **M2/FR1V**-cyano for structural evidence of this phenomena. Although **PS**³³⁰ crystalized several times, X-Ray diffraction data did not provide any conclusive evidence about the binding due to poor electron density of the ligand. We believe this might result from presence of mixture of products, which results in ambiguous electron density around the binding site of the protein. In fact, we observed spectroscopic evidence of a mixed population for **PS**³³⁰ as discussed in the previous section. In addition, photoswitchability between these two states by repeated use of UV and visible light cannot be performed due to unusually high photodegradation of the

complex. Hence, we looked for an alternative fluorescent dye that could display similar dual binding like **FR1V**-cyano, but with less reactivity and increased photostability.

II.2 Modification of the dye to improve the optical properties

An extensive literature research led to the selection of **CM1V**, a fluorescent dye belonging to the coumarin family with conjugated polyene backbone and strong intramolecular charge transfer (ICT) (**Figure**).^{6,26,27} It is a bifunctional fluorescent molecule because of its ability to react either at the electrophilic double bond or the aldehyde. The electron withdrawing ability of the lactone renders the vinyl group electron deficient for covalent addition of a nucleophile. Various chemosensors have taken advantage of changes in optical properties by disrupting the conjugation of the polyene.²⁷ Michael addition of biological thiols (e.g. cysteine, homocysteine and glutathione) to dyes, structurally analogues to **CM1V** has been previously reported, and thus we surmised its suitability as a ligand for labelling hCRBPII.^{26,28-32}

II.2.1 Reversibility of thiol in organic solvent

Prior to *in vitro* studies, the photochemical reversibility of the C-S bond with **CM1V** was examined in organic solvents. β -Mercaptoethanol (β -ME) was used as a surrogate for the active site cysteine residue. The requisite **CM1V**-imine/**CM1V**-SB (obtained from the reaction of **CM1V** and *n*-butylamine) was used to mimic the imine/iminium formed with the engineered lysine residue in the binding pocket of hCRBPII (**Figure**). Addition of excess β -ME to **CM1V**-SB leads to the formation of thioether linkages at both C₁ and C₃. ¹H-NMR analysis confirmed the production of the mixture of the mono adduct (**AD-1**) and the bis-addition product (**AD-2**) (ratio of **AD-1** and **AD-2** is 1:1 after 5 mins and 1:4.5 after 20 mins (**Figure**). Controlling the stoichiometry of β -ME to obtain the mono-addition product was not fruitful, presumably because of competing reactivities at C₁ and C₃. In addition, the reaction was significantly slower with addition of 1 equiv. of thiol,

requiring excess to drive the transformation to completion. Nevertheless, as depicted in **Figure**, the resultant thioether-**CM1V** conjugate leads to a truncation in conjugation, which as expected exhibits a blue shifted absorption ($\lambda_{abs} = 390$ nm) in comparison to **CM1V**-SB ($\lambda_{abs} = 432$ nm) and **CM1V**-PSB ($\lambda_{abs} = 510$ nm). The Michael addition reaction was tested with both

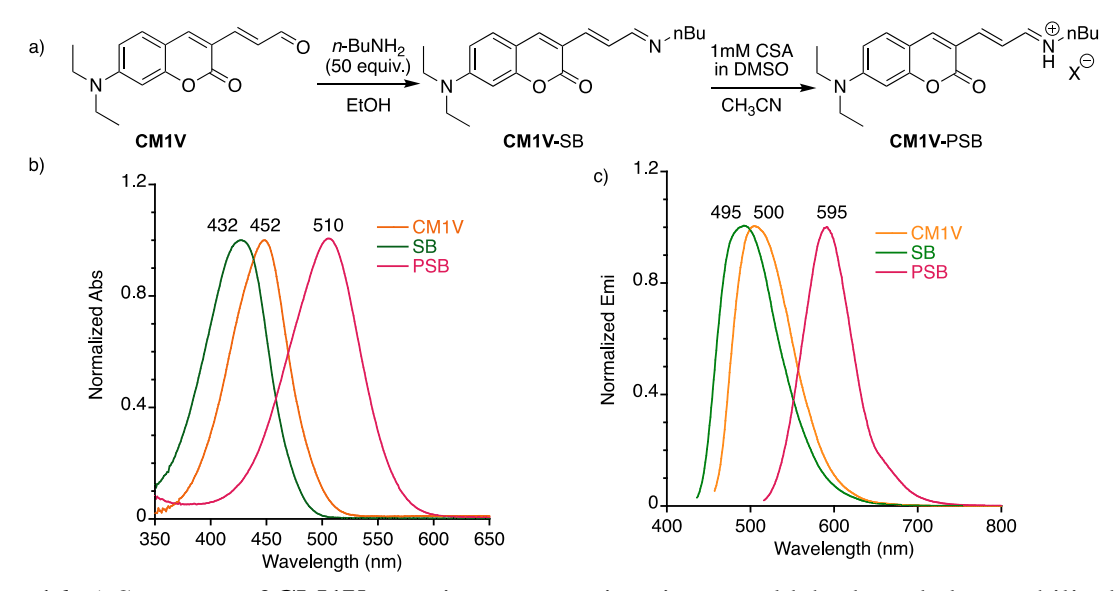


Figure 16. a) Structure of **CM1V** contains two reactive sites, an aldehyde and electrophilic double bond. Reaction of the aldehyde with an amine form either **CM1V**-SB or **CM1V**-PSB. b) Absorption c) emission spectra of **CM1V**-aldehyde, SB and PSB in acetonitrile.

CM1V-SB and **CM1V**-PSB, independently. Surprisingly, full conjugation of **CM1V**-PSB required an excess of β -ME as observed from UV-vis analysis (**Figure**). This is in contrast to the expected reactivity since the PSB is a better nucleophile acceptor and thus should possess higher reactivity as compared to the corresponding SB. We postulate that this is due to the diminished reactivity of β -ME in the acidic environment (depressed nucleophilicity), which was required to form the PSB. It is noteworthy that the use of excess β -ME (>10³ equiv) in basic environment is reported for the optimal photoswitching of cyanine dyes.²⁰ Nonetheless, the room temperature stable thioether conjugates photochemically revert back to the parent **CM1V**-PSB with UV

irradiation (BP300-400 nm) (**Figure**). The resulting PSB absorbs in the visible region with a significant red shift (>130 nm) from the initial complexes **AD-1** and **AD-2**. Hence, this

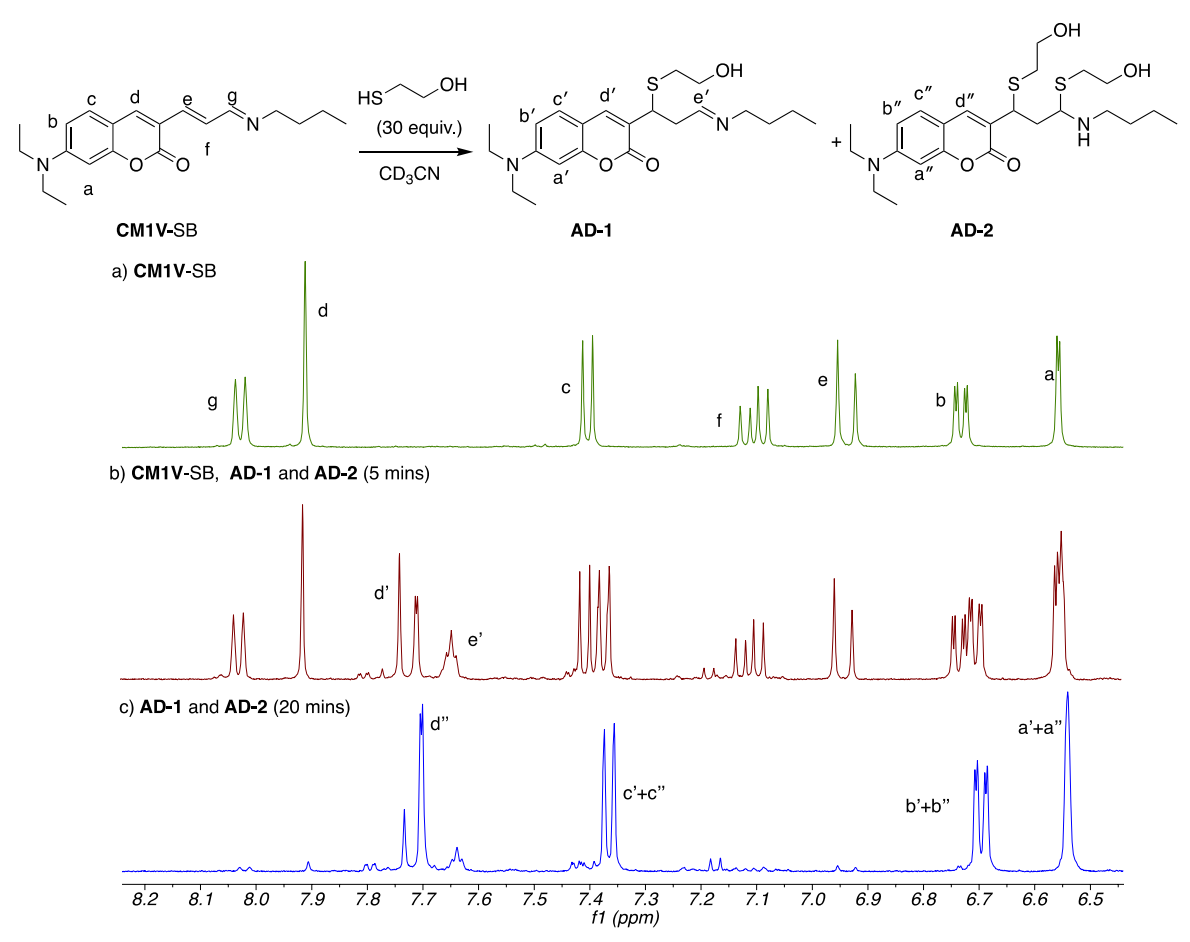


Figure 17. Study of the reaction between **CM1V**-SB and β-ME (30 eq) in CD₃CN using 1 H-NMR a) **CM1V**-SB only b) mixture of starting SB and the products (**AD-1** and **AD-2**) after 5 mins c) **AD-1** and **AD-2** after 20 mins.

describes a photoactivable system, as it displays changes in the spectral properties upon exposure to a specific wavelength of light. Although 1,2 and 1,4 attack of **CM1V**-SB/**CM1V**-PSB with β -ME is observed in solution, we surmised selective Michael addition (C₃ attack) inside an appropriate protein cavity via the incorporation of a single cysteine residue.

II.2.2 Formation of cysteine linkage in hCRBPII/CM1V

Next, our efforts were directed towards the design of a protein host capable of recapitulating the results observed with CM1V-SB/CM1V-PSB and β -ME in acetonitrile. First, an appropriate hCRBPII mutant was required to bind and react with CM1V to form the requisite

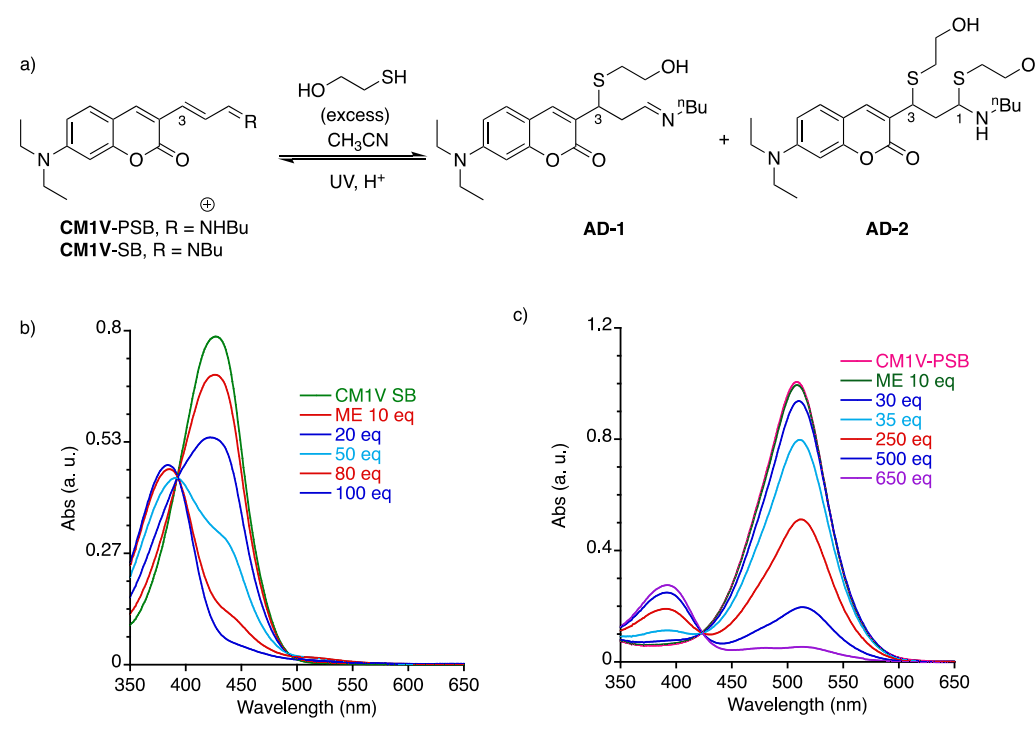


Figure 18. a) Excess addition of β -mercaptoethanol (β -ME) to CM1V-SB/PSB leads to the covalent complexes **AD-1** and **AD-2** b) Change of absorption with addition of β -ME for CM1V-SB and c) CM1V-PSB.

SB/PSB. **M1** (Q108K:K40E:T53A:R58L:Q38F:Q4F), previously used for **FR1V**-cyano, was first tested with **CM1V**. Despite rapid binding of the dye, the complex does not display formation of PSB, probably because of the low pK_a of the imine. PSB, being a red shifted species, would be ideal for further study as it would spectrally distinct than for any other protein bound complexes. Previous study from the group has observed incorporation of a leucine instead of Lys40 increases the pK_a of the imine, yielding the protonated species at physiological pH. Resulting mutant **M3**

(Q108K:K40L:T53A:R58L:Q38F:Q4F) binds with **CM1V** producing a mixture of PSB (λ_{abs} = 550 nm) and the SB (λ_{abs} = 430 nm) at pH 7.2 (**Figure**). The assignment of the peaks was based

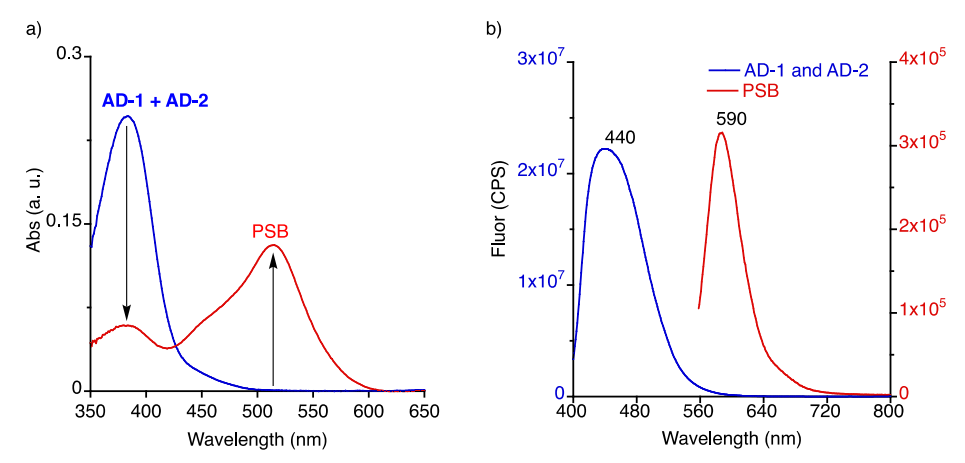


Figure 19. a) **AD-1** and **AD-2** can be reverted to the starting PSB with UV irradiation b) Emission spectrum of thiol bound species (**AD-1** and **AD-2**) and PSB.

on the observed absorptions of the **CM1V** SB/PSB complex formed with *n*-butylamine in acetonitrile (**Figure**). It is worth noting that the PSB formed with **M3** shows a clear bathochromic shift (~40 nm) as compared to that in acetonitrile highlighting the effect of the

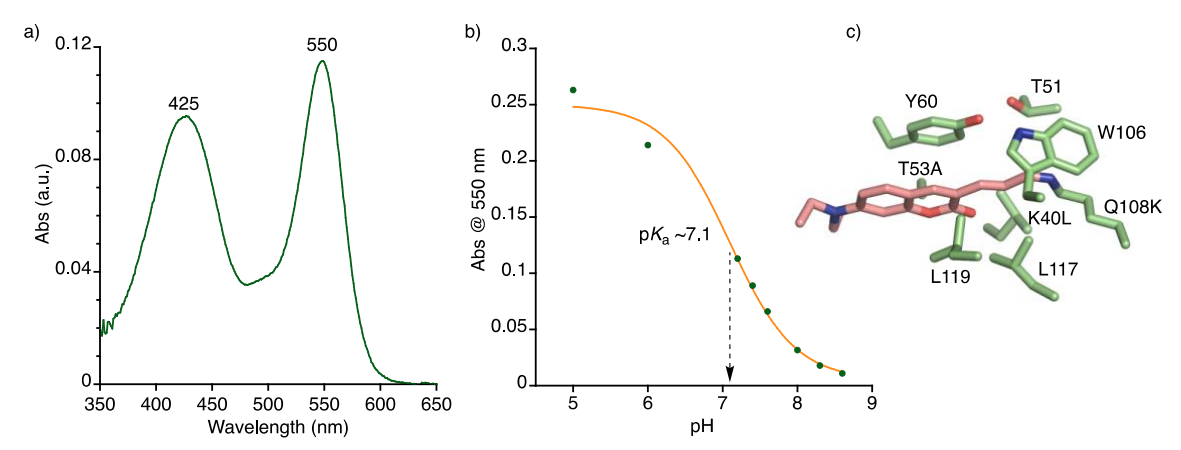


Figure 20. a) Absorption spectrum of M3/CM1V exhibits the formation of SB (425 nm) and PSB (550 nm) at physiological pH. b) The p K_a of M3/CM1V iminium is 7.1, thus explaining the presence of SB and PSB at physiological pH. c) Crystal structure of the complex, showing the conjugation of the fluorophore with the protein through an imine bond. The highlighted residues were targeted to incorporate cysteine, required for the dynamic covalent conjugation.

protein environment on its absorption. The presence of both species at physiological pH suggests a p K_a of the iminium close to the pH of the solution. In fact, the p K_a of the M3/CM1V complex

was measured to be 7.1 (**Figure**). Note that an additional control element available with hCRBPII is the ability to alter the pK_a of the fluorophore/protein complex with the appropriate mutations of residues that line the binding pocket.^{24,33} Fortunately, we obtained the crystal structure of **M3/CM1V** complex which clearly showed the orientation of the ligand inside the binding pocket, identifying nearby amino acid residues within 10 Å of C₃ that could be altered to cysteine. As depicted in **Figure**, **M3** binds **CM1V** to form a *cis*-iminium. The stabilization

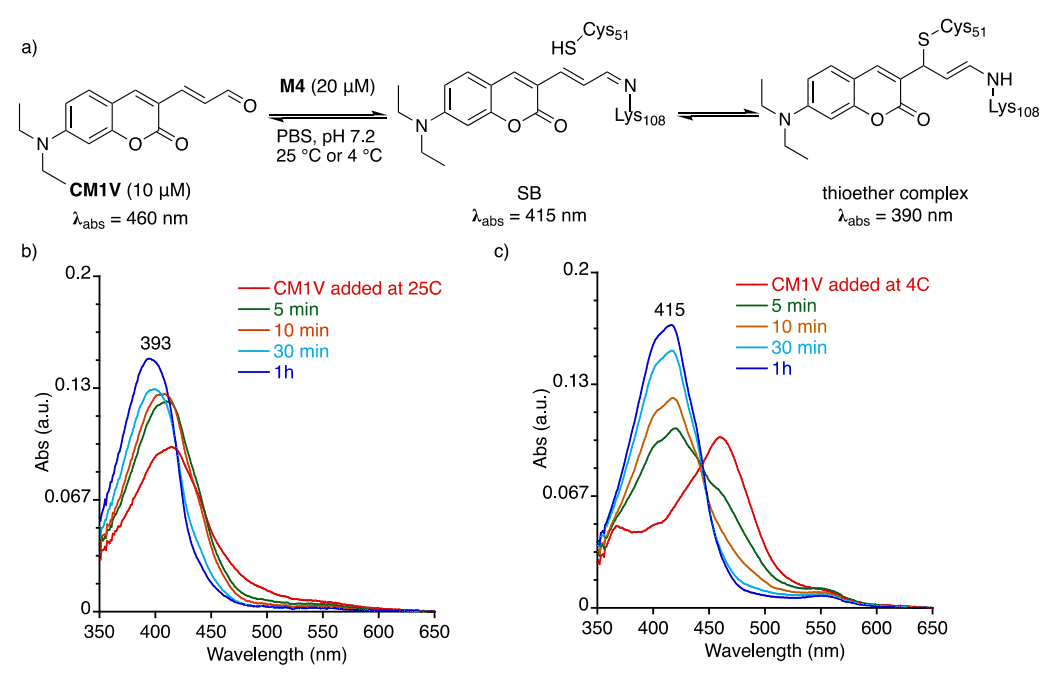


Figure 21. a) The steps of dual binding for M4/CM1V: SB formation is followed by the addition of cysteine b) Change of absorption spectrum with the addition of CM1V (10μM) with M4 (20μM), at 25 °C showing the large blue shift within 1h c) the reaction can be slowed by lowering the temperature to 4 °C, showing the formation intermediate at λ_{max} = 415 nm, close to the absorption of SB of M3/CM1V (λ_{max} = 425 nm).

of the iminium arises from the π -cation interaction of Trp106, positioned 3.6 Å away. Residues L117, L119, Y106, Y60, K40, T51, and T53 were mutated separately to cysteine and the resulting proteins were conjugated with **CM1V**. Among these mutants T51C exhibited the fastest rate of binding with complete conversion to the product within in six hours much like **M2/FR1V**-cyano. Shown in **Figure**, the time-course UV-vis spectra indicate the diminution of the free aldehyde

with increasing conjugate formation ($\lambda_{max} = 395$ nm) upon incubation of **CM1V** with **M4** (Q108K:K40L:**T51C**:T53A:R58L:Q38F:Q4F) at room temperature. The time-dependent blue shift in absorption is indicative of the reduction in conjugation, putatively as a result of the Michael addition of the cysteine residue at position 51 with the polyene. The conjugate is stable for a day at room temperature.

The M4/CM1V-C₅₁ complex was also crystallized, with a clear electron density map consistent with the formation of a thioether linkage via the Michael addition of T51C with the C₃ of the bound ligand (Figure). The overlap of the M3/CM1V and M4/CM1V-C₅₁ structures

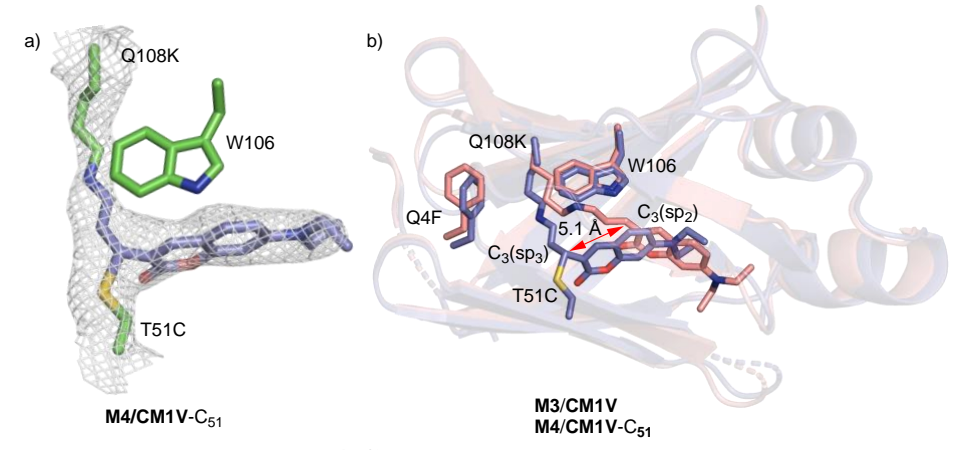


Figure 22. a) Crystal structure of the **M4/CM1V-PSB** reveals the release of Cys51 residue after photoirradiation, b) Its overlay with the structure obtained before photoirradiation illustrates the movement of the chromophore.

reveal a large conformational change of the fluorophore upon covalent attachment (**Figure**). In the new binding orientation, the ligand is forced deeper into the cavity (C_3 has moved by 5.1 Å). Additionally, the chromophore adopts a more twisted conformation to accommodate dual binding with Lys108 and Cys51. As expected, thioether formation changes the hybridization of C_3 (sp² \rightarrow sp³), short-circuiting conjugation of the coumarin unit and the imine that results in the observed blue shifted absorption. It is worth noting the absence of C-S linkage with C_1 unlike that observed with **CM1V** and β -ME in acetonitrile. (**AD-2**, **Figure**). To probe the sequence of

transformations (imine formation vs. Michael addition), complexation of M4 with CM1V was followed spectroscopically at 4 °C to reduce the rate of reaction. The time course study demonstrates the concomitant decrease in the absorption of free CM1V (460 nm), with the appearance of an intermediate peak at 415 nm (Figure). The absorption maximum of this intermediate complex matches well with the M3/CM1V-SB that was incapable of Michael addition (lacking the reactive Cys residue). Hence, SB formation (reaction of Lys108 with the aldehyde to generate the imine) presumably is followed by the Michael addition. Likely, this first step helps to orient the olefin such that the cysteine residue in close proximity can engage in the requisite Michael addition, even in the absence of forming the more reactive iminium.

II.2.3 Photoactivation of hCRBPII/CM1V through dissociation of cysteine linkage

Having established that **CM1V** undergoes facile Michael addition with Cys51 of **M4**, we next investigated the photodissociation of the thioether linkage, similar to that observed with the model compound in acetonitrile. Hence, the protein-fluorophore complex (**M4/CM1V-C**51) was illuminated with UV light (BP300-400 nm) for 1 minute. As illustrated in **Figure**, the photoirradiation results in shifting of the absorption from 390 nm to 415 nm, indicating the formation of the fully conjugated SB. This was the first indication that the photodissociation of the C-S bond is possible inside the protein cavity. The bond cleavage is reversible, as the fully conjugated SB, formed after illumination, thermally reverted to the initial state within an hour. Photoirradiation of the **M4/CM1V-C**51 complex incubated in an acidic buffer (pH = 4.0) promotes the cleavage of the thioether linkage, leading to the formation of the fully conjugated PSB as apparent by its red-shifted absorption (λ_{abs} = 550 nm, **Figure**). In contrast to the SB, the newly generated PSB does not convert back via Michael addition. Although surprising, since the PSB is

a more electrophilic system, the lack of reactivity might be related to an unproductive conformation of the fluorophore in its protonated state. We have previously observed large

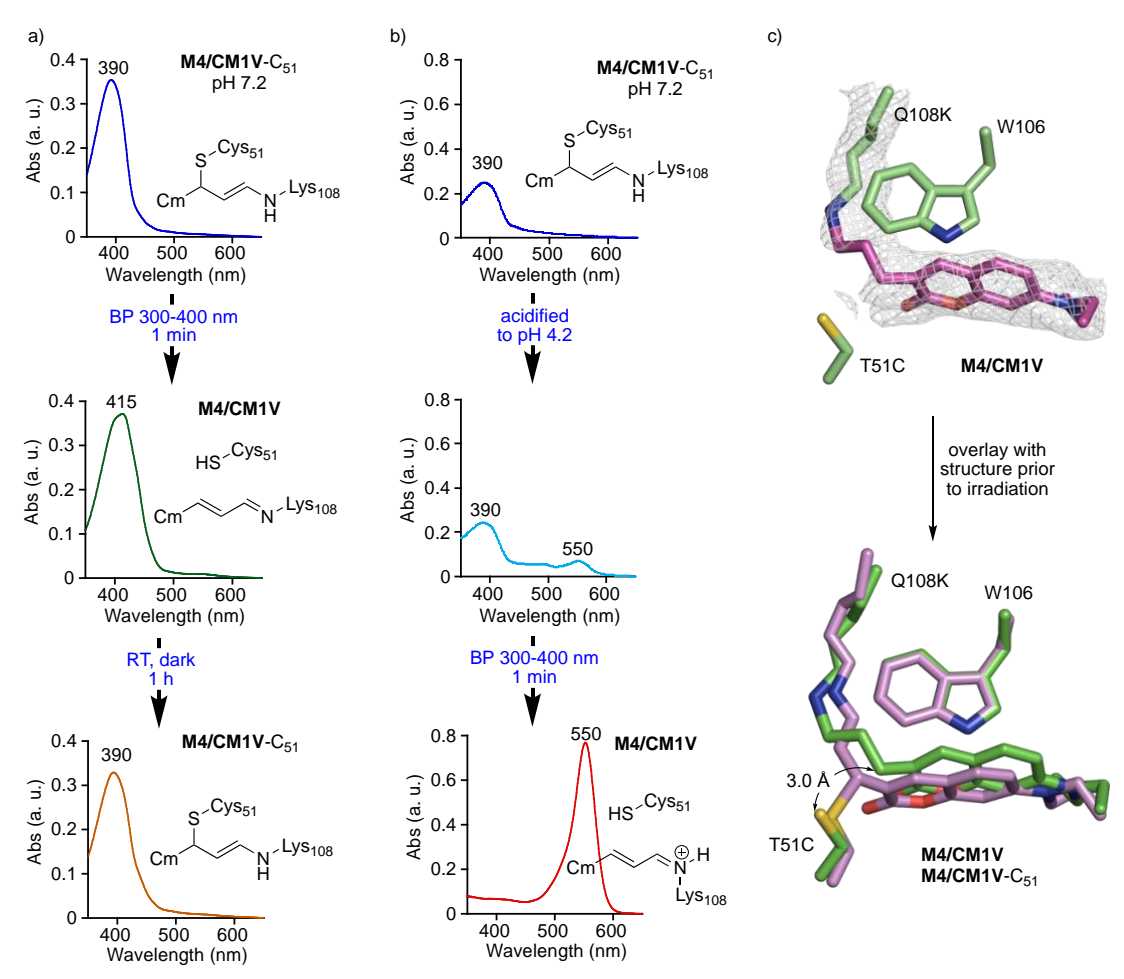


Figure 23. a) UV photoirradiation of the **M4/CM1V**-C51 complex (in blue) at pH 7.2 leads to the formation of **CM1V**-SB (in green), which reverts to the initial complex within 1 h (in orange); b) Acidification of the **M4/CM1V**-C51 complex (blue), presumably leads to the protonation of the imine as the major populated constituent (cyan). UV photoirradiation of the latter solution generates **CM1V**PSB (red) as evident by the large change in absorption; c) Crystal structure of the **M4/CM1V**-PSB reveals the release of Cys51 residue after photoirradiation. Its overlay with the structure obtained before photoirradiation illustrates the movement of the chromophore.

conformational changes of bound ligands upon protonation of the imine.^{24,33,34} It is also possible that under acidic conditions, the nucleophilicity of Cys51 is attenuated to a degree that hinders addition to the polyene. In fact, this was observed in our earlier studies where β -ME was less

reactive with the CM1V-PSB, presumably due to the increased acidity of the solution that was required to generate the PSB.

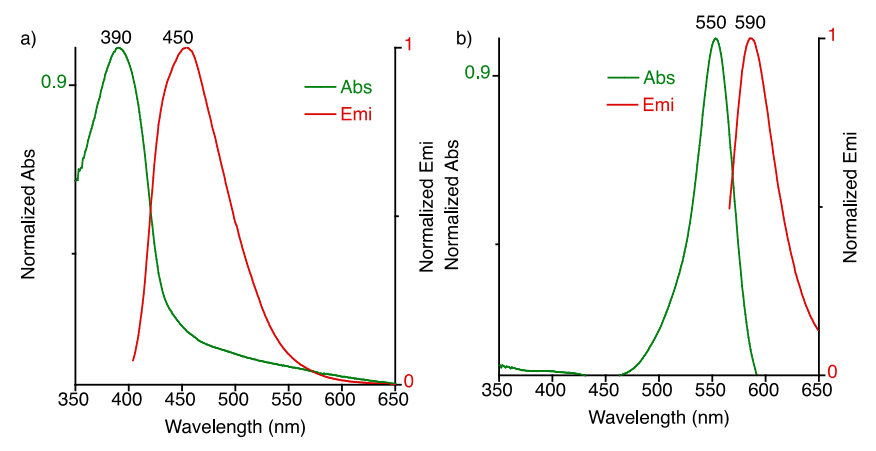


Figure 24. a) Normalized absorption and emission spectrum of **M4/CM1V** OFF state and b) ON state.

With crystals of the M4/CM1V-C₅₁ complex in hand, we explored the potential to promote the bond cleavage in the solid state. Crystals of the M4/CM1V-C₅₁ complex, incubated in pH 7.2 and 4.0 buffers, were irradiated with UV light (380 nm) for 5 minutes and were subsequently frozen in liquid nitrogen within 30 seconds of irradiation. The electron density of photoirradiated crystals incubated at pH 7.2 showed no evidence of bond cleavage. This is either because the cleavage in the solid state does not occur, or that the rebinding of the thiolate with the photodissociated ligand in the crystal is fast and thus cannot be trapped. The results from irradiation of crystals incubated at pH of 4.0 support the latter supposition. Photoirradiated crystals in the acidic media yield structures that lack electron density for the thioether linkage, clearly demonstrating the dissociation of C-S bond (Figure). The red color crystal indicates the presence of the anticipated chromophore as a PSB (red-shifted). The movement of chromophore under photoirradiation can be observed from the overlayed crystal structures of bound and unbound forms despite the proximity between the reactive Cys51 and the C₃ of CMIV (3.0 Å).

Nevertheless, M4/CM1V-C₅₁ acts as a photoactivable system, as UV exposure switches the OFF state ($\lambda_{abs/em} = 390/465$ nm) to the ON state ($\lambda_{abs/em} = 550/580$ nm) (**Figure**).

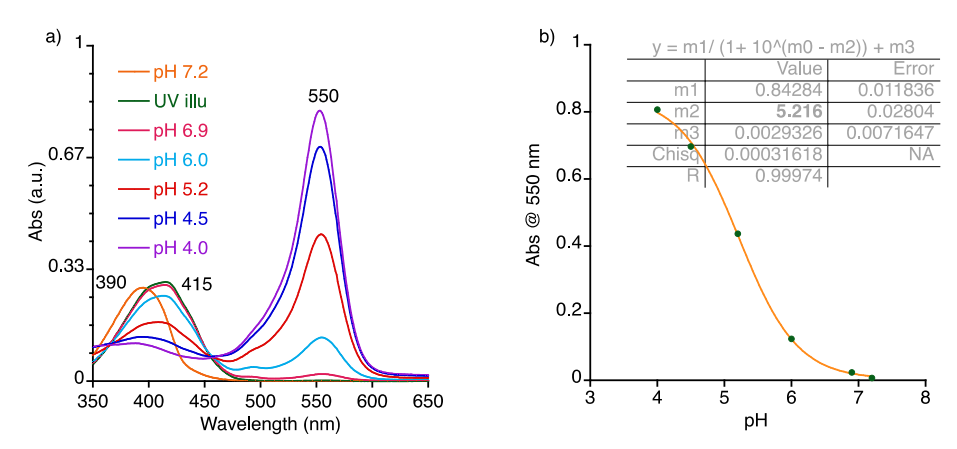


Figure 25. Determination of p K_a for M4/CM1V: a) titration of complex in PBS buffer b) The plot of pH versus absorbance derived from the data in panel a, fitted to the Henderson-Hasselbalch equation, revealing a p K_a of 5.2.

II.2.4 Photoactivation of hCRBPII/CM1V to form PSB at pH 7.2

The M4/CM1V-C₅₁ complex provided proof-of-principle that an active site thiol (Cys51) can engage in Michael addition reaction, and the *retro*-Michael reaction can be triggered with the appropriate wavelength of light. Nonetheless, a system with practical use would benefit from a large change in absorption upon 'ON/OFF' transition, especially at a physiologically relevant pH. The low pK_a of the imine formed in the M4/CM1V complex ($pK_a = 5.2$,) leads to the blue-shifted SB under photo illumination at pH 7.2. To generate a system that would lead to a large shift in absorption, the ground state complex should support the formation of a PSB at physiological pH. Additionally, we would expect an accelerated rate for the Michael addition with the more electrophilic polyene that terminates with the iminium. Note that this scenario is distinctly different from the PSB generated with the M4/CM1V complex, where the thiol seemed unreactive to engage in the Michael addition. In the case above, the PSB was generated by acidifying the medium, potentially attenuating the reactivity of the cysteine residue, while in this case, we desire

a protein with a higher iminium pK_a such that it is protonated at physiological pH. Observation of the **M4/CM1V**-C₅₁ structure showed that Phe4 was well situated to increase the pK_a of the SB if

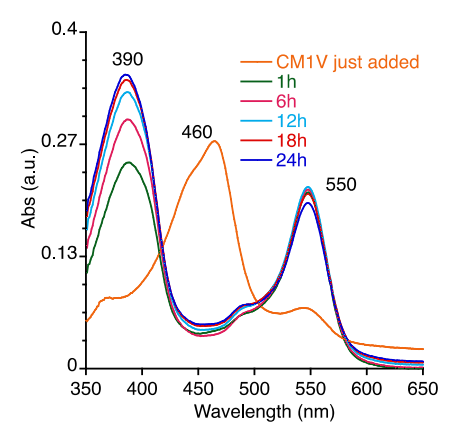


Figure 26. Time course study of M5/CM1V binding: Upon incubation of CM1V (15 μM) with M5 (30 μM), cysteine bound complex at λ_{max} = 390 nm was observed. A non-interconvertible PSB was also observed at λ_{max} = 550 nm.

appropriately mutated (**Figure**). Prior work in hCRBPII engineering efforts had also shown that hydrophilic residues at position 4 resulted in higher p*K*a Schiff bases.³⁵ As predicted, reintroduction of the wild-type Gln4 to generate **M5** (Q108K:K40L:T51C:T53A:R58L:Q38F:Q4) led to a protein host capable of generating the PSB upon incubation of **CM1V** at physiological pH. The putative PSB absorbs at 550 nm, which over time reduced in intensity, presumably as a result of Cys51 Michael addition that interrupts the fully conjugated system (**Figure**). The mature **M5/CM1V**-C₅₁ complex exhibits two peaks (550 nm and 390 nm), apparently due to incomplete conversion to the Michael adduct. Irradiation of the **M5/CM1V**-C₅₁ complex with UV light (BP 300-400 nm) for 1 minute led to a substantial increase in the PSB absorption (550 nm), likely because of the retro-Michael reaction that liberates the fully conjugated PSB complex. During this process, the absorption was increased by 2.8-fold, while the fluorescence observed at 580 nm was enhanced by more than 2-fold (**Figure**). The system turns 'OFF' within 10 minutes in the dark as evident by the decay in the PSB absorption with a half-life (*t1/2*) of 2.8 minutes at room

temperature. The decay could be accelerated by irradiation with visible light (LP500 nm) with an apparent half-life of 1.9 minutes.

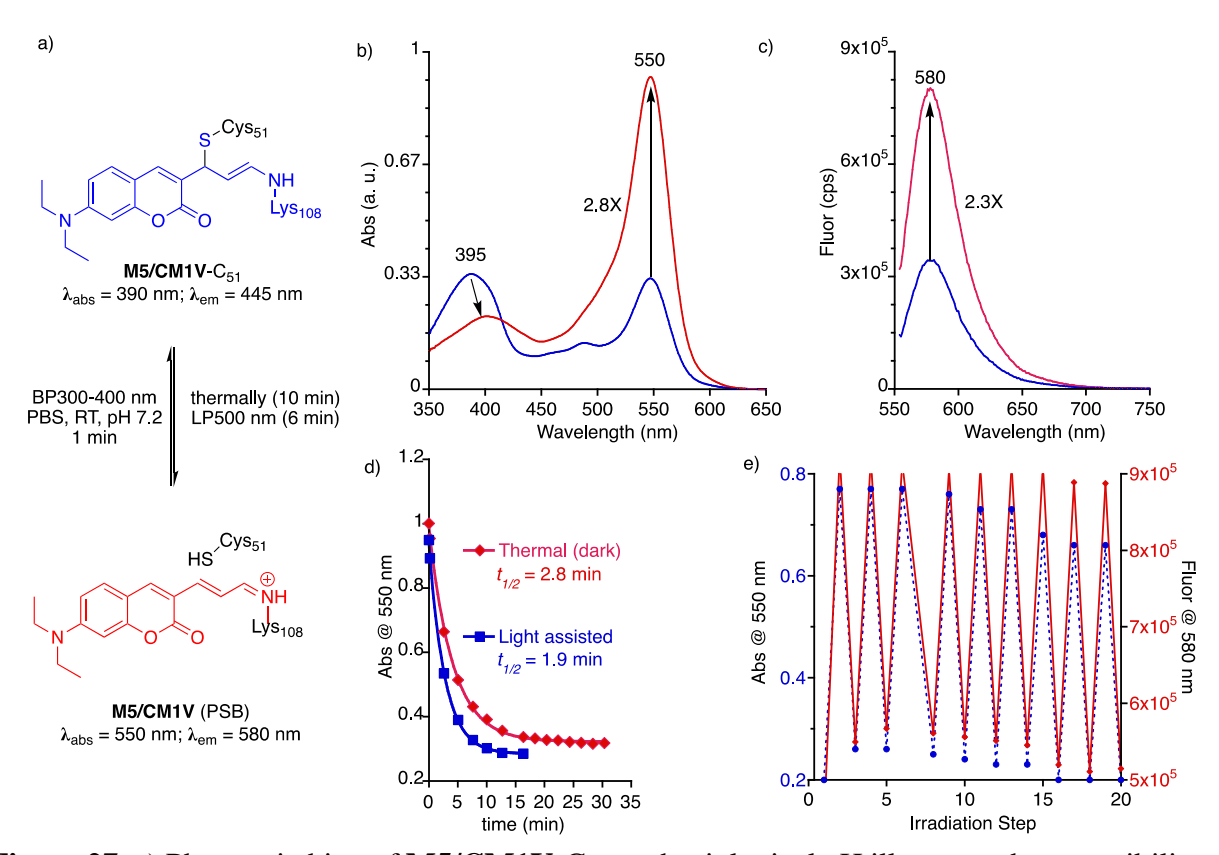


Figure 27. a) Photoswitching of **M5/CM1V**-C₅₁ at physiological pH illustrates the reversibility of the cysteine linkage. Unlike photo-induced cleavage of the C-S bond of **M4/CM1V**-C₅₁ at acidic conditions, the **M5/CM1V** PSB reverts to the initial cysteine bound complex (**M5/CM1V**-C₅₁); b) Photoexcitation (BP300-400 nm) of **M5/CM1V**-C₅₁ leads to a 2.8x increase in absorption, along with a 2.3x increase in the fluorescence (excited at the PSB absorption, 550 nm; c) Decay of the PSB as observed via its absorption through thermal (red) and continuous irradiation (LP500 nm, blue); d) Iterative Michael and retro-Michael addition of Cys51 with the **M5/CM1V** complex is observed with sequential photoirradiation (BP300-400 nm for 1 min, and LP500 nm for 5 min). The change of absorption is denoted by the dashed blue line, while the change in emission is highlighted with the solid red line.

Crystals of the **M5/CM1V** complex were informative in understanding the system (**Figure**). The crystals were deeply red colored, consistent with the presence of a PSB. Efforts at conversion between the PSB and the covalently bonded cysteine adduct at pH 7, however, were unsuccessful in the crystalline form. The PSB is in the *cis* iminium conformation, making a cation-

 π interaction with Trp106, similar to that seen in the M3 variant. The distance between the Cys51 sulfur atom and C₃ of CM1V is 7.0 Å, much too long for a covalent bond to be formed. This leads

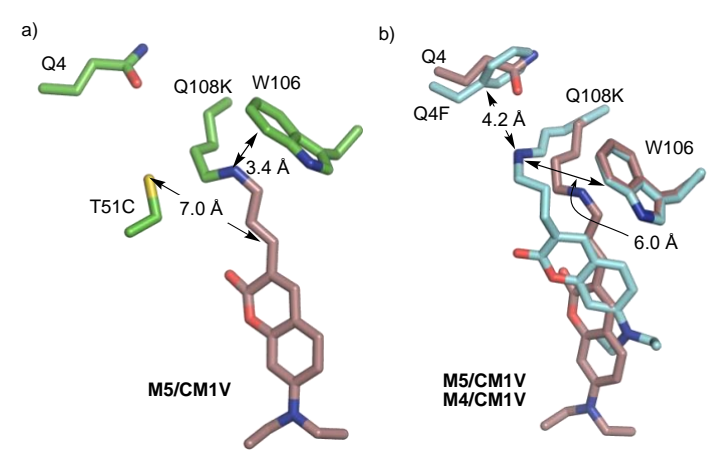


Figure 28. a) X-Ray crystal structure of M5/CM1V representing the non-interconverting PSB where the reactive cysteine is far away from the C₃ of the ligand. b) Overlay of M5/CM1V and UV-irradiated M4/CM1V crystal structures, depicting the role of Q4 in forming a PSB which is interconvertible with cysteine bound form.

us to conclude that the spectroscopically observed mixture (550 and 390 nm absorptions) in the resting state of the M5/CM1V complex were due to two conformations that ultimately has a bearing on the reactivity of the conjugated polyene with the active-site Cys residue. One conformation is competent for photoswitching between a visible light absorbing conjugated form and the covalently bound Cys51 UV absorbing form, while the other is in a conformation consistent with a stable conjugated PSB. The form of the M5/CM1V complex that crystallizes is clearly the non-interconverting permanently conjugated PSB, absorbing at 550 nm. The conformation that interconverts is presumably similar to that seen in the M4/CM1V structure, where the imine points to residue 4 (in this case Phe4) in the visible light absorbing PSB form.

Iterative ON/OFF switching, critical for certain imaging applications, was conducted to probe the stability and resistivity of the complex. As depicted in **Figure**, the conversion between the cysteine bound (*OFF* state) and non-bound form (*ON* state) was performed repeatedly using

UV (BP 300-400 nm) and visible light (LP500 nm) irradiation. The M5/CM1V-C₅₁ complex showed good fatigue resistance, with minimal loss in fluorescence signal upon each ON/OFF cycle. This indicates robustness of the process where the cysteine residue adds reversibly to the fluorophore and undergoes switchability. Analogous to M4/CM1V-C₅₁, the switchability of M5/CM1V-C₅₁ does not occur at acidic pH as the photo illumination leads to formation of stable PSB. However, at physiological pH, cysteine rebinds after photodissociation in both cases. Note that the photo illumination of M4/CM1V-C₅₁ leads to a SB whereas M5/CM1V-C₅₁ generates a PSB at the same pH. In total, the data suggests that cysteine addition is dependent on the pH of the solution regardless of the reactivity of the imine. Thus, the lack of photoswitching at acidic pH is most probably the result of attenuated reactivity of Cys51 even in the presence of the highly reactive iminium. Nonetheless, as the reactivity of cysteine can be finely tuned inside a protein cavity, the photoswitchability of hCRBPII/CM1V complex can be performed by near stoichiometric addition of protein to the fluorophore. Moreover, the switchability is maintained in presence of oxygen, and thus can be useful for imaging under aerobic condition.

II.3 Conclusion and outlook

To the best of our knowledge, we illustrate the first example of a reversible site-specific labelling of a protein with a fluorophore that employs dynamic covalent chemistry of a cysteine residue. The regulation of protein microenvironment by rational mutagenesis yields a photoactivatable protein/fluorophore complex with large shift in absorption at physiological pH. Moreover, the conjugation can be cycled between a cysteine bound and non-bound form repetitively, making it a photoswitchable system. Structural evidence thus far indicates a process involving a Michael type addition reaction of a nucleophilic cysteine residing the binding pocket of the host protein with an electrophilic double bond. The relatively weaker carbon-sulfur bond is

broken under photo irradiation to liberate the cysteine reside to form the fully conjugated polyene through a retro-Michael process. This approach utilizes the reactivity of an α,β -unsaturated aldehyde-based dye, and thus opens the door for expanding the methodology by exploring a broad range of intramolecular charge transfer (ICT) dyes with a similar functional handle for imaging purposes.

II.4 Experimental Section

II.4.1 Site-directed mutagenesis

All site directed mutagenesis were performed in the pET-17b vector containing hCRBPII-Q108K:K40L:T53A:R58L:Q38F:Q4F cloned between NdeI and Xhol.³⁵ Site directed mutagenesis was performed using polymerase chain reaction (PCR), with the following program (**Table 2**):

Table 2. PCR cycling conditions for site-directed mutagenesis

	PCR Program	Time (min)
1X	94 °C	3:00
	94 °C	0:20
20X	3 to 5 °C below T _m	0:55
	72 °C	3:30
1X	72 °C	10:00
1X	4 °C	5:00

Reactant	Volume					
DNA template	$70 \text{ ng } (x \mu L)$					
Forward primer	20 pmol (y μ L)					
Reverse Primer	20 pmol (z μ L)					
10 mM dNTP	1 μL					
50 mM MgCl ₂	1 μL					
DMSO	5 μL					
10X Cloned Pfu Reaction buffer	5 μL					
Pfu Turbo DNA polymerase	1 μL					
$(2.5U/\mu L)$						
Nuclease free water	(50-x-y-z-7) uL					

The primers used for the site directed mutagenesis were purchased from Integrated DNA Technology (IDT), with melting temperature (T_m) from 55 °C to 65 °C. The crude PCR product

was digested with 20 units of DpnI enzyme (New England Biolabs) for 1 h at 37 °C. The digested product was then transformed into *E. coli* XL-1 Blue competent cells (Agilent) for 30 min on ice and then coated on LB-Amp/Tet agar plate. After incubation at 37 °C for 16 h, a single colony was cultured in LB media with antibiotics (100 μg/mL ampicillin and 12.5 μg/mL tetracycline) for 12 h. DNA purification was performed using Wizard Plus SV miniprep DNA purification system (Promega). The concentration of the isolated DNA was measured using Nanodrop® and sequenced at the Research Technology Support Facility at Michigan State University using a primer corresponding to the T7 promoter of the pET-17b plasmid.

II.4.2 Protein expression and purification

hCRBPII mutants in pET-17b vector were expressed in *E. Coli* BL21(DE3)pLyS competent cells (Promega). The target gene (100 ng of DNA for 50 μL of cell solution) was added to the cells on ice for 30 min and spread over LB-Amp/Chl agar plate. The plate was incubated at 37 °C for approximately 12 h and a single colony was picked to grow in a 1 L terrific broth (TB) media supplemented with antibiotics (100 μg/mL ampicillin and 27 μg/mL chloramphenicol). The cells were cultured for 8-10 h at 37 °C until the optical density (OD) reached approximately 1. Subsequently, isopropyl- β-D-thiogalactopyranoside (IPTG, Gold Biotechnology) was added to the culture at a final concentration of 1.0 mM and shaken at 37 °C for additional 16-20 h. The cells were then harvested by centrifugation (3000 rpm, 15 min, 4 °C), resuspended in Tris buffer (10 mM Tris, pH 7.8-8, 50 mL), lysed with ultrasonic homogenizer (Biologics, Inc, power 60%, 3 min), added with 500U of DNase I (recombinant, Roche Diagnostics) and kept at RT for 10 min. The solution was then centrifuged (3000 rpm, 40 min, 4 °C) to separate the pellet. The supernatant was loaded onto a FastQ anion exchange column (resin from GE Healthcare), equilibrated with Tris buffer (10 mM Tris, pH 7.8-8). The resin was subsequently washed with Tris buffer (2X50

mL) and eluted with Tris-elution buffer (10 mM Tris, 200 mM NaCl, pH 7.8-8.0, 50 mL). The eluent was desalted using Amicon® Ultra-15 Centrifugal Filter Units (MW cut-off: 10K), and further purified with a FPLC (NGC chromatography system, Biorad), equipped with a Source 15Q column (Q Sepharose Fast Flow, GE Healthcare) anion exchange resin using 50 mM Tris·HCl (solution A) and 2 M NaCl (solution B) at pH 8.1. All protein samples were collected with 4% of solution B and concentrated using Amicon Ultracentrifugation filter (MW cut-off: 10K) to a final volume of 1 mL. The sample (1 mL) was then loaded to size exclusion chromatography (Superdex 120 16/600 GL column, GE Healthcare) for further purification using a buffer containing solution A and 20% of solution B. Collected protein sample was concentrated (conc. 100-200 μM) and stored at 4 °C for optical studies.

II.4.3 Determination of extinction coefficient of protein

UV-vis spectra were measured with a Cary 300 Bio WinUV, Varian spectrophotometer using 1 cm, 1.0 mL quartz microcuvettes (Starna Cells). The extinction coefficients of the hCRBPII mutants were measured following the method described by Gill and von Hippel.³⁶ The theoretical extinction coefficient (ε_{theo}) is calculated using following equation:

$$\varepsilon_{\textit{theo}} = a \times \varepsilon_{\textit{Trp}} + b \times \varepsilon_{\textit{Tyr}} + c \times \varepsilon_{\textit{cys}}$$

where a, b and c are the number of tryptophan, tyrosine, and cysteine residues in the protein, respectively. ε used for tryptophan, tyrosine, and cysteine are 5690 M⁻¹cm⁻¹, 1280 M⁻¹cm⁻¹ and 120 M⁻¹cm⁻¹, respectively. The absorbance of each protein was measured at 280 nm in 2XPBS and 6M guanidine hydrochloride solution. The absorbance value was used to calculate the experimental ε using the following equation:

$$\varepsilon_{exp} = \frac{A_{native}}{A_{denaturating}} \times \varepsilon_{theo}$$

Table 3. The values of the extinction coefficients

Mutants	Proteins	$\varepsilon_{\rm exp}({ m M}^{-1}{ m cm}^{-1})$
M1	Q108K:K40E:T53A:R58L:Q38F:Q4F	27,681
M2	Q108K:K40E:T51C:T53S:R58L:Q38F:Q4F	28,634
M3	Q108K:K40L:T53A:R58L:Q38F:Q4F	28,000
M4	Q108K:K40L:T51C:T53A:R58L:Q38F:Q4F	28,600
M5	Q108K:K40L:T51C:T53A:R58L:Q38F:Q4	28, 520

II.4.4 UV-Vis measurement of hCRBPII/dye

For UV-vis measurement, a stock solution protein (100-200 μ M) was prepared by concentrating the purified protein, collected from size-exclusion chromatography. In addition, a stock solution of dye (10 mM) was prepared in acetonitrile. For complex formation, 10-30 μ M of protein was incubated with respective dyes (5-15 μ M, 0.5 equiv with respect to the protein) in PBS (pH 7.2) at room temperature, unless otherwise mentioned. The binding was followed by the disappearance of the dye and concomitant formation of complex.

II.4.5 pKa measurements of hCRBPII/CM1V

For p K_a measurement of M3/CM1V, complex was prepared by incubating M3 (20 μ M) and CM1V (10 μ M) PBS (pH 7.2) at RT. Titration was performed with acid (1 M citric acid solution), or base (1 M NaOH) and the absorption spectra was recorded. Absorbance at the λ_{max} of 550 nm was plotted as a function of pH of the solution. A curve fit to the following modified Henderson-Hassebalch equation was applied to determine the p K_a .

$$A = \frac{A_0}{1 + 10^{pH - pK_a}} + \text{constant}$$

where A_0 is the absorbance of the maximum PSB and the p K_a is the mid-point of the titration. A constant is included for the zero absorbance of the deprotonated PSB.

For p K_a measurement of M4/CM1V, first a cysteine bound complex (M4/CM1V-C₅₁) was prepared by incubating M4 (30 μ M) and CM1V (15 μ M) PBS (pH 7.2) at RT. Then M4/CM1V-

SB was formed by photo activation of the complex with UV (discussed in section H) and gradually acidified to form the M4/CM1V-PSB. Absorbance at the λ_{max} of 550 nm was plotted as a function of pH of the solution and p K_a was as described for the M3/CM1V complex. All pH values were recorded with an accumet® Basic pH meter (Fisher Scientific) equipped with a PerpHect® ROSS® Micro Combination pH electrode (Thermo Scientific Orion).

II.4.6 Fluorescence measurements

Fluorescence spectra were recorded using a Fluorolog-3 spectrofluorometer (HORIBA, Ltd.) with a 1 cm, 3.5 mL quartz cuvette or 1 cm, 1.0 mL quartz microcuvette (Starna Cells). An entrance slit of 1 nm and exit slit of 12 nm was used for all measurements.

II.4.7 Photo-irradiations

Photo-irradiation of protein complexes in solution was performed with a Hg(Xe) Arc lamp (Oriel Instrument) attenuated with two neutral-density filters (Edmund Optics Inc.).²⁴ For photoactivation of UV absorbing complexes, solution was illuminated with a 300-400 bandpass filter (Edmund Optics Inc.) at a desired pH (pH 7.2/4.2). Photoswitching between UV and visible absorbing complexes was performed with the use of both a 300-400 bandpass filter (1 min) and 500 nm long pass filter (5 min).

For measuring the half-life of thermal decay, the M5/CM1V-C₅₁ was first illuminated for 1 min and absorbance was followed at 550 nm over time. On the other hand, the rate of photochemical decay was measured under constant irradiation through a 500 nm long pass filter and intermittent collection of the absorbance at 550 nm. The half-life of decay was calculated by fitting the values with a mono-exponential decay function.

 Table 4. Structural data of hCRBPII-CM1V complexes

	M1	M2 before UV	M2 after UV	M3		
Wavelength	1.1272 Å	1.1272 Å	1.1272 Å	1.54184 Å		
Desclution Denga	29.71 - 1.42	33.63 - 1.689	33.49 - 1.601	17.59 - 1.5		
Resolution Range	(1.471 - 1.42)	(1.749 - 1.689)	(1.658 - 1.601)	(1.554 - 1.5)		
Space group	C 1 2 1	C 1 2 1	C 1 2 2	C 1 2 3		
a (Å)	29.612	29.613	29.698	28.71		
b (Å)	67.106	67.25	66.972	66.42		
c (Å)	63.903	63.687	63.817	63.98		
a (°)	90	90	90	90		
b (°)	90.108	92.275	92.102	91.16		
γ (°)	90	90	90	90		
Molecules per Asymmetric Unit	1	1	1	1		
Total reflections	468357	470858	622275	15176		
Unique Reflection	22948 (2284)	13067 (1152)	14890 (1476)	14242		
Multiplicity	6.4	9.8	6.6	2		
Completeness (%)	97.28 (96.21)	93.01 (81.70)	90.18 (88.56)	94.20 (82.71)		
Average I/s	22949	13067	33704	17103		
$R_{ m meas}$ (%)	3.6	4.1	8.0	3.5		
R_{pim} (%)	1.4	1.3	3.4	2.2		
Reflections used in refinement	22934 (2283)	13058 (1152)	14878 (1471)	18241 (1603)		
Reflections used for R _{free}	1987 (201)	1296 (117)	1468 (147)	1807 (152)		
Rwork (%)	22.61	22.09	20.37	22.87		
Rfree (%)	22.85	27.16	26.21	27.98		
RMSD from ideal values						
Bond Angle	1.045	1.71	1.84	1.38		
Bond Length (Å)	0.013	0.022	0.048	1.6		
Average B factor	21.51	46.95	35.42	26.59		
Number of water molecules	53	94	77	76		
PDB IDs	8D6N	8D6L	8D6H	8DB2		

II.4.8 Protein Crystallization and data collection

Pure protein samples were concentrated to 7-10 mg/mL using Amicon® Ultra centrifugal units (5 mL, 10 kDa cutoff), and approximately 4 equivalents of CM1V were added and the solution was allowed to incubate overnight at RT. Crystallization was done by vapor diffusion using 24 well plates (Hampton Research) with 1 mL reservoir volume. For each well, 1 µL of protein was added to 1 µL of well solution. Crystals typically appeared within 1-3 days in well **Table 4** List of crystallographic data solutions containing 25-40% PEG 4000, 0.1 M ammonium acetate, and 0.1 M sodium acetate with a pH range of 4.0 to 4.8. All UV irradiation studies were done using a TLC hand lamp. Crystals were flash frozen in a solution containing the mother liquor and 30% glycerol. Diffraction data was collected at the Advanced Photon Source (APS) (Argonne IL) LS-CAT, (sector 21-ID-D,F, and G) at 1.00 Å wavelength radiation at 100 K, using either an Eiger 9M, MAR300 or MAR350 detector. Data reduction and scaling were performed using the HKL2000 program package.³⁷ All structures were solved by Molecular Replacement using PHASER and refined using the PHENIX program package. 38,39 Three cycles of refinement were implemented for each run. Placement of the CM1V ligand and all ordered water molecules was done using COOT (0.8.9.1).40

II.4.9 Synthesis of FR1V-cyano-acetal

In a mixture of **FR0** (76 mg, 0.26 mmol) and 3,3-dimethoxypropanenitrile (39 mg, 0.34 mmol) in dichloromethane (0.5 mL), NaOMe solution (4.5M, 4.5 mL) was added dropwise over 10 minutes and stirred at room temperature for 24h. Complete consumption of starting material was confirmed by TLC (20:80 ethyl acetate and hexane). The reaction mixture was then extracted

with dichloromethane twice and organic layer was dried through anhydrous sodium sulfate. Finally, dichloromethane was removed in vacuo and purified by preparative TLC using 20% ethyl acetate in hexane to afford **FR1V**-cyano-acetal as orange solid (91 mg, 0.23 mmol, yield 90%). 1 H NMR (500 MHz, CDCl₃) δ 7.93 (d, J = 1.6 Hz, 1H), 7.71 (dd, J = 8.0, 1.7 Hz, 1H), 7.57 (dd, J = 8.2, 5.0 Hz, 2H), 7.34 (s, 1H), 6.70-6.66 (m, 2H), 5.05 (d, J = 1.1 Hz, 1H), 3.44 (m, 10H), 1.49 (s, 6H), 1.23 (t, J = 7.1 Hz, 6H). 13 C NMR (125 MHz, CDCl₃) δ 156.90, 153.29, 148.70, 146.41, 143.65, 129.80, 129.20, 125.92, 123.12, 122.02, 118.51, 117.92, 110.88, 105.58, 105.38, 101.72, 53.36, 53.24, 46.87, 44.84, 29.85, 27.47, 12.76. TOF MS ES⁺(C₂₅H₃₀N₂O₂): Calc. [M+H]⁺: 390.231; found: 391.236.

II.4.10 Synthesis of FR1V-cyano⁴¹

HCl (6 N, 2 mL) was dropwise added to **FR1V**-cyano-acetal (72 mg, 0.18 mmol) and stirred for 30 mins at 0 °C. Reaction mixture was then extracted with ethyl acetate twice from water and washed with brine and finally with water. The organic layer was dried over anhydrous sodium sulfate and concentrated in vacuo to give red solid as crude product. The crude was purified through flash chromatography using 20% ethyl acetate in hexane to afford **FR1V**-cyano as red solid (53 mg, 0.15 mmol, yield 85%). ¹H NMR (500 MHz, CDCl₃) δ 9.57 (s, 1H), 8.04 (s, 1H), 7.88 (dd, J = 8.5, 1.6 Hz, 1H), 7.88 (s, 1H), 7.63 (d, J = 8.2 Hz, 2H), 6.69 (d, J = 8.5 Hz, 2H), 3.47 (q, J = 7.1 Hz, 4H), 1.50 (s, 6H), 1.24 (t, 6H). ¹³C NMR δ (125 MHz, CDCl₃): 187.61, 159.42, 158.11, 153.78, 149.68, 147.81, 133.25, 127.91, 125.06, 124.88, 123.11, 118.85, 115.59, 111.20, 108.42, 104.99, 46.87, 44.92, 27.33, 12.74. Calculated Mass C₂₃H₂₄N₂O: 344.189, [M+H]⁺ = 345.205.

II.4.11 Synthesis of CM1V

$$\begin{array}{c} \text{N} \\ \text{OH} \\ \text{OH} \\ \end{array} \begin{array}{c} \text{1. CH}_2(\text{CO}_2\text{Et})_{2,} \\ \text{piperidine,} \\ \text{dry EtOH} \\ \text{2. AcOH, HCI} \\ \end{array} \begin{array}{c} \text{DMF} \\ \text{POCI}_3 \\ \text{yield over} \\ \text{two steps:} \\ \text{50\%} \\ \end{array} \begin{array}{c} \text{1.} \\ \text{O} \\ \text{PPh}_3 \\ \text{NaOH} \\ \text{dry DCM} \\ \text{2. HCI} \\ \text{yield: 60\%} \\ \end{array} \begin{array}{c} \text{CM1V} \\ \end{array}$$

Compounds 1 and 2 were synthesized following previous literature reported procedures.²⁸ For synthesis of CM1V, compound 2 (73 mg, 0.34 mmol, 1 equiv), ((1,3-dioxolan-2yl)methyl)triphenylphosphonium bromide (175 mg, 0.41 mmol, 1.2 equiv.) were dissolved in dry dichloromethane (5 mL) and stirred for 30 min. Powdered NaOH (15 mg, 0.38 mmol, 1.1 equiv) was added to the mixture and stirred until the spot for the starting material disappeared on TLC (30% ethyl acetate in hexane). Concentrated HCl (1 mL) was added and stirred at RT for 30 min. Subsequently, deionized water (10 mL) and dichloromethane (10 mL) were added, and the organic layer was separated and dried over anhydrous Na₂SO₄. After concentrating under reduced pressure, the product was purified using flash chromatography on silica gel column with a mixture of ethyl acetate in hexane (10-50%) affording compound CM1V as a salmon pink solid (55 mg, 0.20 mmol, yield 60%). The ¹H and ¹³C of the pure compound match with the compound prepared previously. ⁴² ¹H NMR (500 MHz, DMSO- d_6) $\delta = 9.58$ (d, J=8.0 Hz, 1H), 8.34 (s, 1H), 7.57 – 7.48 (m, 2H), 6.93 (dd, J=15.7 Hz, 8.0 Hz, 1H), 6.79 (dd, J=9.0 Hz, 2.5 Hz, 1H), 6.58 (d, J=2.4 Hz, 1H), 3.48 (q, J=7.0 Hz, 4H), 1.14 (t, J=7.0 Hz, 6H). ¹³C NMR (125 MHz, DMSO- d_6) δ 194.91, 159.93, 157.18, 152.68, 148.86, 146.55, 131.51, 128.22, 112.96, 110.48, 108.65, 96.65, 44.83, 12.82.

II.4.12 Synthesis of SB and PSB with *n*-butylamine

For synthesis of SB, respective dyes (\sim 1 mg) were dissolved in ethanol (0.25 mL) and n-butylamine (\sim 20 μ L, 50 equiv) and stirred until the bright color of the aldehyde completely disappeared (\sim 30 min). Subsequently, solvent was completely evaporated under N₂ flow, and the

material was redissolved in acetonitrile to make stock of respective SB (10 mM). To collect the absorption spectrum, 1 μ L of the stock was dissolved in acetonitrile (1 mL). Acidification of the solution with 1 mM camphor sulfonic acid (10 μ L) in DMSO resulted in the formation of PSB.

II.4.13 Studying the formation of AD-1 and AD-2

To study the formation of **AD-1** and **AD-2** by NMR, the 1.1 mg (0.0041 mmol, 1 equiv) of **CM1V**-SB was dissolved in CD₃CN and β -ME (8.6 μ L, 0.12 mmol, 30 equiv) was added. ¹H NMR spectrum of the mixture was collected every 5 minutes until all the starting SB is consumed (after 20 mins). With lower equivalent of β -ME, a single product could not be obtained, and the reaction becomes slower. For UV-vis study, a solution of **CM1V**-SB was prepared in acetonitrile (10 μ M) and β -ME was gradually added, and the absorption spectrum was collected after each addition. Alternatively, **CM1V**-PSB was first formed with addition of CSA (5 μ L of 1 mM solution in DMSO) to **CM1V**-SB (5 μ M) and then β -ME was mixed until the absorption for PSB disappears with concomitant formation absorption maximum around 390 nm. **CM1V**-PSB requires a larger excess of β -ME for the reaction to be complete, possibly because of the lower reactivity of β -ME under acidic condition required to form PSB.

REFERENCES

- (1) Jing, C.; Cornish, V. W. Chemical tags for labeling proteins inside living cells. *Acc. Chem. Res.* **2011**, *44* (9), 784.
- (2) Adumeau, P.; Sharma, S. K.; Brent, C.; Zeglis, B. M. Site-Specifically Labeled Immunoconjugates for Molecular Imaging--Part 1: Cysteine Residues and Glycans. *Mol Imaging Biol* **2016**, *18* (1), 1.
- (3) Liu, W.; Li, F.; Chen, X.; Hou, J.; Yi, L.; Wu, Y. W. A rapid and fluorogenic TMP-AcBOPDIPY probe for covalent labeling of proteins in live cells. *J. Am. Chem. Soc.* **2014**, *136* (12), 4468.
- (4) Chen, Z.; Jing, C.; Gallagher, S. S.; Sheetz, M. P.; Cornish, V. W. Second-generation covalent TMP-tag for live cell imaging. *J. Am. Chem. Soc.* **2012**, *134* (33), 13692.
- (5) Canovas, C.; Bellaye, P. S.; Moreau, M.; Romieu, A.; Denat, F.; Goncalves, V. Sitespecific near-infrared fluorescent labelling of proteins on cysteine residues with mesochloro-substituted heptamethine cyanine dyes. *Org Biomol Chem* **2018**, *16* (45), 8831.
- (6) Chen, Y.; Clouthier, C. M.; Tsao, K.; Strmiskova, M.; Lachance, H.; Keillor, J. W. Coumarin-based fluorogenic probes for no-wash protein labeling. *Angew. Chem. Int. Ed. Engl.* **2014**, *53* (50), 13785.
- (7) Hori, Y.; Norinobu, T.; Sato, M.; Arita, K.; Shirakawa, M.; Kikuchi, K. Development of Fluorogenic Probes for Quick No-Wash Live-Cell Imaging of Intracellular Proteins. *Journal of the American Chemical Society* **2013**, *135* (33), 12360.
- (8) Girouard, S.; Houle, M. H.; Grandbois, A.; Keillor, J. W.; Michnick, S. W. Synthesis and characterization of dimaleimide fluorogens designed for specific labeling of proteins. *J. Am. Chem. Soc.* **2005**, *127* (2), 559.
- (9) Hu, W.; He, T.; Zhao, H.; Tao, H.; Chen, R.; Jin, L.; Li, J.; Fan, Q.; Huang, W.; Baev, A.et al. Stimuli-Responsive Reversible Switching of Intersystem Crossing in Pure Organic Material for Smart Photodynamic Therapy. *Angew. Chem. Int. Ed. Engl.* **2019**, *58* (32), 11105.
- (10) Kuriki, Y.; Kamiya, M.; Kubo, H.; Komatsu, T.; Ueno, T.; Tachibana, R.; Hayashi, K.; Hanaoka, K.; Yamashita, S.; Ishizawa, T.et al. Establishment of Molecular Design Strategy To Obtain Activatable Fluorescent Probes for Carboxypeptidases. *J. Am. Chem. Soc.* **2018**, *140* (5), 1767.
- (11) Sayresmith, N. A.; Saminathan, A.; Sailer, J. K.; Patberg, S. M.; Sandor, K.; Krishnan, Y.; Walter, M. G. Photostable Voltage-Sensitive Dyes Based on Simple, Solvatofluorochromic, Asymmetric Thiazolothiazoles. *J. Am. Chem. Soc.* **2019**, *141* (47), 18780.

- (12) Zhang, W.; Huo, F.; Yue, Y.; Zhang, Y.; Chao, J.; Cheng, F.; Yin, C. Heat Stroke in Cell Tissues Related to Sulfur Dioxide Level Is Precisely Monitored by Light-Controlled Fluorescent Probes. *J. Am. Chem. Soc.* **2020**, *142* (6), 3262.
- (13) Tang, J.; Robichaux, M. A.; Wu, K. L.; Pei, J.; Nguyen, N. T.; Zhou, Y.; Wensel, T. G.; Xiao, H. Single-Atom Fluorescence Switch: A General Approach toward Visible-Light-Activated Dyes for Biological Imaging. *J. Am. Chem. Soc.* **2019**, *141* (37), 14699.
- (14) Dai, S. Y.; Yang, D. A Visible and Near-Infrared Light Activatable Diazocoumarin Probe for Fluorogenic Protein Labeling in Living Cells. *J. Am. Chem. Soc.* **2020**, *142* (40), 17156.
- Usama, S. M.; Inagaki, F.; Kobayashi, H.; Schnermann, M. J. Norcyanine-Carbamates Are Versatile Near-Infrared Fluorogenic Probes. *J. Am. Chem. Soc.* **2021**, *143* (15), 5674.
- (16) Toussaint, S. N. W.; Calkins, R. T.; Lee, S.; Michel, B. W. Olefin Metathesis-Based Fluorescent Probes for the Selective Detection of Ethylene in Live Cells. *J. Am. Chem. Soc.* **2018**, *140* (41), 13151.
- (17) Aggarwal, K.; Kuka, T. P.; Banik, M.; Medellin, B. P.; Ngo, C. Q.; Xie, D.; Fernandes, Y.; Dangerfield, T. L.; Ye, E.; Bouley, B.et al. Visible Light Mediated Bidirectional Control over Carbonic Anhydrase Activity in Cells and in Vivo Using Azobenzenesulfonamides. *J. Am. Chem. Soc.* **2020**, *142* (34), 14522.
- (18) Mayer, G.; Heckel, A. Biologically active molecules with a "light switch". *Angew. Chem. Int. Ed. Engl.* **2006**, *45* (30), 4900.
- (19) Szymanski, W.; Beierle, J. M.; Kistemaker, H. A.; Velema, W. A.; Feringa, B. L. Reversible photocontrol of biological systems by the incorporation of molecular photoswitches. *Chem Rev* **2013**, *113* (8), 6114.
- (20) Dempsey, G. T.; Bates, M.; Kowtoniuk, W. E.; Liu, D. R.; Tsien, R. Y.; Zhuang, X. Photoswitching mechanism of cyanine dyes. *J. Am. Chem. Soc.* **2009**, *131* (51), 18192.
- (21) Gidi, Y.; Payne, L.; Glembockyte, V.; Michie, M. S.; Schnermann, M. J.; Cosa, G. Unifying Mechanism for Thiol-Induced Photoswitching and Photostability of Cyanine Dyes. *J. Am. Chem. Soc.* **2020**, *142* (29), 12681.
- (22) Chozinski, T. J.; Gagnon, L. A.; Vaughan, J. C. Twinkle, twinkle little star: photoswitchable fluorophores for super-resolution imaging. *FEBS Lett.* **2014**, *588* (19), 3603.
- (23) Zhou, X. X.; Lin, M. Z. Photoswitchable fluorescent proteins: ten years of colorful chemistry and exciting applications. *Curr. Opin. Chem. Biol.* **2013**, *17* (4), 682.

- (24) Sheng, W.; Nick, S. T.; Santos, E. M.; Ding, X.; Zhang, J.; Vasileiou, C.; Geiger, J. H.; Borhan, B. A Near-Infrared Photoswitchable Protein-Fluorophore Tag for No-Wash Live Cell Imaging. *Angew. Chem. Int. Ed. Engl.* **2018**, *57* (49), 16083.
- (25) Wang, W.; Nossoni, Z.; Berbasova, T.; Watson, C. T.; Yapici, I.; Lee, K. S.; Vasileiou, C.; Geiger, J. H.; Borhan, B. Tuning the electronic absorption of protein-embedded all-transretinal. *Science* **2012**, *338* (6112), 1340.
- (26) Cho, A. Y.; Choi, K. A Coumarin-based Fluorescence Sensor for the Reversible Detection of Thiols. *Chem. Lett.* **2012**, *41* (12), 1611.
- (27) Cao, D.; Liu, Z.; Verwilst, P.; Koo, S.; Jangjili, P.; Kim, J. S.; Lin, W. Coumarin-Based Small-Molecule Fluorescent Chemosensors. *Chem Rev* **2019**, *119* (18), 10403.
- (28) Jiang, X.; Yu, Y.; Chen, J.; Zhao, M.; Chen, H.; Song, X.; Matzuk, A. J.; Carroll, S. L.; Tan, X.; Sizovs, A.et al. Quantitative imaging of glutathione in live cells using a reversible reaction-based ratiometric fluorescent probe. *ACS Chem Biol* **2015**, *10* (3), 864.
- (29) Kim, G.-J.; Yoon, D.-H.; Yun, M.-Y.; Kwon, H.; Ha, H.-J.; Kim, H.-J. Ratiometric fluorescence probes based on a Michael acceptor type of coumarin and their application for the multichannel imaging of in vivo glutathione. *RSC Advances* **2014**, *4* (36), 18731.
- (30) Yue, Y.; Huo, F.; Ning, P.; Zhang, Y.; Chao, J.; Meng, X.; Yin, C. Dual-Site Fluorescent Probe for Visualizing the Metabolism of Cys in Living Cells. *J. Am. Chem. Soc.* **2017**, *139* (8), 3181.
- (31) Liu, J.; Sun, Y. Q.; Huo, Y.; Zhang, H.; Wang, L.; Zhang, P.; Song, D.; Shi, Y.; Guo, W. Simultaneous fluorescence sensing of Cys and GSH from different emission channels. *J. Am. Chem. Soc.* **2014**, *136* (2), 574.
- (32) Yin, G. X.; Niu, T. T.; Gan, Y. B.; Yu, T.; Yin, P.; Chen, H. M.; Zhang, Y. Y.; Li, H. T.; Yao, S. Z. A Multi-signal Fluorescent Probe with Multiple Binding Sites for Simultaneous Sensing of Cysteine, Homocysteine, and Glutathione. *Angew. Chem. Int. Ed. Engl.* **2018**, 57 (18), 4991.
- (33) Berbasova, T.; Tahmasebi Nick, S.; Nosrati, M.; Nossoni, Z.; Santos, E. M.; Vasileiou, C.; Geiger, J. H.; Borhan, B. A Genetically Encoded Ratiometric pH Probe: Wavelength Regulation-Inspired Design of pH Indicators. *Chembiochem* **2018**, *19* (12), 1288.
- (34) Nosrati, M.; Berbasova, T.; Vasileiou, C.; Borhan, B.; Geiger, J. H. A Photoisomerizing Rhodopsin Mimic Observed at Atomic Resolution. *J. Am. Chem. Soc.* **2016**, *138* (28), 8802.
- (35) Santos, E. M.; Sheng, W.; Esmatpour Salmani, R.; Tahmasebi Nick, S.; Ghanbarpour, A.; Gholami, H.; Vasileiou, C.; Geiger, J. H.; Borhan, B. Design of Large Stokes Shift

- Fluorescent Proteins Based on Excited State Proton Transfer of an Engineered Photobase. *J. Am. Chem. Soc.* **2021**, *143* (37), 15091.
- (36) Gill, S. C.; von Hippel, P. H. Calculation of protein extinction coefficients from amino acid sequence data. *Anal. Biochem.* **1989**, *182* (2), 319.
- (37) Otwinowski, Z.; Minor, W. In *Methods Enzymol.*; Academic Press, 1997; Vol. 276.
- (38) Winn, M. D.; Ballard, C. C.; Cowtan, K. D.; Dodson, E. J.; Emsley, P.; Evans, P. R.; Keegan, R. M.; Krissinel, E. B.; Leslie, A. G.; McCoy, A.et al. Overview of the CCP4 suite and current developments. *Acta Crystallogr D Biol Crystallogr* **2011**, *67* (Pt 4), 235.
- (39) Adams, P. D.; Afonine, P. V.; Bunkoczi, G.; Chen, V. B.; Davis, I. W.; Echols, N.; Headd, J. J.; Hung, L. W.; Kapral, G. J.; Grosse-Kunstleve, R. W. et al. PHENIX: a comprehensive Python-based system for macromolecular structure solution. *Acta Crystallogr D Biol Crystallogr* **2010**, *66* (Pt 2), 213.
- (40) Emsley, P.; Lohkamp, B.; Scott, W. G.; Cowtan, K. Features and development of Coot. *Acta Crystallogr D Biol Crystallogr* **2010**, *66* (Pt 4), 486.
- (41) Erichsen, M. N.; Huynh, T. H. V.; Abrahamsen, B.; Bastlund, J. F.; Bundgaard, C.; Monrad, O.; Bekker-Jensen, A.; Nielsen, C. W.; Frydenvang, K.; Jensen, A. A.et al. Structure—Activity Relationship Study of First Selective Inhibitor of Excitatory Amino Acid Transporter Subtype 1: 2-Amino-4-(4-methoxyphenyl)-7-(naphthalen-1-yl)-5-oxo-5,6,7,8-tetrahydro-4H-chromene-3-carbonitrile (UCPH-101). *Journal of Medicinal Chemistry* **2010**, *53* (19), 7180.
- (42) Yuan, L.; Lin, W.; Yang, Y. A ratiometric fluorescent probe for specific detection of cysteine over homocysteine and glutathione based on the drastic distinction in the kinetic profiles. *Chem Commun (Camb)* **2011**, *47* (22), 6275.

Chapter III: Deciphering the Mechanism of NIR Emitting hCRBPII/FR1V Based Photoswitchable Protein

Reversibly photoswitchable fluorescent probes are a class of fluorescent molecules that can transit between two different optical states when triggered by light.^{1,2} Because of the ability to switch, they become useful in live cell super-resolution microscopies (e.g., RESOLFT, psSIM, STORM, PALM), information storage and optical control of protein activity.³⁻⁷ This is largely because of the availability of several reversibly switchable fluorescent proteins (RSFPs) with

Figure 28. Proposed mechanism for the cis-trans isomerization of the chromophore in Dronpa. Bright and dark states correspond to the cis and trans forms of the chromophore, respectively. The two forms are determined by the pK_a difference in the acid-base equilibrium. In Dronpa, the cis form is anionic and bright.

broad range of emission. The switchability of these RSFPs arises from the photoinduced reaction of the chromophore inside the protein. Out of different RSFPs, Dronpa, which was engineered from Pectiniidae coral FP, has gained popularity and has led to important improvements in superresolution imaging.⁸ Dronpa can exist in two different states- an anionic form having absorption maximum at 503 nm and emission maximum at 513 nm (ON state) (**Figure**).^{8,9} The other form is neutral, absorbs at 390 nm, but does not show significant fluorescence (OFF state).

Several experimental and computational studies were performed to understand the mechanism of the photoswitching and to improve its optical properties. These studies revealed an ultrafast photoinduced *cis-trans* isomerization of the chromophore that is followed by a rapid ground-state proton transfer (GSPT).8 The structural reorganization of the chromophore and the amino acid residues inside the protein cavity is believed to be responsible for the difference in the pK_a of the two conformations. In the cis form, intramolecular charge transfer (ICT) from the electron donating alkoxide to the electron withdrawing amide group leads to fluorescence. But the ICT property of the chromophore weakens when the alkoxide is protonated in the trans form and the molecule becomes non-fluorescent. However, this stable neutral trans form can be converted to the unstable cis form with irradiation at 405 nm. Reversely, the neutral form can be brought back upon laser excitation at 488 nm. Reversible switching with high fatigue resistance and good onoff contrast ratio makes Dronpa one of best photoswitchable proteins. ¹⁰ Several mutants of Dronpa such as PDMI-4, Dronpa-2, Dronpa-3, rsFastLime and bsDronpa were later evolved with different photoswitching kinetics. 11,12 Padron, another mutant that displays baseline OFF state can be switched ON by light, opposite to the original Dronpa. ¹³ In recent years, Mut2Q, EYQ1, rsEGFP and mGeos were reported to exhibit different switching speed, maturation, stability and localization precision potential, serving as potential candidates to replace Dronpa in various biological applications. 14-16

Despite the availability of several RSFPs, there is a growing interest in developing novel RSFP that can emit in the far-red/NIR. These are of particular importance as the emission channel has lower signal from the cellular autofluorescence. ¹⁷⁻²⁴ In addition, longer wavelengths allow greater tissue penetrability and less damage to protein and DNA components of the cells. For example, to expand the spectral window of RSFPs several proteins such as cyan-emitting mTFP1

and red photoswitchable FPs rsCherry, rsCherryRev, rsTagRFP and mApple were generated after Dronpa. Our group has recently developed a synthetic photoswitchable fluorescent protein, named CrimFluors (**CF**), which emits in NIR region with emission maximum close to 700 nm.²⁵ No oxygen dependency, small size, fast labelling kinetics and rapid ON-OFF switching are hallmarks of **CF**, which makes it complementary to the naturally occurring Dronpa and its variants.

III.1 Preliminary work towards hCRBPII based photoswitchable proteins

Previous work from our research group has focused on the development of soluble, easily manipulated rhodopsin mimics derived from the reengineering of cellular retinoid binding proteins namely human cellular retinoic acid binding protein II (hCRABPII) and human cellular retinol binding protein II (hCRBPII).^{26,27} As described in previous studies by Nosrati *et al*, a number of

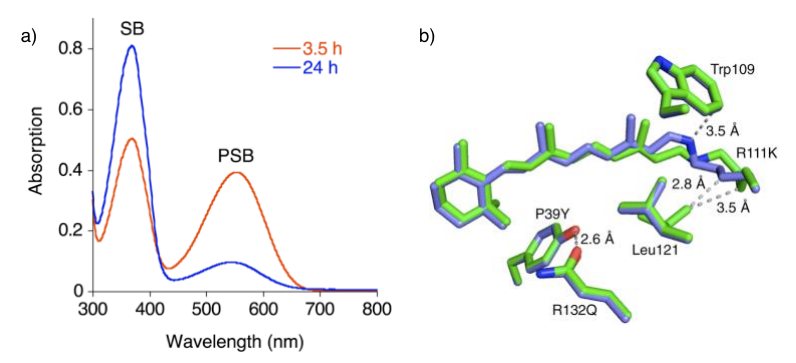


Figure 29. a) UV spectrum of hCRBPII/retinal after 3.5 h and 24 h of addition of retinal to the protein. b) Overlayed crystal structures of *cis*-PSB (blue) and *trans*-SB (green), revealing the difference that corelates the changes in the p K_a . The pictures were copied from reference ²⁶

hCRABPII variants exhibited changes in the protonation state of retinylidene bound protein, namely an initially observed pigmented protein-chromophore complex reverts to a colorless state in time (**Figure a**). 26 X-ray crystallography and UV vis spectroscopy disclosed imine bond isomerization from 15-*cis* to 15-*anti* is responsible for this change. The initial kinetically formed 15-*cis* isomer orients the imine nitrogen atom in a polar environment that supports a high p K_a regime, and thus yields a protonated Schiff base (PSB) that is a colored pigment. Time-dependent 15-*cis* to 15-*trans* imine isomerization yields a thermodynamic product that places the nitrogen

atom in a low pK_a regime, leading to the unprotonated Schiff base (SB) that is colorless. Additionally, green and UV light irradiation interconverts between the PSB and SB, respectively,

PSB,
$$\lambda_{max} > 440 \text{ nm}$$

high p K_a

N

N

R₁₁₁K

SB, $\lambda_{max} \sim 360 \text{ nm}$

W light $\sim 360 \text{ nm}$

PSB, $\lambda_{max} \sim 360 \text{ nm}$

PSB, $\lambda_{max} \sim 360 \text{ nm}$

PSB, $\lambda_{max} \sim 360 \text{ nm}$

SB, $\lambda_{max} \sim 360 \text{ nm}$

Figure 30. Thermodynamic and light-induced *cis*, *trans*-retinal iminium isomerization in hCRABPII protein.

in solution and crystalline states (**Figure**). The light driven isomerization and consequent formation of two optical states set a robust platform to design photoswitchable fluorescent protein. In fact, previous work by Dr. Wei Sheng showed this can be accomplished with a fluorescent dye (e.g., **FR1V**).²⁵ Additionally, using human cellular retinol binding protein II (hCRBPII) in place of hCRABPII, a synthetic photoswitchable protein was used for *in-vivo* fluorescence imaging.²⁵

III.1.1 FR1V, a NIR emitting fluorescent dye

FR1V, a fluorene based highly conjugated dye with emission maximum deep in the red region of spectrum.²⁵ FR0, a precursor of FR1V is reported as a fluorescent scaffold with its high quantum yield and relatively high extinction coefficient.^{28,29} It has a diethylamino group as a strong electron donor, and a formyl group as a strong electron acceptor, spaced by a 9,9-dimethylfluorenyl fragment. In the nomenclature of FR1V, "1V" is used to denote presence of a vinyl group which is installed between the aldehyde and the fluorenyl scaffold to extend the conjugation from FR0. To mimic the formation of SB and PSB in hCRBPII and study the optical properties, *n*-butylamine was used as a surrogate of the active lysine residue (Figure). The SB corresponding to FR1V can

FR1V-SB exhibits hypsochromic shifts in both absorption and emission compared to **FR1V** due to decreased electron withdrawing ability. In contrast, the absorption and emission maximum dramatically red-shifted upon protonation of the amine. In fact, the PSB is even more bathochromically shifted than the free aldehyde. As shown in **Figure 30**, the aldehyde, SB and PSB emits at maximum of 630, 510 and 709 nm, respectively. This sets the background for NIR fluorescence imaging by forming the PSB between hCRBPII and **FR1V**.

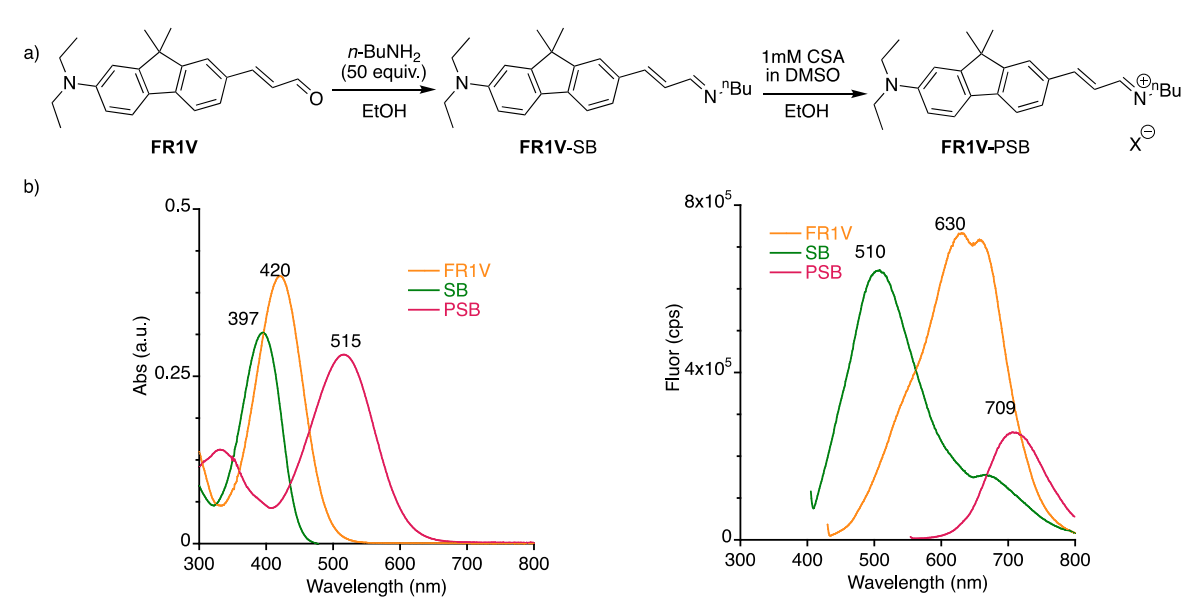


Figure 31. a) Synthesis of SB and PSB from **FR1V** using *n*-butylamine. b) Absorption and emission spectrum of **FR1V** aldehyde, SB and PSB in ethanol.

III.1.2 NIR emitting hCRBPII/FR1V fluorescent tag

As seen from the solution study, the emission spectra of SB and PSB are distinct. Thus, with the selection of a proper dichroic mirror in the microscope, SB can appear as fluorescence

OFF and PSB can appear as ON. Based on this idea, a suitable hCRBPII/FR1V complex was selected by site directed mutagenesis of the residues in the binding cavity of the protein. Previous

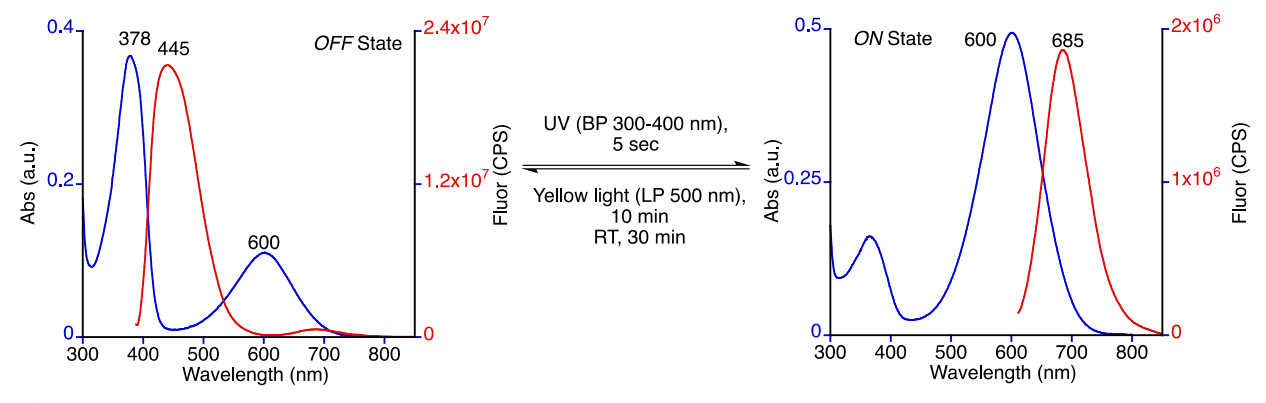


Figure 32. Absorption and emission spectra of the two photoswitching states of **psHex/FR1V** complex. OFF state: the colorless thermal equilibrated state after binding. ON state: the blue-colored state after UV irradiation. The equilibrium illustrates the reversible switching under different conditions.

experience of working with hCRBPII has shown the Q108K and K40L mutations are key for the formation of SB/PSB, with Lys108 as the anchor for covalent linkage. In addition to that, T51V, T53S/C, Y19W were seen to be critical for the photoswitching event of the complex. **psHex** (Q108K:K40L:T51V:T53S:Y19W:R58Y) is one such representative hCRBPII mutant which binds with **FR1V** to form two photoswitchable optical states- OFF ($\lambda_{abs/em} = 378/445$ nm) and ON state ($\lambda_{abs/em} = 600/685$ nm) (**Figure**). Similar to hCRABPII/retinal, a 5-second UV irradiation (using a ~ 365 nm handset or a Xenon lamp equipped with BP 300-400 nm band filter) can switch the thermal OFF state to a kinetic ON state. On the other hand, ON-to-OFF switching can be driven either by a thermal process (30 min at room temperature in dark) or a photochemical process (10 min irradiation with yellow light, LP 500 nm). The two states can be interconverted repeatedly by UV and yellow light irradiation with good fatigue resistance. This light-triggered OFF-to-ON

switchability enables spatiotemporal control of activation for the NIR fluorescence of imaging of the complex. In addition to **psHex**, the protein was further engineered to suppress the

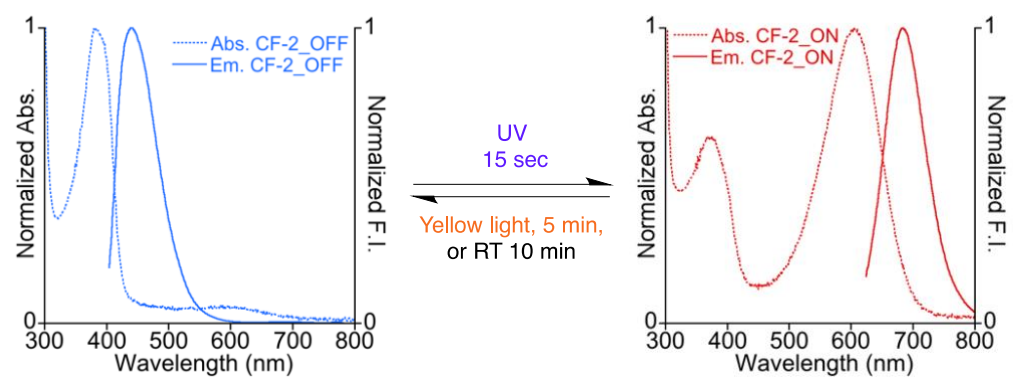


Figure 33. Absorption and emission spectra of the two photoswitching states of **psNona/FR1V**. The thermally equilibrated OFF state does not display any residual PSB unlike **psHex/FR1V**. The image is copied from reference. ²⁵

residual PSB in the resting state, as this could reduce the contrast between OFF and ON state (Figure). Incorporation of hydrophobic residues such as T29L, Q38L and Q128L serves this purpose, without sacrificing red-shifted absorption and emission maxima (Figure). Resulting mutant psNona (psHex- T29L:Q38L:Q128L) binds with FR1V with negligible PSB in the OFF state. In addition, psNona/FR1V displays 6-fold increase in the *in vitro* ON to OFF switching (Table). As photoswitching event to form PSB only happens inside the engineered protein, non-specifically bound fluorophore does not interfere with the image. This led to background free no wash cell imaging in the NIR.

Table 5. Optical properties of hCRBPII/**FR1V** variants

		OFF state		ON state		
Mutant		λ_{abs}	$\lambda_{\rm em}$	λabs	$\lambda_{\rm em}$	ON/OFF time
psHex	Q108K:K40L: T51V:T53S:	378	445	600	686	7.4
	Y19W:R58Y					
psNona	psHex: R58W:T29L: Q38L:Q128L	382	440	604	684	1.2

III.1.3 Structural study to understand the photoswitching mechanism (at pH 7.2)

The success of hCRBPII/FR1V as a synthetic photoswitchable protein inspired us to study the underlying mechanism in more detail. Note that for hCRBPII/FR1V, no structural evidence of the two optical states was achieved and a pathway like hCRABPII/retinal is proposed. This resulted from the numerous unfruitful attempts to crystalize psHex/FRIV and psNona/FR1V.²⁵ Hence, we searched for alternative hCRBPII variants which were readily crystallizable, giving well-ordered density for the fluorophore and exhibit photoswitching behavior in both solution and crystal. This would not only elucidate the switching pathway but may further help to improve the optical properties of photoswitchable states. Based on our experience on crystalizing several hCRBPII variants, we found the Q128L mutation (in **psNona**) to be problematic for both protein stability and crystallization. Additionally, Y19W was usually helpful in both crystallization and in stabilizing the conformation of the chromophore in the binding pocket. Further, we obtained a large number of high-resolution structures containing the T53C, Q38L and Q4A mutations. These observations led us to the M1variant (Q108K:K40L:T51V:T53C:Y19W:T29L:R58Y:Q38L:Q4A), which we successfully studied both in solution and in the crystalline state upon complexation with FR1V. As shown in Figure, UVvis spectra taken over a period of twelve hours after addition of FRIV to M1 show conversion of the free aldehyde (absorbing at 440 nm) to the SB (absorbing at 380 nm), indicating binding of the aldehyde to form a SB, with no evidence of PSB formation. Note that, in addition to a slower binding rate compared to psHex/psNona, the complex does not show any evidence of PSB formation during the initial binding. Irradiation of the resulting complex with UV light (BP300-400 nm) light results in a reduction of the SB absorbance with a concomitant increase in absorbance at 598 nm, consistent with absorbance of a protein bound PSB (Figure). However,

substantial SB absorption remains, even after irradiation for 2 full minutes, indicating either incomplete photoswitching or a PSB with a pK_a too low to be completely protonated at pH

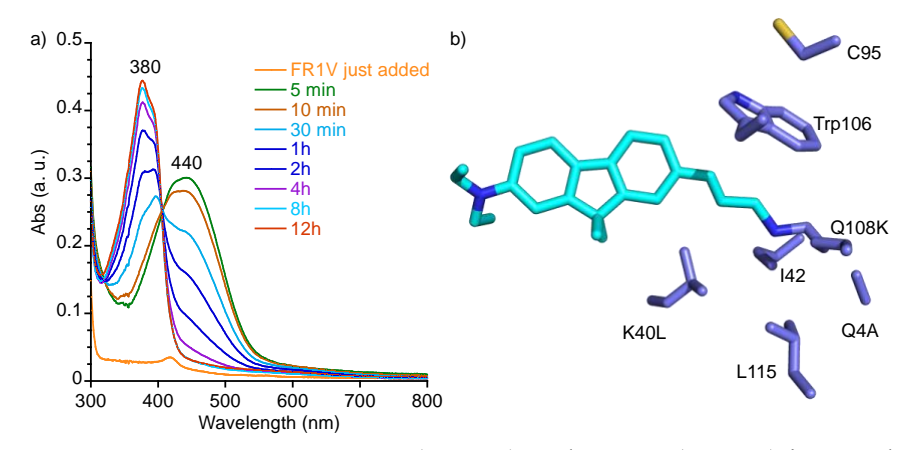


Figure 34. a) Time course of binding of **M1** (20 μ M) and **FR1V** (10 μ M) in PBS buffer (pH 7.2) over time, incubated at 25 °C. b) X-Ray crystal structure of **M1/FR1V** at pH 7.2 depicting the *trans*-imine, pointing towards hydrophobic residues.

of 7.2. Efforts to measure the pK_a of this SB were thwarted by the relatively rapid thermal loss of the PSB. Nonetheless, the data supports a photoswitching mechanism involving the conversion of the SB from a lower to higher pK_a environment, analogous to that seen for **psHex** and **psNona**. In collaboration with Ms. Courtney R. Bringham from Professor James H. Geiger's lab, we were successful to crystalize the mutant and study the crystal at pH 7.2. The colorless crystal of **M1/FR1V** shows a *trans*-SB isomer of the bound **FR1V** analogous to the thermodynamically stable retinal complex with hCRABPII. The imine in this isomer is surrounded by hydrophobic residues (K40L, L115, I42, Q4A) that lead to a suppressed pK_a , resulting in the formation of SB at physiological pH. With this structure in hand, efforts were made to photoirradiate the crystals with UV and subsequently freeze under liquid N₂ for further study using X-ray diffraction. As shown in **Figure a**, the UV-irradiated structure reveals a *cis* geometry with the imine projecting towards Trp106. The measured distance between the imine nitrogen atom and tryptophan is 3.5 Å, indicating a π -cation interaction. The biggest difference between the two structures before and after the UV irradiation is the movement of the chromophore as shown in **Figure b**. Note that for

hCRABPII/retinal, despite the change in the trajectory of R111K, no such chromophore movement was observed (**Figure b**). This large conformational change of chromophore can contribute to the incomplete photoswitching of **M1/FR1V**.

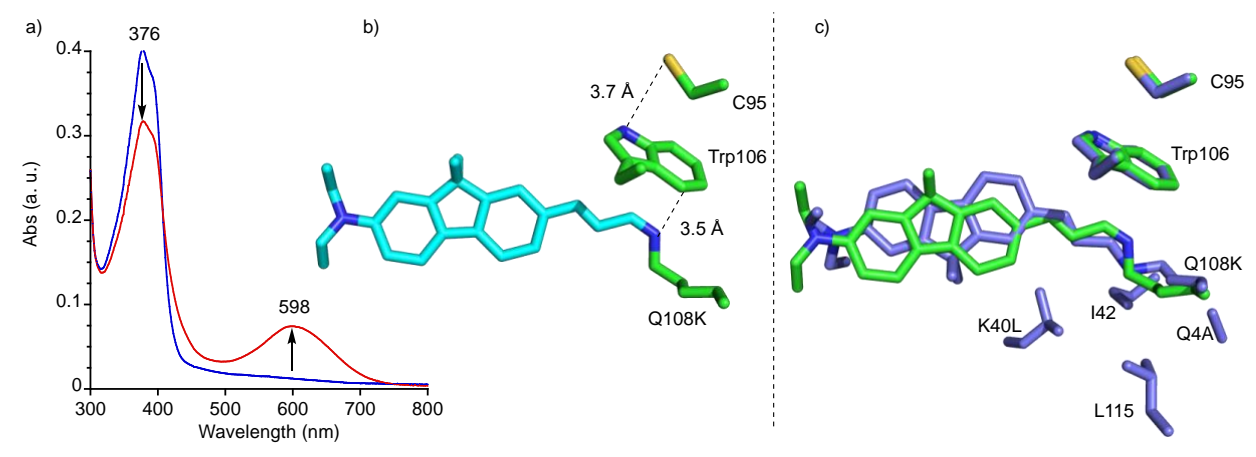


Figure 35. a) UV irradiation (BP300-400 nm) of **M1/FR1V**-SB results in the formation to PSB at pH 7.2; the conversion was incomplete even after irradiation of 2 mins b) X-Ray crystal structure UV-irradiated crystal, depicting a *cis* geometry of the imine, weekly stabilized by Trp106. c) the overlayed crystal structure before and after UV irradiation displays the isomerization process along with the flipping of the chromophore inside the hCRBPII binding pocket.

III.2 Discovery of a new optical state of M1/FR1V at pH 2.8 (PS³²⁵)

Structural analysis of M1/FR1V crystal shows a *trans*-SB is formed inside hydrophobic pocket of the protein. Next, we titrated this species in an effort to measure its pK_a but were met with a surprise in this experiment. Instead of the complete conversion of SB to a red-shifted PSB, absorbing at 598 nm, we instead witnessed the loss of the SB correlated with an increase in a *blue-shifted* absorbance at 325 and 345 nm (Figure). This state is labelled as PS³²⁵ for further discussion because of its maximum absorbance at 325 nm. This large blue shift of absorption is suggesting the loss of conjugation in the chromophore, possibly due to protonation of the electron donating amine unit. To understand this phenomenon, a parallel study with FR1V in organic solvent was performed where the compound was acidified to protonate the amine. As shown in Figure, the free aldehyde FR1V absorbs at 420 nm. Upon acidification the absorption is blue shifted by 95

nm presumably as a result of protonation of the amine, with maximum of absorption at 320 nm. The similarity of absorption of PS^{325} and protonated FR1V indicate the generation of an ammonium inside the protein.

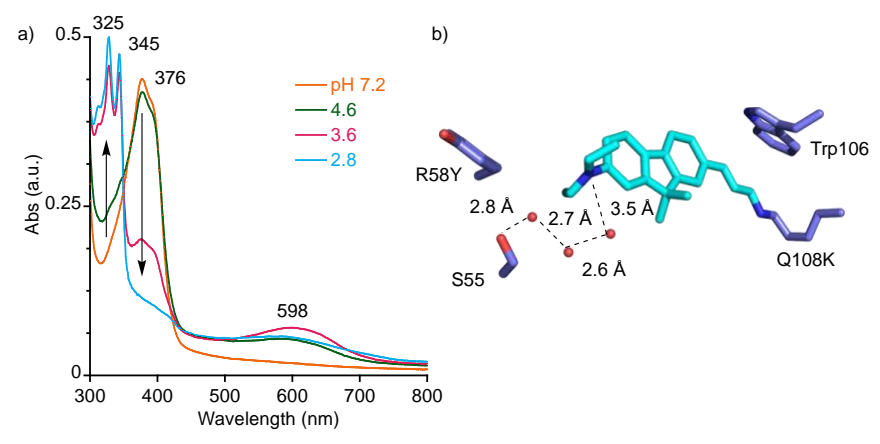


Figure 36. Titration of M1/FR1V-SB with gradual addition of acid leads to the formation of blue-shifted species PS³²⁵ without the formation of PSB. b) the X-Ray crystal structure of M1/FR1V at pH 3.0 indicates formation of an ammonium ion, stabilized by the hydrogen bonded network of three nearby water molecules.

The acidification data of M1/FR1V is surprising as the pK_a of PSB is expected to be higher than that of an ammonium, where the values for these groups in solution are typically around 8 and 5, respectively. To verify, FR1V-SB was acidified gradually in ethanol (Figure). As expected, it first leads to protonation of the imine, followed by the protonation of amine, evident from the absorption spectra. The absorption maximum of the protonated FR1V is approximately 50 nm blue-shifted as compared to that of the doubly protonated FR1V-SB. Although protonation of the amine leads to a hypsochromic shift in both compounds, the effect is less in case of FR1V-PSB due to presence of a stronger electron withdrawing group on the other end.

To understand the anomalous protonation of the fluorophore inside protein in comparison to the organic solvent, M1/FR1V was crystalized at pH 3.0. As expected, the crystals were colorless. The X-Ray diffraction data shows evidence for the ammonium that is embedded in a hydrophilic

cavity and hydrogen bonded with a Ser55 through a network of water molecules (**Figure**). The protonation is also possibly facilitated by the presence of a nearby hydrophilic tyrosine residue.

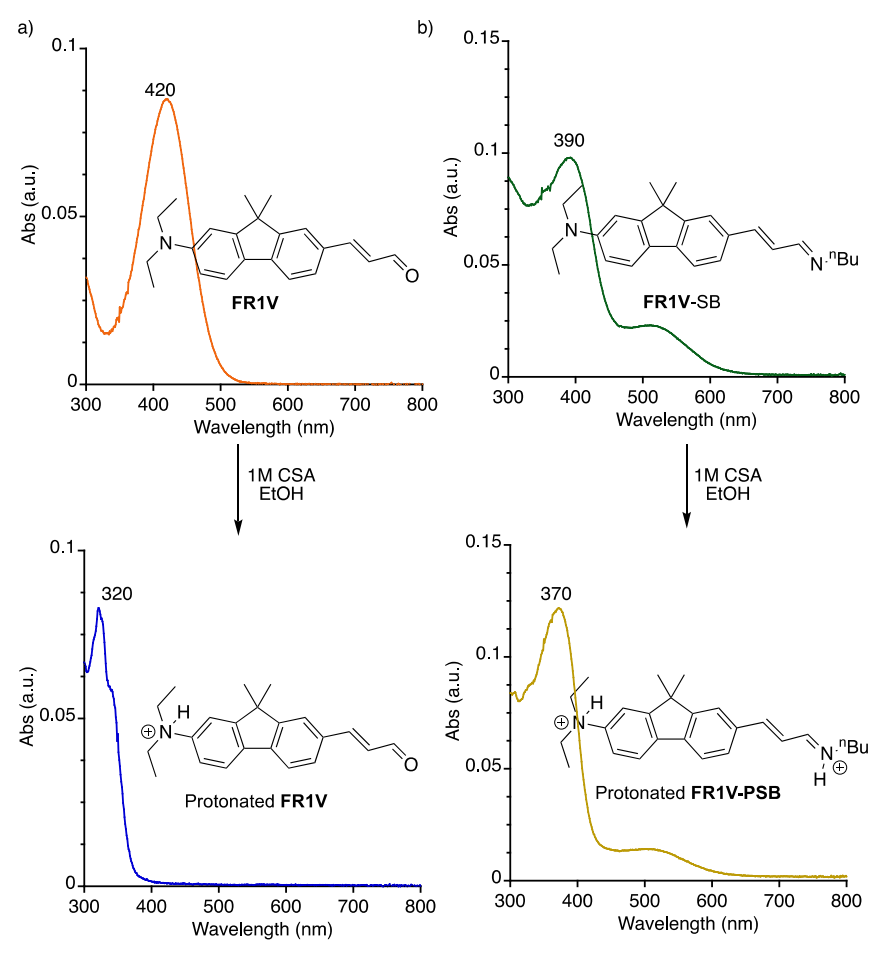


Figure 37. Monitoring the protonation of a) **FR1V** and b) **FR1V**-SB (with *n*-butylamine) by absorption spectra. The protonation was performed by gradual acidification of the respective compound in ethanol by addition of 1M camphor sulfonic acid (CSA).

Note that, no such evidence of protonation is observed when the **M1/FR1V** is crystalized at pH of 7.2. On the other hand, the SB as a *trans* isomer is surrounded by hydrophobic residues that does not favor protonation even at a lower pH. In addition to that, formation of ammonium and consequent strong electron withdrawing effect further disfavors the protonation of the imine.

III.2.1 Discovery of a new photoswitching pathway at pH 2.8

We next explored potential photoswitching of the system at lower pH. As shown in **Figure a**, irradiation of **PS**³²⁵ with UV light (BP 300-400 nm) results in a reduction of the 325 and 345

nm absorptions correlated with the appearance of an absorbance at 590 nm, consistent with the absorbance the **FR1V**-PSB. This seems to indicate a process where UV light irradiation propels a change in the pK_a of the diethylamine moiety, resulting in the loss of the proton. This solution result is supported by the aqua color of the photoirradiated crystals, consistent with PSB formation. The X-ray diffraction data of **PS**³²⁵ displays no movement of the chromophore or isomerization with the photoirradiation of the crystal. However, three critical water molecules, responsible for the hydrogen bonding with the ammonium ion disappeared. This further supports the loss of proton and consequent color change of the crystal during the photoirradiation. Despite the lack of movement of the chromophore, overlayed crystal before and after UV irradiation shows Leu38 has rotated away from the amine, possibly altering the environment. Additionally, a slight conformational change of R58Y was observed. The mechanism of this side chain movement is unclear, but one possibility is that the photoinduced motion of the chromophore induces the conformational change of the side chain. Upon absorption of photon, the excited chromophore can experience higher vibrational actively which increases the motion of the bonds. This increased movement can impact nearby amino acid residues, which can respond by rearrangement to a state that would allow the chromophore to escape the excitation by continuous irradiation. Presence of an aromatic amino acid residue, capable of absorbing the photon in the range (BP300-400), can potentially participate in the process, as well.

It is important to point out that the motion is only for the side chain, not the main chain. Nonetheless, the mechanism of photoactivation at pH 3.0 is distinct from the one at pH 7.2 despite the fact that both processes lead to **FR1V**-PSB as the end product. As the proton loss happens upon UV exposure, the ammonium ion can be considered as a photoacid. Similarly, the imine acts as a photoabse as it is protonated upon exposure to light. A fluorophore that is bound with hCRBPII

and can participate as a photoacid and a photobase simultaneously was previously observed from the study our group with another fluorophore. This phenomenon is referred as double excited state

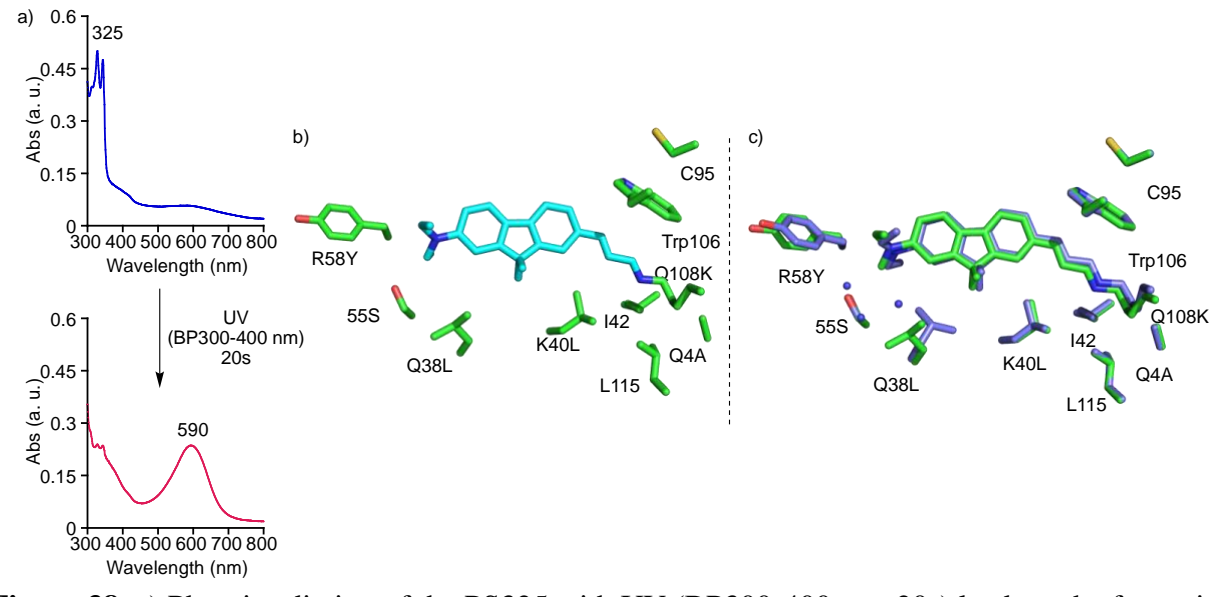


Figure 38. a) Photoirradiation of the PS325 with UV (BP300-400 nm, 20s) leads to the formation of PSB with absorption maximum at 590 nm. b) Structure of the UV-irradiated crystal does not display a hydrogen bonded network of water molecules, indicating loss of the proton from the ammonium ion. c) Overlayed crystal structure shows minimal change in the conformation of the chromophore before and after irradiation. However, residues such as Q38L and R58Y display conformational change.

proton transfer (double-ESPT). In **M1/FR1V** this results in a large change in the absorption spectra (>250 nm), hence it can be called as a photoactivable system. Several proteins (e.g. PAGFP, PAmcherry1, CFP, Dendra2, EosFP) and organic dyes (e.g., rhodamine, DMNB, DCDHF) are reported to exhibit photoactivation and are used for super- resolution imaging protocols such as STORM, STED and PALM. ^{10,30,31} Through a double ESPT, **M1/FR1V** represents a mechanically distinct photoactivable system.

III.2.2 Photoswitchability with both R58W and R58F

M1/FR1V complex provided proof-of-principle that through engineering the protein cavity, the pK_a of the chromophore can be influenced, resulting in a protonation state that is not obtainable with free chromophore in organic solvents. Next, we explored the role of the side chain

on the photoswitching of the chromophore at pH 3. We hypothesized, Tyr58 being close to the chromophore, can influence the pK_a of the ammonium. Hence, two mutants were prepared with other aromatic side chains. We have previously observed spectral property of the protein-bound chromophore can be greatly impacted by changes to Arg58 as it resides at the opening of the protein cavity. Large aromatic residues such as tryptophan can isolate the protein interior from the outside medium and influence the polarity of the protein cavity. As an example, absorption of hCRBPII/retinal was seen to red shift by 50 nm with incorporation of R58W.³² We hypothesized a similar spectral shift can also be obtained with hCRBPII/**FR1V**.

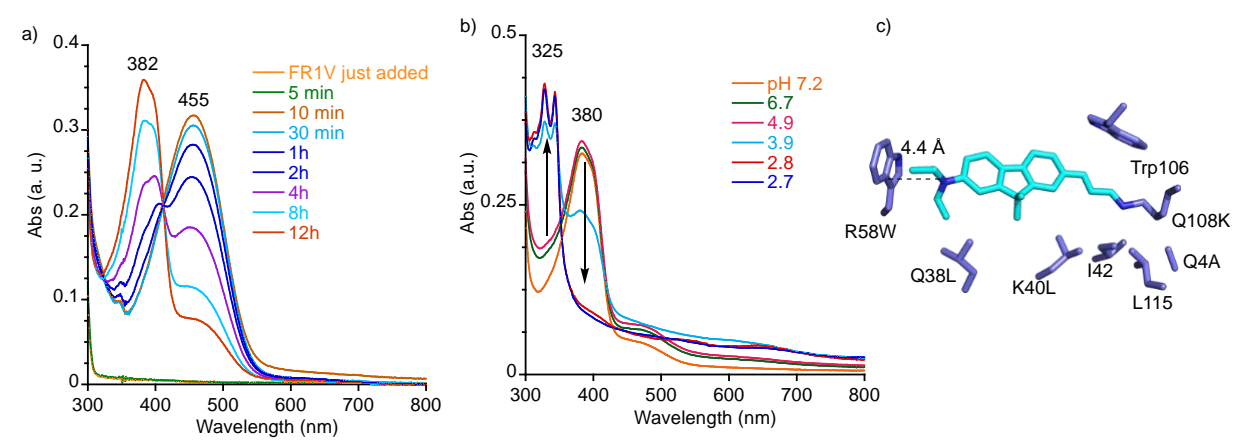


Figure 39. a) Time course study of the binding of **M2** (20 μ M) with **FR1V** (10 μ M), displaying the complex formation within 12h. b) Titration of **M2/FR1V**-SB also results in the formation of **PS**³²⁵ similar to **M1/FR1V** with blue-shifted absorption. c) X-ray crystal structure of the **M2/FR1V** at pH 3.0 display formation of ammonium which is stabilized by the nearby aromatic residue Trp58 through a cation- π interaction.

Mutant **M2** (Q108K:K40L: T51V:T53C: Y19W:T29L: R58W:Q38L:Q4A) with Trp58 binds with **FR1V** within 12 h, forming SB with absorption maximum at 380 nm (**Figure**). Similar to **M1/FR1V**, titration of the complex does not result in the formation of PSB, rather forms the **PS**³²⁵ which fully forms at pH 2.7. This shows that the Trp58 is equally effective towards selective protonation of amine. Photoirradiation of the solution leads to the formation of PSB with

absorption maximum at 630 nm. Note that the absorption maximum of **M2/FR1V**-PSB is 40 nm red-shifted than **M1/FR1V**-PSB, displaying the role of Trp58 protein environments.

With a red-shifted PSB, the photoirradiation results in a change of the absorption by 305 nm (**Figure a**). Further, **M2/FR1V-**PSB emits in NIR region of spectrum with emission maximum at 700 nm. Fluorescence spectra of **M2/FR1V**, before and after UV irradiation show a change in emission by 240 nm consistent with the switch in absorption, demonstrating the protein complex to be a photoswitchable fluorescent protein at pH 3.0 (**Figure b**).

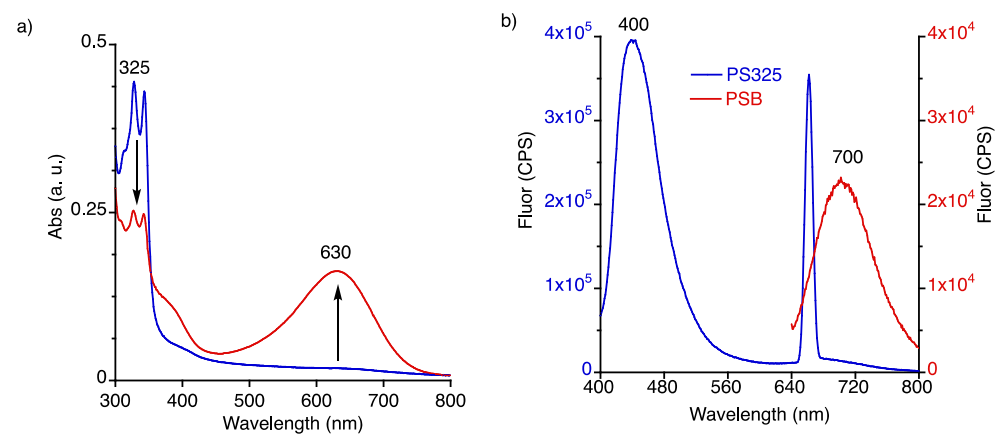


Figure 40. a) Photoirradiation of M2/FR1V-PS³²⁵ results in the formation of PSB similar to M1/FR1V. However, the PSB is red shifted compared to M1/FR1V, with maximum of absorption at 630 nm. b) Fluorescence spectra of PS³²⁵ and PSB, displaying the mega-shift of emission corresponding to the absorption spectra. The PSB emits at NIR region with maximum at 700 nm.

Overlay of M2/FR1V pre- and post-UV irradiated structures show a similar conformation of the chromophore, but with a conformational movement of Trp58 sidechain (Figure a). In both cases the chromophore is bound with the protein through a trans imine. The most significant difference is in the position of the tryptophan ring close to the diethylamine moiety of ligand, well positioned to make a cation- π interaction (consistent with an ammonium ion). In contrast, in the UV irradiated structure, the tryptophan ring is flipped away from the diethylamine, which breaks the cation- π interaction. This conformational change of Trp58 possibly involves coupling with the vibrational states of chromophore, brought on by photon absorption. The conclusion we draw from

these observations are that the cation- π interaction, fostered by the "flipped in" conformation of Trp58, leads to the UV absorbing **PS**³²⁵. UV light irradiation results in the "flipped out" conformation, which disfavor the ammonium ion and produces the visible light absorbing PSB. Unlike **M1/FR1V**, no water molecules capable of hydrogen bonding with the positively charged

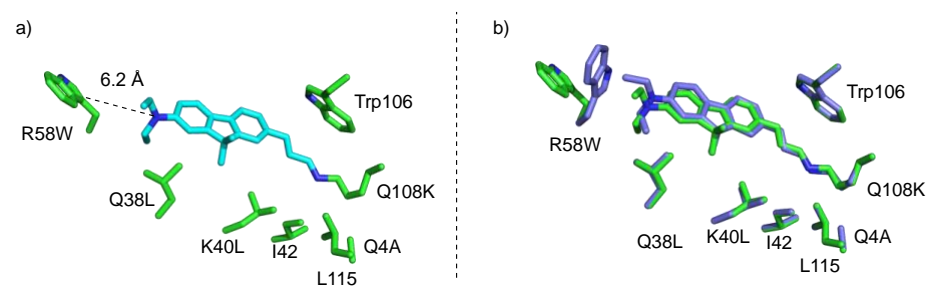


Figure 41. a) X-Ray of crystal structure of **M2/FR1V** at pH 3.0 after UV irradiation. The chromophore shows no conformational change and remain connected with the protein through a *trans*-imine bond. 6b) Overlayed crystal structure of **M2/FR1V** before and after UV highlights the movement of Trp58 side chain.

chromophore was observed. Further, photoswitching was observed with phenylalanine (R58F) in place of tryptophan. As shown in **Figure**, the observed **M3** (Q108K:K40L: T51V:T53C:Y19W:T29L:R58F:Q38L:Q4A) can similarly bind with **FR1V** to form **M3/FR1V**-SB, which on acidification results in **PS**³²⁵. In contrast to **M1** and **M2**, **M3/FR1V** forms a significant amount of PSB upon acidification. Nonetheless, UV excitation of **PS**³²⁵ results in the formation of more PSB, albeit with slight redshift. To this end, we were interested to see if photoswitching of **PS**³²⁵ to PSB at pH 3.0 is possible with a non-aromatic amino acid at position

58. Hence, **M4** (Q108K:K40L: T51V:T53C:Y19W:T29L:R58A:Q38L:Q4A) with R58A mutation was studied with **FR1V**. As shown in **Figure**, acidification of **M4/FR1V**-SB similarly

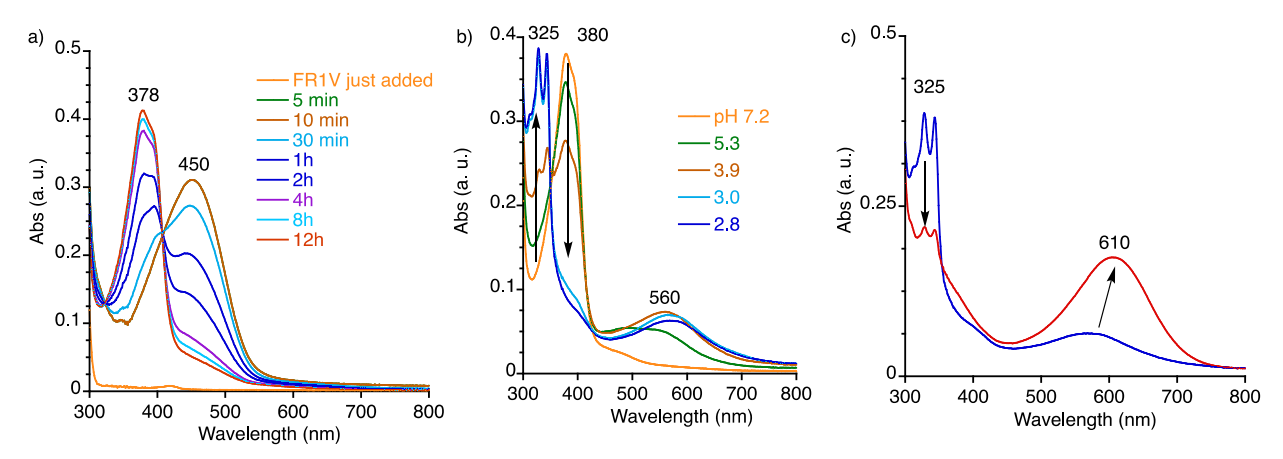


Figure 42. a) Time course study of the binding of M3 (20 μM) with FR1V (10 μM), displaying the complex formation within 12h. b) Titration of M3/FR1V-SB also results in the formation of PS^{325} similar to M1-M2/FR1V with blue-shifted absorption. c) Photoirradiation of M3/FR1V- PS^{325} results in the formation of PSB.

shows formation of \mathbf{PS}^{325} upon acidification to pH 3. However, unlike M1-M3, even with prolonged exposure to UV, the visible light absorbing PSB is not formed. This is interesting as it shows despite formation of \mathbf{PS}^{325} with both aromatic and non-aromatic residues, the

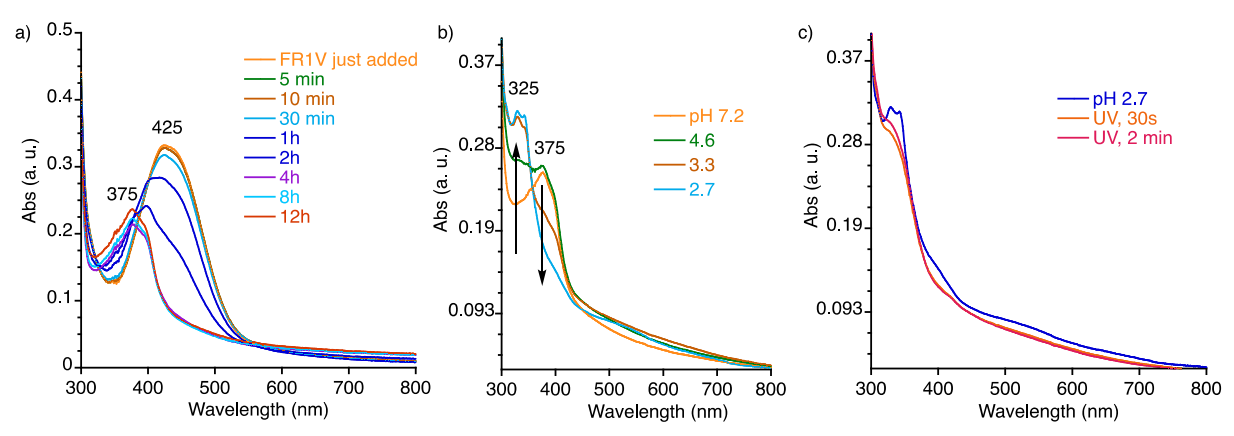


Figure 43. a) Time course study of the binding of M4 (20 μ M) with FR1V (10 μ M), displaying the complex formation within 12h. b) Titration of M4/FR1V-SB also results in the formation of PS³²⁵ similar to M1-M3/FR1V with blue-shifted absorption. c) Photoirradiation of solution does not result in the formation of any PSB unlike M1-M3.

photoswitching occurs only with the former. This supports our previous hypothesis that the photoinduced movement of the chromophore is associated with the motion of UV absorbing aromatic residues like tyrosine, tryptophan and phenyl alanine. This overall movement results in decreased stability of the ammonium compared to the unirradiated structure and loss of the proton to from the amine. The conformational movement of tyrosine and tryptophan residue in M1/FR1V and M2/FR1V supports this idea. It is of note, residues around the imine bond were kept same in all the hCRBPII mutants. This finely tuned hydrophobic environment only supports the protonation of the imine upon deprotonation of the ammonium with the UV irradiation.

III.2.3 Photoswitchable property of M2/FR1V

M2/FR1V, exhibiting the most red-shifted PSB of the series, was further studied to see if the photoactivable behavior at pH 3.0 is reversible. For this purpose, **PS**³²⁵ was irradiated with UV for 30 sec and the absorption was monitored over time. The absorption of the PSB drops in the

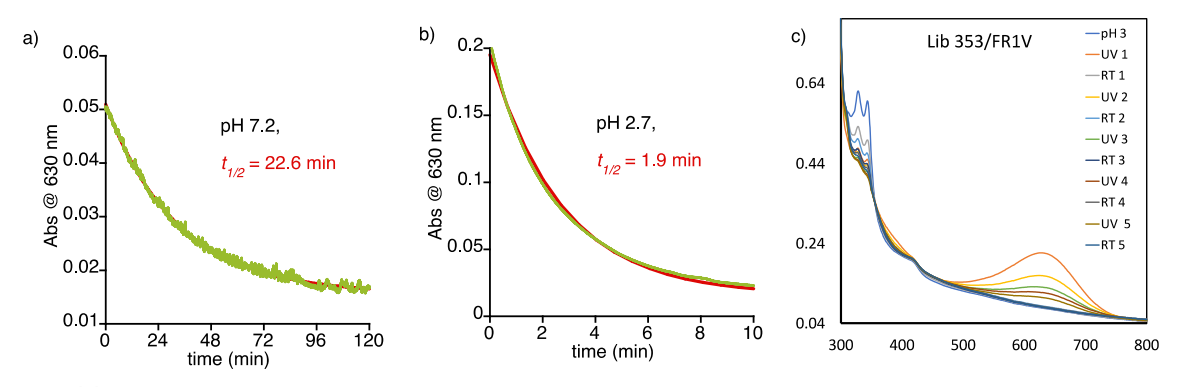


Figure 44. Decay of the M2/FR1V-PSB after initial UV irradiation at a) pH 7.2 and b) pH 2.7. The half-life ($t_{1/2}$), measured from fitting the decay curve is 22.6 and 1.9 min respectively. The variation in the $t_{1/2}$ also indicates difference the pathway of decay. c) Sequential UV irradiation change **PS**³²⁵ to PSB several times but with significant photobleaching.

dark within 10 min with a half-life of $(t_{1/2})$ of 1.9 min at room temperature. It is important to note that, PSB formed at pH 7.2 decays at a slower rate with $(t_{1/2})$ of 22.6 min. Although the end product is same at both pHs, the noticeably altered $t_{1/2}$ value at pH 2.7 potentially indicates a different

pathway of switching, correlating with previous data in solution and crystal. Nonetheless, photoswitching between the **PS**³²⁵ and PSB can be repeatedly performed with UV (BP 300-400 nm, 20 s) and dark (5 min). This result is interesting as it depicts the conformational change of Trp58 can be reversible. However, a rapid photodegradation of **PS**³²⁵ was observed with repeated UV irradiation. This likely results from the photobleaching of both the chromophore and the tryptophan residue. Nonetheless, with a large shift of the spectrum and unique pathway of photoswitching, **M2/FR1V** sets the stage for further study.

III.3 Conclusions and outlook

Herein we have described a system that exhibits two distinct photoswitching processes, one at neutral pH and one at acidic pH. We were able to elucidate the two distinct mechanisms involved in these processes by irradiating single crystals and observing, at atomic resolution, the photoswitching process. The neutral pH switch involves imine cis- to trans- isomerization, where the SB switches from a cation- π tryptophan interaction to an almost exclusively hydrophobic environment, similar to that seen in the rhodopsin family members and in our own rhodopsin mimics^{26,33-35}. In contrast, the low pH photoswitch mechanism does not involve a photoisomerization, conformational or even orientational change of the protein-imbedded chromophore. Instead, photoswitching is caused by interaction of the aromatic residue with the protonated diethylamine on the opposite end of the chromophore. Photoswitching is therefore caused exclusively by motions in the surrounding protein environment, not in the chromophore or fluorophore itself. This creates the opportunity to reimagine the design of photoswitchable systems that do not require any photoreaction by the fluorophore but can be designed purely by manipulation of the protein structure. Further, this shows how a photoactive system can be used to probe dynamic changes in a protein electrostatic environment, leading to large dynamic changes in the pK_a of groups imbedded in the protein environment. Indeed, it has been appreciated that protein environments are responsible for massive changes in the pK_a of important reactive moieties; we now see how relatively subtle changes in structure can make these large changes dynamic, possibly driving chemical reactivity inside protein binding cavities.

III.4 Experimental Section

III.4.1 Site-directed mutagenesis

All site directed mutagenesis were performed in the pET-17b vector containing hCRBPII-Q108K:K40L:T53A:R58L:Q38F:Q4F cloned between NdeI and Xhol.³⁶ Site directed mutagenesis was performed using polymerase chain reaction (PCR), with the following program (**Table 6**):

Table 6. PCR cycling conditions for site-directed mutagenesis

	PCR Program	Time (min)
1X	94 °C	3:00
	94 °C	0:20
20X	3 to 5 °C below T _m	0:55
	72 °C	3:30
1X	72 °C	10:00
1X	4 °C	5:00

Reactant	Volume		
DNA template	$70 \text{ ng } (x \mu L)$		
Forward primer	20 pmol (y μ L)		
Reverse Primer	$20 \text{ pmol} (z \mu L)$		
10 mM dNTP	1 μL		
50 mM MgCl ₂	1 μL		
DMSO	5 μL		
10X Cloned Pfu Reaction buffer	5 μL		
Pfu Turbo DNA polymerase	1 μL		
$(2.5U/\mu L)$			
Nuclease free water	(50-x-y-z-7) uL		

The primers used for the site directed mutagenesis were purchased from Integrated DNA Technology (IDT), with melting temperature (T_m) from 55 °C to 65 °C. The crude PCR product

was digested with 20 units of DpnI enzyme (New England Biolabs) for 1h at 37 °C. The digested product was then transformed into *E. coli* XL-1 Blue competent cells (Agilent) for 30 min on ice and then coated on LB-Amp/Tet agar plate. After incubation at 37 °C for 16 h, a single colony was cultured in LB media with antibiotics (100 μg/mL ampicillin and 12.5 μg/mL tetracycline) for 12 h. DNA purification was performed using Wizard Plus SV miniprep DNA purification system (Promega). The concentration of the isolated DNA was measured using Nanodrop® and sequenced at the Research Technology Support Facility at Michigan State University using a primer corresponding to the T7 promoter of the pET-17b plasmid.

M2 was used as template DNA for all mutation studies and the primers used where mutations are shown in bold.

R58A forward: 5'-CTAGCACATTCGCGAACTATGATGTG-3',

R58A reverse: 5'-CACATCATAGTTCGCGAATGTGCTAG-3',

R58F forward: 5'-CTAGCACATTCTTCAACTATGATGTG-3',

R58F reverse: 5'-CACATCATAGTTGAAGAATGTGCTAG-3',

R58Y forward: 5'-CTAGCACATTCTACAACTATGATGAG-3',

R58Y reverse: 5'-CTCATCATAGTTGTAGAATGTGCTAG-3'.

III.4.2 Protein expression and purification

hCRBPII mutants in pET-17b vector were expressed in *E. Coli* BL21(DE3)pLyS competent cells (Promega). The target gene (100 ng of DNA for 50 μL of cell solution) was added to the cells on ice for 30 min and spread over LB-Amp/Chl agar plate. The plate was incubated at 37 °C for approximately 12 h and a single colony was picked to grow in a 1 L terrific broth (TB) media supplemented with antibiotics (100 μg/mL ampicillin and 27 μg/mL chloramphenicol). The cells were cultured for 8-10 h at 37 °C until the optical density (OD) reached approximately 1.

Subsequently, isopropyl- β -D-thiogalactopyranoside (IPTG, Gold Biotechnology) was added to the culture at a final concentration of 1.0 mM and shaken at 37 °C for additional 16-20 h. The cells were then harvested by centrifugation (3000 rpm, 15 min, 4 °C), resuspended in Tris buffer (10 mM Tris, pH 7.8-8, 50 mL), lysed with ultrasonic homogenizer (Biologics, Inc, power 60%, 3 min), added with 500U of DNase I (recombinant, Roche Diagnostics) and kept at RT for 10 min. The solution was then centrifuged (3000 rpm, 40 min, 4 °C) to separate the pellet. The supernatant was loaded onto a FastQ anion exchange column (resin from GE Healthcare), equilibrated with Tris buffer (10 mM Tris, pH 7.8-8). The resin was subsequently washed with Tris buffer (2X50 mL) and eluted with Tris-elution buffer (10 mM Tris, 200 mM NaCl, pH 7.8-8.0, 50 mL). The eluent was desalted using Amicon® Ultra-15 Centrifugal Filter Units (MW cut-off: 10K), and further purified with a FPLC (NGC chromatography system, Biorad), equipped with a Source 15Q column (Q Sepharose Fast Flow, GE Healthcare) anion exchange resin using 50 mM Tris·HCl (solution A) and 2 M NaCl (solution B) at pH 8.1. All protein samples were collected with 4% of solution B and concentrated using Amicon Ultracentrifugation filter (MW cut-off: 10K) to a final volume of 1 mL. The sample (1 mL) was then loaded to size exclusion chromatography (Superdex 120 16/600 GL column, GE Healthcare) for further purification using a buffer containing solution A and 20% of solution B. Collected protein sample was concentrated (conc. 100-200 µM) and stored at 4 °C for optical studies.

III.4.3 Determination of extinction coefficient of protein

UV-vis spectra were measured with a Cary 300 Bio WinUV, Varian spectrophotometer using 1 cm, 1.0 mL quartz microcuvettes (Starna Cells). The extinction coefficients of the hCRBPII mutants were measured following the method described by Gill and von Hippel.³⁷ The theoretical extinction coefficient (ε_{theo}) is calculated using following equation:

$$\varepsilon_{theo} = \mathbf{a} \times \varepsilon_{Trp} + \mathbf{b} \times \varepsilon_{Tyr} + \mathbf{c} \times \varepsilon_{cys}$$

where a, b and c are the number of tryptophan, tyrosine, and cysteine residues in the protein, respectively. ε used for tryptophan, tyrosine, and cysteine are 5690 M⁻¹cm⁻¹, 1280 M⁻¹cm⁻¹ and 120 M⁻¹cm⁻¹, respectively. The absorbance of each protein was measured at 280 nm in 2XPBS and 6M guanidine hydrochloride solution. The absorbance value was used to calculate the experimental ε using the following equation:

$$\varepsilon_{exp} = rac{A_{native}}{A_{denaturating}} imes \varepsilon_{theo}$$

Table 7. The values of the extinction coefficients

Mutants	Proteins	$\varepsilon_{\rm exp}({ m M}^{\text{-1}}{ m cm}^{\text{-1}})$
M1	Q108K:K40L: T51V:T53C: Y19W:T29L: R58Y:Q38L:Q4A	35,780
M2	Q108K:K40L:T51V:T53C:Y19W:T29L: R58W:Q38L:Q4A	36,220
M3	Q108K:K40L: T51V:T53C: Y19W:T29L: R58F:Q38L:Q4A	34,680
M4	Q108K:K40L: T51V:T53C: Y19W:T29L: R58A:Q38L:Q4A	34,500

III.4.4 UV/Vis study of M1-M4/FR1V:

hCRBPII mutant was incubated with **FR1V** in PBS buffer (pH 7.2) with final concentration of protein 20 μM and 0.5 equivalent of chromophore. The binding was monitored using UV-vis spectroscopy at 23 °C. The pH of the solution was verified each time after the addition of components and spectra was recorded immediately after the addition of chromophore. For *in vitro* photoconversion study, samples in PBS were illuminated with an Hg(Xe) Arc lamp (Oriel® Instruments) attenuated with one neutral density filter (Edmund Optics Inc.) Illumination using UV 300-400 nm bandpass filter leads to conversion of **PS**³²⁵ protonated species to PSB within a timescale of 20 s.

III.4.5 Acidification of the complex and determination of pK_a

The solution containing the hCRBPII mutant and **FR1V** was left to bind until the chromophore is fully bound. SB and PSB peaks were assigned based on the wavelength of the absorption. Next the solution was acidified from pH 7.3 to pH 2.7 by gradual addition of citric acid (1 M). Absorption spectra of the solution was collected at different pHs and continued until the absorption for SB completely disappears leading to the gradual formation of **PS**³²⁵ or formation of PSB followed by **PS**³²⁵. Absorption maxima of the double protonated species was plotted as a function of pH. The scatter plot was fitted to a sigmoidal curve to determine the p K_a using equation

$$A = \frac{A_0}{1 + 10^{pH - pK_a}} + \text{constant}$$

where A_0 is the absorbance of the maximum PS^{325} and the pK_a is the mid-point of the titration. A constant is included for the zero absorbance of the deprotonated PSB.

REFERENCES

- (1) Hell, S. W.; Sahl, S. J.; Bates, M.; Zhuang, X.; Heintzmann, R.; Booth, M. J.; Bewersdorf, J.; Shtengel, G.; Hess, H.; Tinnefeld, P.et al. The 2015 super-resolution microscopy roadmap. *J. Phys. D: Appl. Phys.* **2015**, *48* (44), 443001.
- (2) Shcherbakova, D. M.; Sengupta, P.; Lippincott-Schwartz, J.; Verkhusha, V. V. Photocontrollable fluorescent proteins for superresolution imaging. *Annu. Rev. Biophys.* **2014**, *43* (1), 303.
- (3) Hell, S. W.; Wichmann, J. Breaking the diffraction resolution limit by stimulated emission: stimulated-emission-depletion fluorescence microscopy. *Opt. Lett.* **1994,** *19* (11), 780.
- (4) Gustafsson, M. G. Nonlinear structured-illumination microscopy: wide-field fluorescence imaging with theoretically unlimited resolution. *Proc. Natl. Acad. Sci. U. S. A.* **2005,** *102* (37), 13081.
- (5) Rust, M. J.; Bates, M.; Zhuang, X. Sub-diffraction-limit imaging by stochastic optical reconstruction microscopy (STORM). *Nat. Methods* **2006**, *3* (10), 793.
- (6) Betzig, E.; Patterson, G. H.; Sougrat, R.; Lindwasser, O. W.; Olenych, S.; Bonifacino, J. S.; Davidson, M. W.; Lippincott-Schwartz, J.; Hess, H. F. Imaging Intracellular Fluorescent Proteins at Nanometer Resolution. *Science* **2006**, *313* (5793), 1642.
- (7) Hess, S. T.; Girirajan, T. P.; Mason, M. D. Ultra-high resolution imaging by fluorescence photoactivation localization microscopy. *Biophys. J.* **2006**, *91* (11), 4258.
- (8) Acharya, A.; Bogdanov, A. M.; Grigorenko, B. L.; Bravaya, K. B.; Nemukhin, A. V.; Lukyanov, K. A.; Krylov, A. I. Photoinduced Chemistry in Fluorescent Proteins: Curse or Blessing? *Chem. Rev.* **2017**, *117* (2), 758.
- (9) Zhou, X. X.; Lin, M. Z. Photoswitchable fluorescent proteins: ten years of colorful chemistry and exciting applications. *Curr. Opin. Chem. Biol.* **2013**, *17* (4), 682.
- (10) Lippincott-Schwartz, J.; Patterson, G. H. Photoactivatable fluorescent proteins for diffraction-limited and super-resolution imaging. *Trends Cell Biol.* **2009**, *19* (11), 555.
- (11) Ando, R.; Flors, C.; Mizuno, H.; Hofkens, J.; Miyawaki, A. Highlighted generation of fluorescence signals using simultaneous two-color irradiation on Dronpa mutants. *Biophys. J.* **2007**, *92* (12), L97.
- (12) Stiel, A. C.; Trowitzsch, S.; Weber, G.; Andresen, M.; Eggeling, C.; Hell, S. W.; Jakobs, S.; Wahl, M. C. 1.8 A bright-state structure of the reversibly switchable fluorescent protein Dronpa guides the generation of fast switching variants. *Biochem. J* **2007**, *402* (1), 35.
- (13) Andresen, M.; Stiel, A. C.; Fölling, J.; Wenzel, D.; Schönle, A.; Egner, A.; Eggeling, C.; Hell, S. W.; Jakobs, S. Photoswitchable fluorescent proteins enable monochromatic

- multilabel imaging and dual color fluorescence nanoscopy. *Nat. Biotechnol.* **2008**, *26* (9), 1035.
- (14) Bizzarri, R.; Serresi, M.; Cardarelli, F.; Abbruzzetti, S.; Campanini, B.; Viappiani, C.; Beltram, F. Single amino acid replacement makes Aequorea victoria fluorescent proteins reversibly photoswitchable. *J. Am. Chem. Soc.* **2010**, *132* (1), 85.
- (15) Grotjohann, T.; Testa, I.; Leutenegger, M.; Bock, H.; Urban, N. T.; Lavoie-Cardinal, F.; Willig, K. I.; Eggeling, C.; Jakobs, S.; Hell, S. W. Diffraction-unlimited all-optical imaging and writing with a photochromic GFP. *Nature* **2011**, *478* (7368), 204.
- (16) Chang, H.; Zhang, M.; Ji, W.; Chen, J.; Zhang, Y.; Liu, B.; Lu, J.; Zhang, J.; Xu, P.; Xu, T. A unique series of reversibly switchable fluorescent proteins with beneficial properties for various applications. *Proc. Natl. Acad. Sci. U. S. A.* **2012**, *109* (12), 4455.
- (17) Subach, F. V.; Verkhusha, V. V. Chromophore transformations in red fluorescent proteins. *Chem. Rev.* **2012**, *112* (7), 4308.
- (18) Shaner, N. C.; Campbell, R. E.; Steinbach, P. A.; Giepmans, B. N.; Palmer, A. E.; Tsien, R. Y. Improved monomeric red, orange and yellow fluorescent proteins derived from Discosoma sp. red fluorescent protein. *Nat. Biotechnol.* **2004**, 22 (12), 1567.
- (19) Piatkevich, K. D.; Efremenko, E. N.; Verkhusha, V. V.; Varfolomeev, S. D. Red fluorescent proteins and their properties. *Russian Chem. Rev.* **2010**, *79* (3), 243.
- (20) Shcherbakova, D. M.; Subach, O. M.; Verkhusha, V. V. Red fluorescent proteins: advanced imaging applications and future design. *Angew. Chem. Int. Ed. Engl.* **2012**, *51* (43), 10724.
- (21) Piatkevich, K. D.; Verkhusha, V. V. Advances in engineering of fluorescent proteins and photoactivatable proteins with red emission. *Curr. Opin. Chem. Biol.* **2010**, *14* (1), 23.
- (22) Campbell, R. E.; Tour, O.; Palmer, A. E.; Steinbach, P. A.; Baird, G. S.; Zacharias, D. A.; Tsien, R. Y. A monomeric red fluorescent protein. *Proc. Natl. Acad. Sci. U. S. A.* **2002**, *99* (12), 7877.
- (23) Subach, F. V.; Piatkevich, K. D.; Verkhusha, V. V. Directed molecular evolution to design advanced red fluorescent proteins. *Nat. Methods* **2011**, *8* (12), 1019.
- (24) Shcherbakova, D. M.; Baloban, M.; Emelyanov, A. V.; Brenowitz, M.; Guo, P.; Verkhusha, V. V. Bright monomeric near-infrared fluorescent proteins as tags and biosensors for multiscale imaging. *Nat. Commun.* **2016,** 7 (1), 12405.
- (25) Sheng, W.; Nick, S. T.; Santos, E. M.; Ding, X.; Zhang, J.; Vasileiou, C.; Geiger, J. H.; Borhan, B. A Near-Infrared Photoswitchable Protein-Fluorophore Tag for No-Wash Live Cell Imaging. *Angew. Chem. Int. Ed. Engl.* **2018**, *57* (49), 16083.

- (26) Nosrati, M.; Berbasova, T.; Vasileiou, C.; Borhan, B.; Geiger, J. H. A Photoisomerizing Rhodopsin Mimic Observed at Atomic Resolution. *J. Am. Chem. Soc.* **2016**, *138* (28), 8802.
- (27) Berbasova, T.; Santos, E. M.; Nosrati, M.; Vasileiou, C.; Geiger, J. H.; Borhan, B. Light-Activated Reversible Imine Isomerization: Towards a Photochromic Protein Switch. *Chembiochem* **2016**, *17* (5), 407.
- (28) Kucherak, O. A.; Didier, P.; Mély, Y.; Klymchenko, A. S. Fluorene Analogues of Prodan with Superior Fluorescence Brightness and Solvatochromism. *J. Phy. Chem. Lett.* **2010,** *1* (3), 616.
- (29) Shaya, J.; Fontaine-Vive, F.; Michel, B. Y.; Burger, A. Rational Design of Push-Pull Fluorene Dyes: Synthesis and Structure-Photophysics Relationship. *Chemistry* **2016**, 22 (30), 10627.
- (30) Wang, S.; Moffitt, J. R.; Dempsey, G. T.; Xie, X. S.; Zhuang, X. Characterization and development of photoactivatable fluorescent proteins for single-molecule-based superresolution imaging. *Proc. Natl. Acad. Sci. U. S. A.* **2014**, *111* (23), 8452.
- (31) Li, H.; Vaughan, J. C. Switchable Fluorophores for Single-Molecule Localization Microscopy. *Chem. Rev.* **2018**, *118* (18), 9412.
- (32) Wang, W.; Nossoni, Z.; Berbasova, T.; Watson, C. T.; Yapici, I.; Lee, K. S.; Vasileiou, C.; Geiger, J. H.; Borhan, B. Tuning the electronic absorption of protein-embedded all-transretinal. *Science* **2012**, *338* (6112), 1340.
- (33) Sheves, M.; Albeck, A.; Friedman, N.; Ottolenghi, M. Controlling the pKa of the bacteriorhodopsin Schiff base by use of artificial retinal analogues. *Proc. Natl. Acad. Sci. U. S. A.* **1986**, *83* (10), 3262.
- (34) Ghanbarpour, A.; Nairat, M.; Nosrati, M.; Santos, E. M.; Vasileiou, C.; Dantus, M.; Borhan, B.; Geiger, J. H. Mimicking Microbial Rhodopsin Isomerization in a Single Crystal. *J. Am. Chem. Soc.* **2019**, *141* (4), 1735.
- (35) Ghanbarpour, A.; Pinger, C.; Esmatpour Salmani, R.; Assar, Z.; Santos, E. M.; Nosrati, M.; Pawlowski, K.; Spence, D.; Vasileiou, C.; Jin, X.et al. Engineering the hCRBPII Domain-Swapped Dimer into a New Class of Protein Switches. *J. Am. Chem. Soc.* **2019**, *141* (43), 17125.
- (36) Santos, E. M.; Sheng, W.; Esmatpour Salmani, R.; Tahmasebi Nick, S.; Ghanbarpour, A.; Gholami, H.; Vasileiou, C.; Geiger, J. H.; Borhan, B. Design of Large Stokes Shift Fluorescent Proteins Based on Excited State Proton Transfer of an Engineered Photobase. *J. Am. Chem. Soc.* **2021**, *143* (37), 15091.

(37)	Gill, S. C.; von Hippel, P. H. Calculation of protein extinction coefficients from amino acid sequence data. <i>Anal. Biochem.</i> 1989, <i>182</i> (2), 319.

Chapter IV: Rational Design of Fluorene Dyes: Synthesis and Structure-Photophysical Relationship

New fluorescent dyes are of high demand because of their application in several areas including biomolecular labeling and as environmental indicators ¹⁻⁵ Among them, many are donoracceptor (D-A) dyes, which can be identified by the presence of an electron-donating and electronwithdrawing group (EDG and EWG) at two ends of the molecules, connected with a conjugated backbone.^{6,7} Under photoexcitation, this system undergoes intramolecular charge transfer (ICT), making them highly colored.⁸ Among different D-A dyes, environmentally sensitive dyes are of special interest as they exhibit strong change in the dipole moment upon electronic excitation. As the energy of the excited state can vary depending on the polarity of the medium, their emission properties are largely dependent on the solvent used. Due to this sensitivity towards the polarity, they are also referred as solvatochromic dyes. 9,10 Example of such dyes include dansyl derivatives, Prodan, Anthradan, Dapoxyl, dimethylaminophthalimide (DMAP), NileRed, and fluorene based dyes. 11 Due to their sensitivity to the local environment, these dyes have found a number of applications for monitoring protein and DNA interactions and probing biophysical properties of biomembranes. 12-15 A successful fluorescent probe for such applications should exhibit high extinction coefficient and fluorescence quantum yield (QY). The product of these two determines the absolute brightness, high value of which is the overarching goal for a fluorescent probe. However, many of the dyes mentioned above are limited, often because of low fluorescence quantum yield in polar solvents. Along the charge transfer coordinate, the larger momentum change is usually correlated to a longer timescale that may allow for more non-radiative decay pathways to occur and lead to lower QYs. Hence, rational molecular engineering of fluorophores,

based on understanding the working mechanism is crucial to yield novel fluorophores with superior brightness.

IV.1 Current approaches to minimize the non-radiating decay pathways

In recent years, a great deal of effort has led to the development of more effective fluorophores with improved fluorescence QY for application in biological research and photocatalysis. ¹⁶ Previous studies have indicated that the mechanism that governs non-radiative decay and affects the QY of dyes include formation of twisted intramolecular charge transfer (TICT) state, internal conversion to lower energy non-emissive exited state, aggregation, intermolecular hydrogen bonding, and heat loss to the solvent upon intramolecular charge

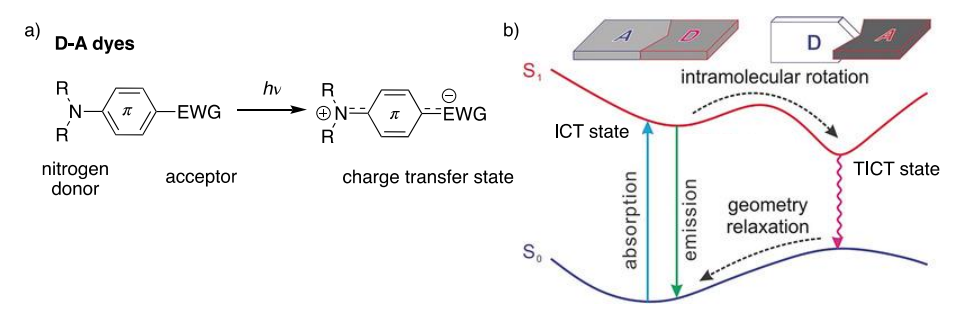


Figure 45. a) Formation of charge transfer state in donor (D) acceptor (A) dyes b) intramolecular rotation of the single bond can form a lower energy twisted intramolecular charge transfer state (TICT). Formation of such TICT can result rapid non-radiative decay. Image is copied from reference¹⁷

transfer. ¹⁸⁻²⁰ Assuming, the donor and acceptor moieties are in the same plane in the ground state, excitation could result in an intramolecular charge transfer from the donor to acceptor. Subsequent relaxation in the excited state is achieved by rotation around the single bond connecting the donor and acceptor, yielding a perpendicular conformation, known as TICT state (**Figure**). Previous studies indicated presence of TICT state in the Rhodamine dyes can significantly increase the non-radiative decay, causing the decrease in QY. ^{21,22} It is also suggested the reactivity of the TICT state is significantly high, increasing photodegradability. ¹⁶ A strongly polar medium like water can

stabilize the charge separated TICT state. Dyes often have higher propensity to form the TICT state in aqueous solution, thereby resulting in moderate to low QY. Hence, a significant effort was

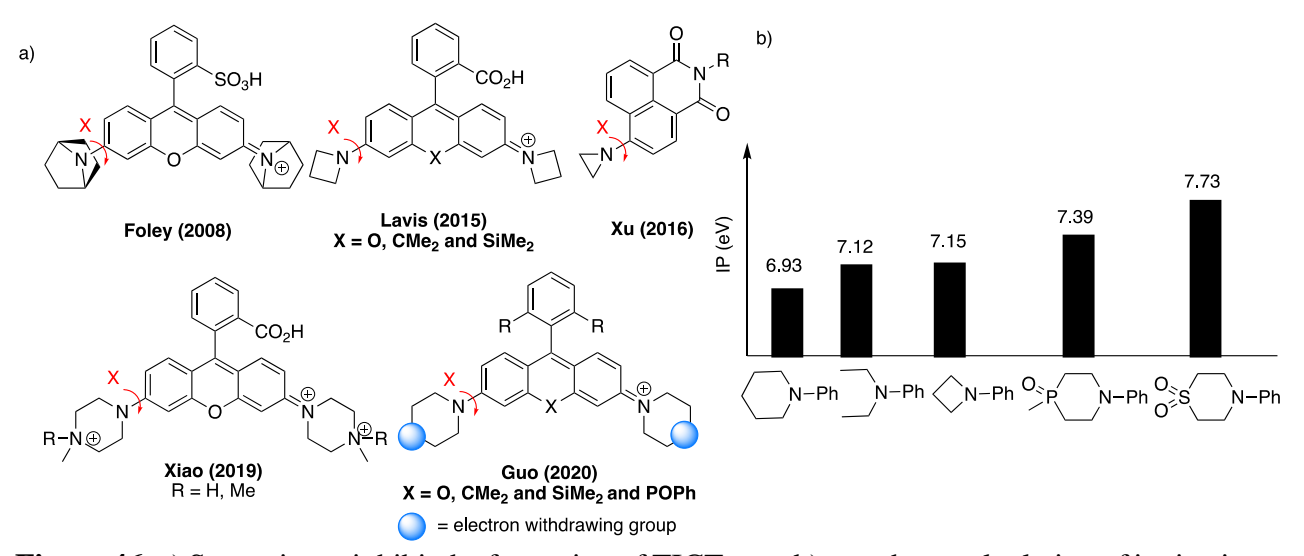


Figure 46. a) Strategies to inhibit the formation of TICT state b) gas phase calculation of ionization potential (IP) of different donor groups. Values in Figure b is adapted from ref .²³

focused on modifications of the structure of existing dyes to reduce the possibility of TICT state.

Table highlights some of the structural engineering of well-known rhodamine, fluorescein and coumarin based fluorescent dyes. One of the early methods to inhibit TICT includes rigidification of the dialkylamino donor by forming a ring structure.²⁴ As shown in

Table, compound **1b** with cyclic amine donor displays an enhanced QY compared to linear counterpart **1a**. the More recently, Foley *et al.* demonstrates incorporation of 7-azabicyclo[2.2.1]heptane enhances the QY of rhodamine based compounds (**Figure**). Alternatively Lavis and co-workers showed replacement of N,N-dimethylamino substituent with an azetidine ring is effective in suppressing the TICT (**Figure** and **Table 8**, entry **1c-1k**). Later, Xu and co-workers disclosed similar effect can also be achieved with substitution of aziridine. It was further realized that the basic principle to prevent the formation of TICT state is improving the ionization potential IP) of the amino auxochrome. With a geometrically constrained azacyclic substituents (e.g. 7- azabicyclo[2.2.1]heptane, azetidine, and aziridine), rise in the IP results from

the increase in the *s*- character of the nitrogen lone pair.²³ Using this principle, a number of recent studies were focused

Table 8. Reported structural modification of dyes and comparison of QY with parent compounds in ethanol and water.

Entry	Structure	Solvents	λ _{abs} (nm)	λ _{em} (nm)	ε (M ⁻¹ cm ⁻¹)	Φ
1a ²⁴	$\begin{array}{c} \\ \\ \\ \\ \\ \\ \\ \\ \\ \\ \\ \\ \\ \\ \\ \\ \\ \\ \\$	EtOH	543	563	111,000	0.70
1b	$\begin{array}{c} \\ \\ \\ \\ \\ \\ \\ \\ \\ \\ \\ \\ \\ \\ \\ \\ \\ \\ \\$	EtOH	568	590	95,000	0.98
1c ²⁵ 1d	$R_{2}N = N_{5}s^{5}$ $CO_{2}H \qquad R_{2}N = N_{5}s^{5}$	H ₂ O	518 519	546 546	60,000 59,000	0.21 0.85
1e 1f	$\begin{array}{cccccccccccccccccccccccccccccccccccc$	H ₂ O	606 608	626 631	121,000 99,000	0.52 0.67
1j 1k	$R_{2}N \longrightarrow O \qquad O \qquad R_{2}N = N \qquad N_{3}s^{5}$ $CH_{3} \qquad R_{2}N = N_{3}s^{5}$	H ₂ O	372 354	470 467	18,000 15,000	0.19 0.96
1g ²⁷ 1h 1i	$\begin{array}{cccccccccccccccccccccccccccccccccccc$	H ₂ O	548 524 526	571 552 557	78,000 87,000 87,000	0.47 0.93 0.92

(on improving the QY of existing dyes. Xiao and co-workers have shown that replacing the dimehtylamino group with a quaternary piperazine moiety is effective in enhancing the brightness (**Figure 46** and **Table 8, entry 1g-1i**).²⁷ A positively charged quaternary ammonium ion reduces the electron withdrawing ability of the amino group inductively (-I effect) and thereby

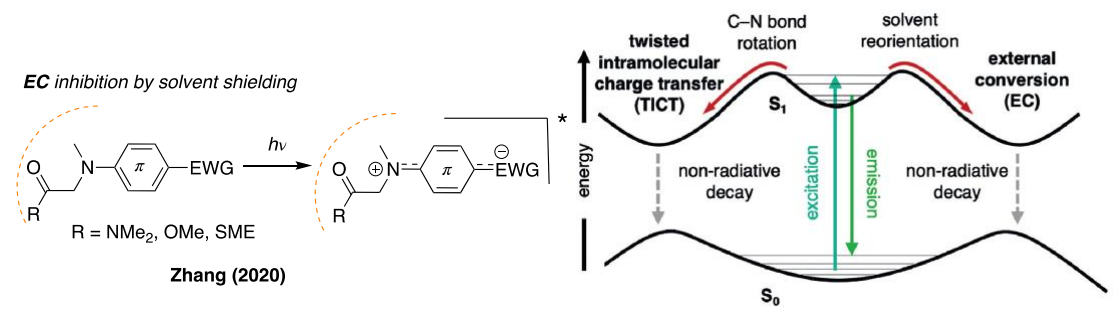


Figure 47. a) Possible shielding effect of a β -carbonyl on the amine group can reduce the solvent induced quenching. b) presence of solvent induced quenching pathway, also known as external conversion (EC).

destabilize the TICT state and increase the energy barrier to enter such a state. This idea is further extended by incorporating a strong electron withdrawing sulfone functionality to improve the IP values of amino auxochromes. **Figure** shows a comparison of the IP values for different amine donors calculated in gas phase. As can be seen, similar to sulfone; a phosphine group is also effective in reducing TICT. It is of note, IP values for both sulfone and phosphine are not only higher than their open chain diethylamine analogue but also the aziridine donor, previously seen to be effective in increasing the QY. Consistent with the enhancement in QY, the fluorescence lifetime (*t*) of these derivatives also showed a similar increasing trend.²³ It is important to mention most of these studies are limited to rhodamine, carbo-rhodamine, silicon-rhodamine coumarin derivatives.

Despite significant progress in studying TICT, its presence is poorly understood in case of solvatochromic dyes. Such dyes are highly fluorescent in non-polar mediums, but the florescence QY drastically reduces in protic solvent such as ethanol.²⁸ Even more dramatically, QY is

practically negligible in aqueous medium for most dyes. However, there are only a few studies aiming to improve the QY of these dyes. In fact, current literature provides conflicting evidence about the existence of TICT state in solvatochromic dyes. For example, Abelt's group studied several different rigidified versions of a prodan dye and compared its optical properties with the open chain analogue. Although the derivatives hold the solvatochromic features of the parent

Table 9. Effect of the structural modification to suppress the solvent induced quenching

Entry	Structure	Solvents	λ _{abs} (nm)	λ _{emi} (nm)	ε (M ⁻ ¹ cm ⁻¹)	Φ
2a ²⁸ 2b	CH ₃ N 254	EtOH H ₂ O EtOH H ₂ O	367 372 363 367	449 467 440 455	20,880 16,380 12,680 11,970	0.84 0.21 0.95 0.98
2c 2d	N 2222	EtOH H ₂ O EtOH H ₂ O	360 356 356 360	491 526 485 514	17,920 5,190 15,400 14,390	0.71 0.25 0.82 0.76

prodan, none show any improvement in the fluorescence QY.²⁹ Hence, a planar ICT state is proposed as the excited state. However, theoretical, and experimental study by Liu *et. al.* proposed a possibility of TICT state and an enhanced QY is shown for azetidinyl, and pyrrolidine substituted prodan compound.³⁰ Nonetheless, it is important to mention excited state phenomena such as fluorescence is affected not only by the structure of the molecules, but also the surrounding medium. Thus, consideration of one factor like rotation of single bonds and hence formation TICT state is often not enough to describe the fluorescence properties.

As discussed earlier, interaction with solvents can also induce non-radiative pathways, known as external conversion (EC) (**Figure**).²⁸ Additionally, an intermolecular hydrogen bond interaction in protic solvents can lead to rapid non-radiative decay. We previously discussed a

possible role of the positively charged methyl-piperazine unit has on suppressing the TICT. In addition to that, such functionality is also believed to reduce non-radiative decays by hydrogen bonding. Xin *et al.* reports installation of a polar functional group at the β -position relative to the nitrogen donor is effective in shielding the amino auxochrome from solvent interactions, and thereby attenuates the influence of solvent dependent quenching pathways (**Table 9**).²⁸ It is also proposed that the carbonyl functionality can inhibit the formation of TICT by increasing the rotational barrier of the donating group. Example of fluorophores that were studied includes coumarin and prodan derivatives. It was also observed that β -esters and thioesters are more effective in increasing the brightness than amides.

Table 10. Reported fluorene-based dyes with their optical properties in protic mediums.

Entry	Structure Structure	Solvents	λ_{Abs} (nm)	λ _{Emi} (nm)	ε (M ⁻¹ cm ⁻¹)	Φ
3a ³¹	O N FR0	EtOH MeOH	395 396	554 570	43,000	0.33 0.19
3b	O C ₈ H ₁₇	EtOH MeOH	383 384	536 555	-	0.47 0.35
$3c^{32}$	$R_2N = N$	EtOH	388	562	35,500	0.48
3d 3e	R_2N H $R_2N = N_{5}^{5}$	EtOH	380	572	36,000	0.44
	$R_2N = N_{x_2}$	EtOH	342	522	24,000	0.33
	$R_2N = N_{\gamma}^{\gamma}$	H ₂ O	386	624	35,500	0.04
3f 3g	R_2N H $R_2N = N_{2}p^5$	H ₂ O	377	621	36,000	0.05
3h	$R_2N = N_{c}^{c}$ $R_2N = N_{c}^{c}$	H_2O	345	555	24,000	0.16

IV.2 Structural modification of fluorene dyes to improve QY

In the previous section, different strategies to improve the QY of fluorescent dyes were discussed. These studies sparsely describe solvatochromic dyes despite their importance as environmentally sensitive probes. Fluorene based dyes are analogous to the well-known prodan derivatives but with remarkable improvement of optical properties including red-shifted emission, enhanced brightness and photostability.³¹ As first reported in 2009, fluorene dyes undergo a large change in the diploe moment from ground to excited state, making them sensitive towards solvent polarity.³¹ Despite their large Stoke's shift, these dyes display negligible fluorescence QY in protic solvents (**Table 10**). Shaya *et. al* developed a series of fluorene-based dyes with different heterocyclic amines as the donor unit including the aziridine and azetidine (**Table 10**, entry 3c-3h).³² However, the QY of these derivatives remain insignificant in aqueous medium, similar to the dimethylamine donor. We wondered if other strategies such a rigidification of the structure or introduction of a negative inductive group is effective in improving the QY. In addition, such studies may also help to understand the nature of the dye's excited state.

To examine the effect of rigidification of structure on the optical properties of fluorene dyes, we designed and synthesized six fluorene derivatives **4-9** (**Figure**). As previously observed, a dialkylamine is effective as a strong EDG and to maintain good solubility of the

Figure 48. Structures of fluorene derivatives 4 -9.

compound in organic solvents. A ketone functional moiety is introduced as a uniform EWG. In compound 5, the rotation of the diethylamine group is prevented by locking it in a cyclic structure. On the other hand, conformation of the carbonyl group is restricted in compound 6. We surmised comparing the optical properties of 4-6 will be useful in understanding the effect of the rigidification on structure. Additionally, to test the effect of positively charged ammonium ion and a β -carbonyl substituent on fluorene derivatives, we synthesized compounds 7-9. As reported this functionality is either effective in suppressing TICT formation or solvent induced quenching.

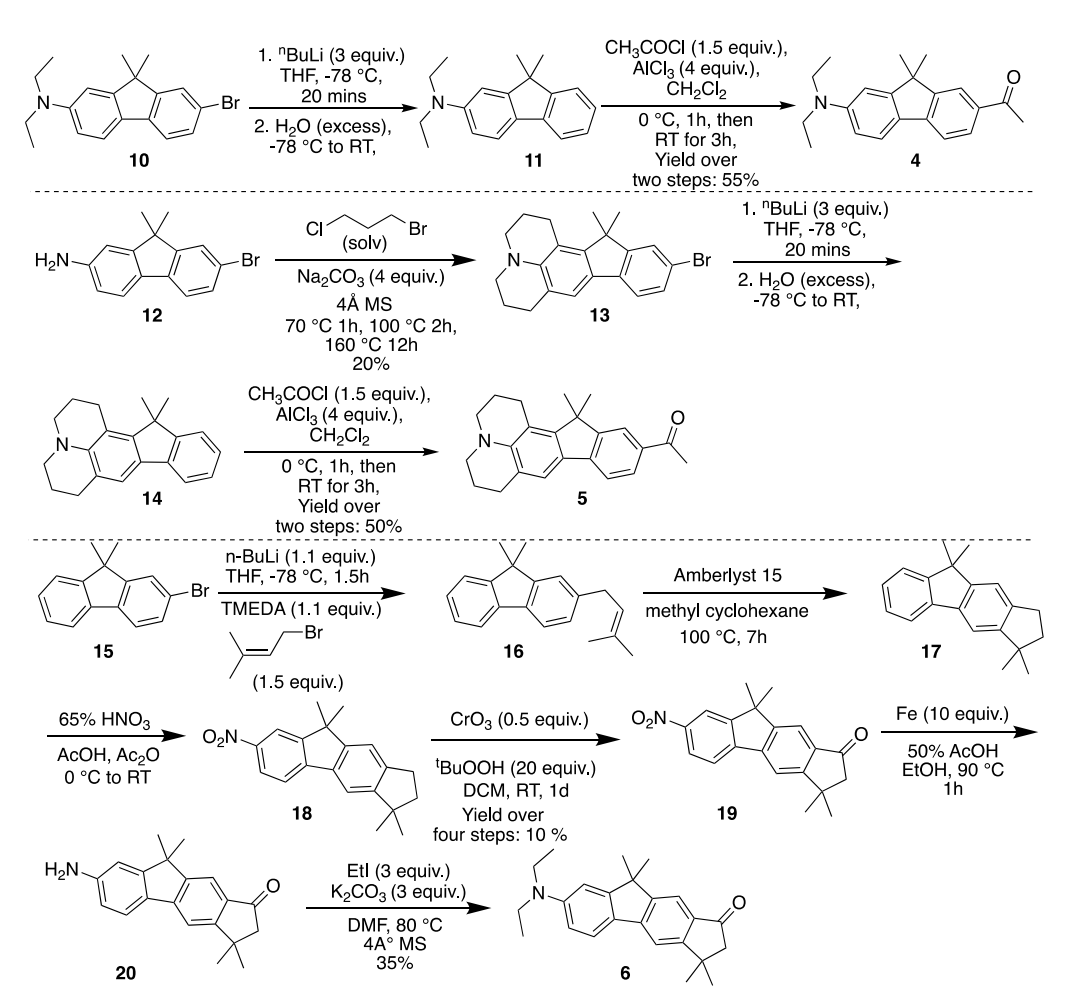


Figure 49. Steps for synthesis of 4-6.

IV.3 Synthesis of fluorene dyes 4-9

Synthesis of **4** started from **10** which was obtained from a previously developed method (**Figure**).³¹ Subsequently debromination was accomplished by metal-halogen exchange, followed by incorporation of the carbonyl using Friedel-Craft acetylation. For synthesizing compound **5**, a vicinal dihalide was used to alkylate and cyclize the amine, yielding **13**. Further acetylation was accomplished following similar procedure as that for compound **4**. Synthesis of compound **6** was performed first by introducing a cyclopentane ring, followed by nitration of fluorene core structure. A carbonyl group was introduced at a later stage by oxidizing compound **18** with chromium trioxide. Introduction of the cyclopentane ring was not successful with amine

Figure 50. Steps for synthesis of 7-9.

functionalized fluorene due to decreased reactivity of the compound under acidic condition. A methyl-piperazine donor unit on the fluorene is installed by Pd-catalyzed C-N cross coupling method to synthesize **7** (**Figure**). Acidification of the solution of compound **7** in polar protic

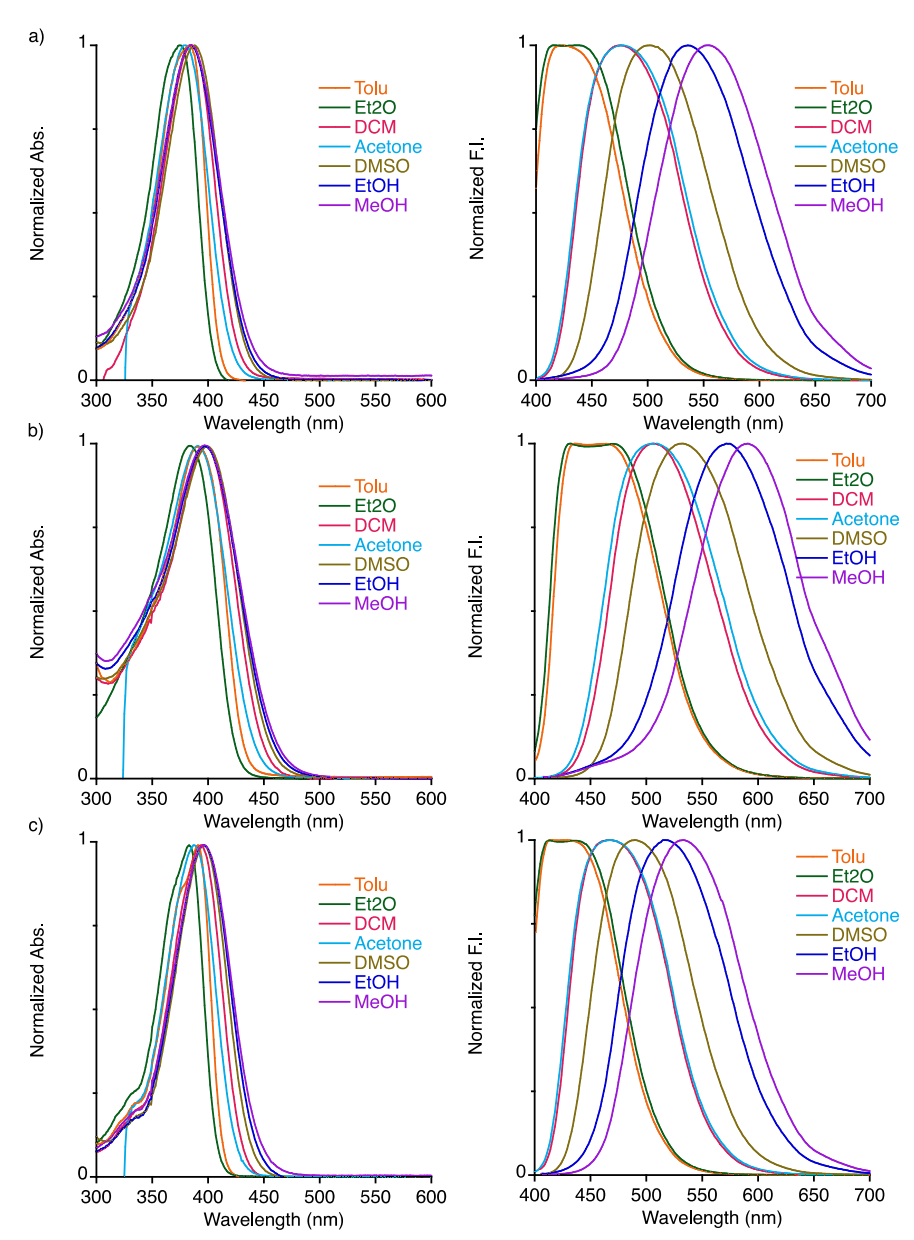


Figure 51. Normalized absorption and emission spectra in various solvents for a) **4**, b) **5** and c) **6.** solvents result in formation of compound **8** through selective protonation of aliphatic amine. Lastly, synthesis of **9** was accomplished first through mono-alkylation of the amine through acylation and borane reduction (**Figure**). The mono-ethylamine was subjected to further alkylation with ethyl bromoacetate to introduce the β -carbonyl on the amine group (compound **25**). Acetylation of compound **25** was performed as the last step similar to the other previously

discussed derivatives. All compounds are bright yellow/orange in color except **7** which is pale yellow, both as solid and solution.

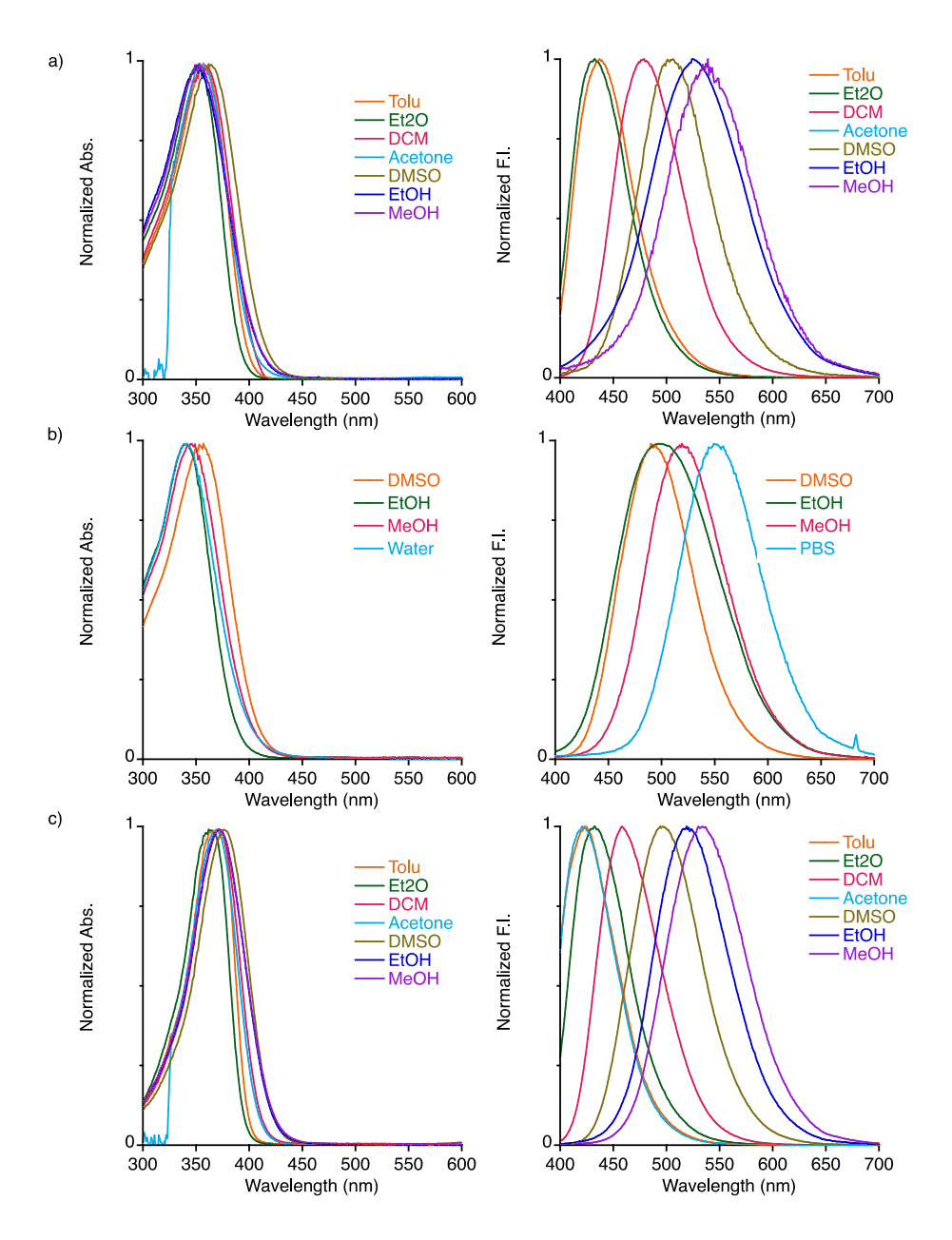


Figure 52. Normalized absorption and fluorescence spectra in various solvents for a) **7**, b) **8** and c) **9**.

IV.4 Optical properties

IV.4.1 Absorption and emission:

Optical properties of synthesized fluorene derivatives **4-9** were studied in different organic solvents as shown in **Figure** and **Figure** and respective values are summarized in **Table**. All six dyes absorb in the UV, displaying a larger Stoke's shift in polar solvents (122-171 nm in ethanol) compared to non-polar solvents (30-79 nm in toluene). Incorporation of extra ring in **5** and **6** shifts the absorption to longer wavelengths as compared to **4** in accordance with the increased inductive effect of the alkyl groups. On the other hand, compounds **7-9** show a significant hypsochromic shift in the absorption. The hypsochromic shift can be explained by the decreased

Table 11. Comparison of spectral properties of fluorene-based dyes **4-9** in different solvents

Table 11. Col	4				5				6			
$\varepsilon (M^{-1}cm^{-1})$		23	,500		24,600				18,400			
	$\lambda_{ m Abs}$	$\lambda_{ m Emi}$	Δλ	Φ	$\lambda_{ m Abs}$	$\lambda_{ m Emi}$	Δλ	Φ	$\lambda_{ m Abs}$	$\lambda_{ m Emi}$	Δλ	Φ
Toluene	384	424	40	0.75	391	467	76	0.75	391	427	36	0.81
Et ₂ O	375	436	61	0.70	384	470	86	0.78	383	435	52	0.78
DCM	385	474	89	0.87	398	506	108	0.82	393	466	73	0.90
Acetone	379	479	90	0.82	390	506	116	0.70	388	467	79	0.82
DMSO	387	502	115	0.94	400	532	132	0.84	397	489	92	0.96
Ethanol	385	537	152	0.79	397	571	174	0.52	396	518	122	0.85
Methanol	386	554	168	0.63	397	590	193	0.32	396	532	136	0.80
H_2O	-	-	-	-	-	-	-	-	394	553	159	0.18
			7				8			9	9	
ε (M ⁻¹ cm ⁻¹)			7 ,000			23	8 ,152			-	9 500	
ε (M ⁻¹ cm ⁻¹)	$\lambda_{ m Abs}$		-	Φ	$\lambda_{ m Abs}$	23 λ _{Emi}		Φ	$\lambda_{ m Abs}$	-		Φ
ε (M ⁻¹ cm ⁻¹) Toluene	λ _{Abs}	21	,000	Φ 0.66	λ _{Abs}		,152	Φ-	λ _{Abs} 372	22,	500	Φ 0.36
	-	21 λ _{Emi}	,000, Δλ		λAbs -		,152	Φ - -	-	22, λ _{Emi}	500 Δλ	
Toluene	357	21 λ _{Emi} 436	,000 Δλ 79	0.66	λAbs		,152	Φ - -	372	22, λ _{Emi} 422	$\frac{500}{\Delta \lambda}$ 50	0.36
Toluene Et ₂ O	357 352	21 λ _{Emi} 436 430	,000 Δλ 79 78	0.66 0.54	λAbs		,152	Φ - - -	372 364	22, λ _{Emi} 422 421	500 Δλ 50 57	0.36 0.32
Toluene Et ₂ O DCM	357 352 359	21 λ _{Emi} 436 430 476	79 78 117	0.66 0.54 0.90	λAbs		,152	Φ - - - - -	372 364 371	22, λ _{Emi} 422 421 457	500 Δλ 50 57 86	0.36 0.32 0.95
Toluene Et ₂ O DCM Acetone	357 352 359 355	21 λ _{Emi} 436 430 476 480	79 78 117 125	0.66 0.54 0.90 0.22	λAbs 340		,152	Φ 0.45	372 364 371 369	22, λ _{Emi} 422 421 457 467	500 Δλ 50 57 86 98	0.36 0.32 0.95 0.85
Toluene Et ₂ O DCM Acetone DMSO	357 352 359 355 364	21 λ _{Emi} 436 430 476 480 503	79 78 117 125 139	0.66 0.54 0.90 0.22 0.14	- - - -	λEmi		- - - -	372 364 371 369 376	22, λ _{Emi} 422 421 457 467 497	500 Δλ 50 57 86 98 121	0.36 0.32 0.95 0.85 1.00

electron donating ability due to increased s-character of the nitrogen lone pair in such cyclic amines.³² In addition, the steric factor may also contribute by rotating the nitrogen atom out of the

plane of the conjugated backbone. With the presence of an ammonium ion, compound 8 displays the most blue-shifted absorption and emission. This indicates a strong negative inductive effect (-I) of the positively charged ammonium ion on the charge redistribution of the fluorene derivatives. It is worth noting that 8 only can be generated in protic solvents, hence optical properties in other solvents are not reported. Among all the fluorene derivatives synthesized, compound 5 displays most red-shifted absorption with a dramatic Stoke's shift in protic solvents such as ethanol. Molar absorptivity or molar extinction coefficient is a measure of how strongly a compound absorbs photons at a wavelength and is an intrinsic property of the molecule. Compound 5 displays the highest molar absorptivity (24,600 M⁻¹cm⁻¹ in ethanol), presumably because of its increased surface area due to the rigidification.

Similar to absorption, emission maximum for all the dyes shift to lower energy going from most apolar aprotic solvents to polar protic solvents. In fact, such variation in the emission maximum is common to other solvatochromic dyes due to their sensitivity to the surrounding environments. The magnitude of the fluorescence solvatochromism is determined by the degree of charge transfer in the excited state, which can be quantified by Reichardt's $E_T(30)$ scale of polarity. This $E_T(30)$ parameter is broadly a measure of the solvent polarity, but it also reflects the hydrogen-bonding ability of the solvents. **Figure** plots the emission maxima vs the Reichardt $E_T(30)$ parameter for five derivatives **4-7** and **9**. As can be seen, the maximum wavelength of emission energy increases linearly with increasing polarity of the solvents. The slopes of these best-fit lines indicate the sensitivity of the dyes to polarity, follows the order: **7>5>6>9>4**. The strong positive solvatochromism of the dyes emissions emphasizes the large ICT character of their excited states. Due to optical values in a limited number of solvents, **5** is not considered for

comparison with other compounds. To summarize, all the newly synthesized fluorene-based dyes retain the solvatochromic nature despite the structural modification.

QY for compounds **4-9** collected in different solvents, are higher in non-polar solvents but markedly decreased in protic mediums (**Table**). This is generally true for solvatochromic dyes displaying a large ICT character in the excited states. QY of rigidified amine derivative **5** is comparable to the open chain analogue **4** in most non-polar and polar solvents. However, it is significantly reduced in protic mediums, with sharp decline in going from ethanol to methanol.

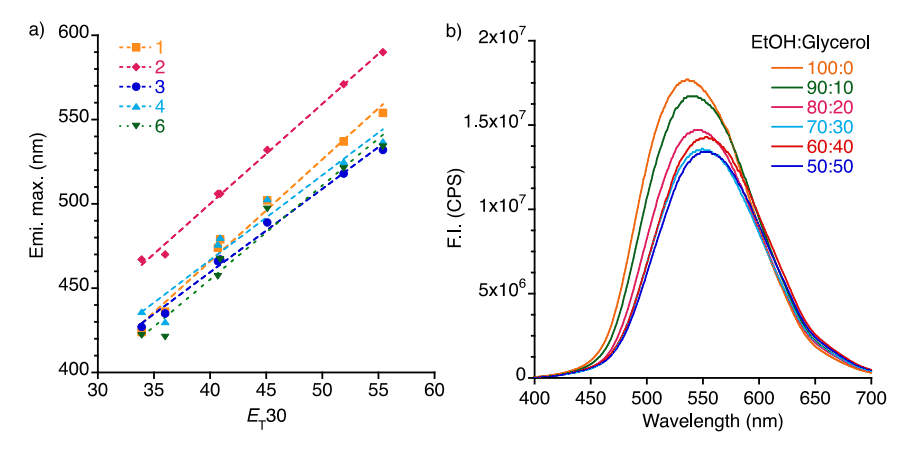


Figure 53. a) Plot of emission maxima versus solvents polarity. The E_T30 values for toluene, diethyl ether, dichloromethane, acetone, dimethyl sulfoxide, ethanol, methanol, water is 33.9, 36.0, 400.7, 40.9, 45.1, 51.9, 55.4, 63.1. \mathbb{R}^2 values for the best-fit lines are 0.99, 0.99, 0.99, 0.97 and 0.98 respectively. b). Emission spectrum of **4** in a solvent mixture with varying ratio of ethanol and glycerol.

This result shows despite the red-shifted absorption and emission, the restriction of the C-N bond rotation does not suppress the non-radiative decay. Similarly, QYs of 6 are comparable to 4 in all organic solvents but with slightly increased values in protic mediums. Of note, the emission maximum of 6 is blue shifted compared to 4 in most solvents. Interestingly, molecule 6 exhibits fluorescence in the aqueous medium which is uncommon to fluorene dyes. This might be associated with the increased solubility of the compound in aqueous medium. To elucidate the relationship between QY and possible formation of TICT in protic mediums, we measured the fluorescence intensities of 4 in ethanol–glycerol mixtures of varying volume ratios (100:0 to 50:50)

(**Figure b**). Glycerol being a viscous medium, would reduce the rotational movement, hence suppress the formation TICT.³⁰ In other word, the emission intensity of a dye possessing TICT would increase in glycerol rich medium. As can be seen from **Figure b**, the fluorescence intensity of **4** does not show any noticeable change with increasing amount of glycerol in the mixture. This result indicates likelihood of planar ICT state for the fluorene-based dyes in the protic mediums. In fact, no or marginal increase of QY of the constrained fluorene derivative **5** and **6** compared to **4**, supports this idea. Nevertheless, large polarity of these dyes in the excited state can result in the augmented ability for hydrogen bonding. This can result in increased non-radiative decay in polar mediums and can reduce the QY.

The QY of other fluorene derivatives **7-9** are also measured in different solvents. Among them, **7** is weakly fluorescent in most solvents, especially in polar mediums. Despite the blue-shifted emission, the decreased QY may arise because of the weakly donating amine similar to other heterocyclic amine substituted fluorene dyes. In addition to this, the presence of aliphatic amine on the methyl-piperazine unit can act as quencher through photoinduced electron transfer (PeT). Interestingly, with protonation of that amine, QY increased by almost 2-4-fold as can be seen for **8**. Strong fluorescence quenching for **7** and significant increase of fluorescence upon protonation (compound **9**) opens the opportunities of developing turn-on fluorescence sensor. Notably, the fluorescence QY of **8** is remarkably high in aqueous medium, despite the relatively lower value in other protic solvents compared to **4**. Lastly, as shown in **Table**, compound **9** maintains a relatively high QY even in all protic mediums. To the best of our knowledge, **8** and **9** report one of the highest fluorescence quantum yields achieved to date for the fluorene derivatives in aqueous medium. As discussed earlier, dyes can display an enhanced QY through shielding the amino auxochrome from solvent-induced quenching. Thus, the increased QY for **8** and **9** may

result from such shielding effect of the positively charged methyl piperazine or β -ester substituent. Additionally, both these derivatives maintain large Stoke's shift similar to **4**, making them promising candidates for fluorescence imaging.

IV.5 Aldehyde as an electron withdrawing unit

As discussed earlier, an aldehyde functionality is instrumental for the design of our fluorescent dyes for rapid binding with engineered hCRBPII mutants. The aldehyde can react with the lysine group to form an imine/iminium, and thus, covalently binds the protein. Based on our discussion of fluorene derivatives **4-9**, we have seen compound **5** with the most red-shifted emission and **8** with high QY in aqueous medium. Hence, we choose these two scaffolds for further engineering of the dyes. Both these D-A dyes contain an acetyl group as an electron withdrawing group, which is not suitable for binding with hCRBPII. Hence, we synthesized two aldehyde-based dyes **26** and **27**, containing a cyclic amine and methyl piperazine as electron donating unit (**Figure**). Compound **27** can be protonated in aqueous medium to form **28**, which is expected to show a large increase in QY as observed with its ketone analogue (compound **8**). Previously, our group

Figure 54. Fluorene derivatives with aldehyde as electron withdrawing group

has synthesized and studied the photophysical properties of **FR0**, an aldehyde containing dye with diethylamine as the electron donor. Hence, **FR0** can be used as a reference for comparing the optical properties with compound **26-28**.

IV.5.1 Synthesis and optical properties of aldehyde analogues

Figure shows the steps for the synthesis of compounds **26-28**. Compound **13** was previously used as a precursor for synthesizing **5** and is also used for synthesizing **26**. An aldehyde

functional group was introduced by metal-halogen exchange of the bromide in **13** with *n*-BuLi, which was subsequently formylated with DMF. For the synthesis of **27**, the aldehyde functional

Figure 55. Steps to synthesize aldehyde containing fluorene dyes 26 -28.

group was introduced onto the **15** by Fridel-Crafts reaction using zirconium tetrachloride. Subsequently, Buchwald–Hartwig amination of **29** with N-methylpiperazine leads to **27**, following the protocol developed by Shaya *et. al.*³² Compound **26** is bright orange whereas **27** is pale yellow

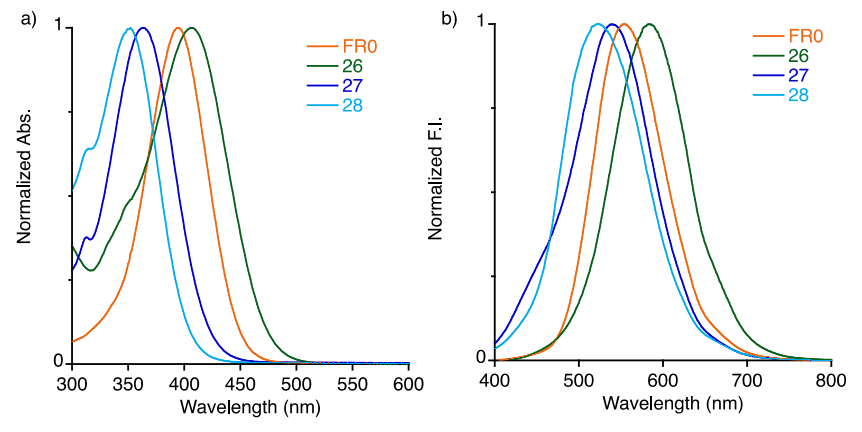


Figure 56. Normalized absorption and fluorescence spectra of **FR0** and **26-28** in ethanol. in color.

Optical properties of compounds **26-28** were measured in ethanol and compared with parent compound **FR0**. As can be seen from **Figure** and **Table**, compound **26** with rigidified amine displays the most red-shifted absorption and emission among all the aldehyde-based fluorene derivatives. Additionally, stronger electron withdrawing effect of the aldehyde further red

shifts (by 11 nm) the absorption and emission when compared to the ketone analogue 5. The maximum of absorption of 26 lies in the visible spectrum, matching the argon laser line. In contrast, incorporation of methyl-piperazine as an electron donating unit in 27 results in large hypsochromic shift (32 nm) of absorption as compared to FR0. Protonation of the methyl-

Table 12. Comparison of spectral properties of fluorene-based dyes FR0, 26-28

	FR0			26			27			28		
	$\lambda_{ m Abs}$	$\lambda_{ m Emi}$	Φ	$\lambda_{ m Abs}$	$\lambda_{ m Emi}$	Φ	$\lambda_{ m Abs}$	$\lambda_{ m Emi}$	Φ	$\lambda_{ m Abs}$	$\lambda_{ m Emi}$	Φ
Ethanol	396	556	0.66	408	585	0.36	364	540	0.10	348	520	0.40

piperazine (compound **28**) further blue-shifted the absorption. The QY of the rigidified **FR0** derivative **26** is unusually low in ethanol albeit large, red-shifted emission spectrum than **FR0**. This shows rigidification of C-N does not improve the QY and further support a possible existence of planar ICT state in these derivatives. Compared to other members, compound **27** was characterized by reduced QY which increases with protonation of the amine (compound **28**).

Figure 57. Synthesis of imine (SB) and iminium (PSB) using *n*-butylamine.

To mimic the active site lysine group of protein, *n*-butylamine was used as surrogate to form an imine (SB) upon reaction with aldehyde-based dyes **26-28** (**Figure**). Resulting imine can be protonated to form iminium (PSB) and its optical properties can be studied. Previous study from our group has shown the positively charged iminium is a strongly electron withdrawing unit that results in large red shift of absorption and emission compared to both free aldehyde and SB.³³⁻³⁶ Similar effect on optical properties is also observed upon binding of the dye with hCRBPII

mutants. Previously, **FR1V**, a homologue of **FR0** was used with hCRBPII as a NIR emitting fluorescent tag with emission around 680 nm.³⁵ Despite the success as a highly red-shifted imaging tag, the QY of the complex tends to be low (QY: 0.13-0.16). Hence, study of QY of PSB of **FR0** and the newly engineered dye **26** and **28** in solution can be useful to design a brighter fluorescent tag.

As shown in **Figure** and **Table**, emission of **26**-PSB is red-shifted by 30 nm compared to the analogous **FR0**, reaching to the NIR region of visible spectrum. As biological samples have minimal interference in the NIR region of spectrum, such a dye can be useful for

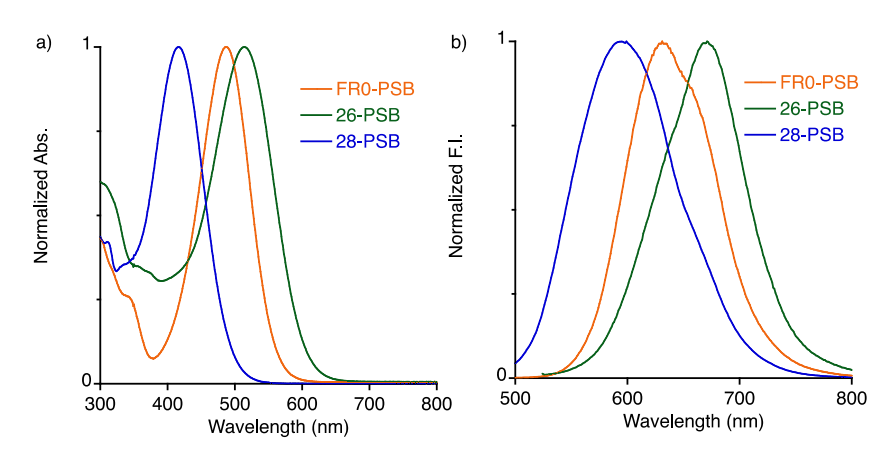


Figure 58. Normalized absorption and fluorescence spectra of PSB corresponding to **FR0**, **26** and **28**.

fluorescence imaging. Interestingly, despite the red-shift of emission, QY 26-PSB is higher than FR0-PSB unlike their aldehyde counterpart. Selective protonation of the imine to form 28-PSB was not fruitful as it also results in protonation of amine of methyl-piperazine. (Figure). Gratifyingly, QY of the resulting PSB has doubled compared to the parent compound FR0, highlighting the role of the positively charged ammonium ion on the electron donating amine group. In addition, 28-PSB displays the largest Stoke's shift among all dyes examined. This is important as it can reduce self-quenching of the dye and increase the depth of the fluorescence imaging.

Table 13. Comparison of spectral properties of PSB for FR0, 26-28

	FR0-PSB				26-P	SB			28-PSB			
	λabs	$\lambda_{\rm em}$	Δλ	Φ	λ _{abs}	$\lambda_{\rm em}$	Δλ	Φ	λ _{abs}	$\lambda_{\rm em}$	Δλ	Φ
Ethanol	487	631	144	0.23	514	671	157	0.30	418	596	178	0.47

IV.6 Conclusion and Future Scope

A number of fluorene-based dyes were synthesized, and optical properties were compared, focusing on the fluorescence QY. Despite different structural modifications, newly designed dyes display solvatochromic behavior similar to their parent dyes. Rigidification of the dye through restricting the single bond rotation did not significantly impact the QY in most examples. Additional experiment on fluorescence behavior in ethanol-glycerol mixture cast doubt on the presence of a TICT state in fluorene-based dyes. Incorporation of a positively charged methyl-piperazine or β -ester substituent on the amino auxochrome improved the QY, especially in protic mediums including water. It can be postulated that these substitutions are effective in reducing the solvent induced quenching of highly polar excited state of these solvatochromic dyes. Compound 26 and 28 with superior QY can be used for conjugating with hCRBPII for imaging tag. Additionally different spacer group can be incorporated between the fluorene core and the aldehyde to further shift the spectrum. Finally, with week fluorescence of 27 and selective protonation of the methyl-piperazine inside the protein, the dye can be used for fluorogenic labelling of hCRBPII.

IV.7 Experimental Section

Synthesis of 1-(7-(diethylamino)-9,9-dimethyl-9H-fluoren-2-yl)ethan-1one (4): 10 (500 mg, 1.5 mmol, 1 equiv.) was dissolved in dry THF (5 mL) and the solution was cooled down to -78 °C under argon atmosphere. n-Buli (2.5 M in hexane, 1.7 mL, 3 equiv.) was added to the resulting solution dropwise and stirred for 20 min at that temperature. Then of water (1 mL) was added dropwise at -78 °C and the temperature was raised to RT. The organic layer was extracted with ethyl acetate three times, dried over anhydrous sodium sulphate and concentrated. The dried crude of 11 was directly used for the next reaction. Compound 11 (457 mg, 1.7 mmol, 1 equiv.) was dissolved in dry CH₂Cl₂ in (20 mL) and the solution was cooled to 0 °C under argon atmosphere. Anhydrous aluminum chloride (0.9 g, 6.9 mmol, 4 equiv.) was added to at once, followed by dropwise addition of acetyl chloride (0.18 mL, 2.6 mmol, 1.5 equiv.) in 30 min. The reaction was run at 0 °C for 1 h and subsequently at RT for 3 h. The reaction mixture was then slowly poured into a saturated sodium bicarbonate solution (200 mL). After extraction with dichloromethane (100 mL × 2), the organic layer was dried with anhydrous Na₂SO₄. The crude product was purified by column chromatography on silica gel eluting with ethyl acetate/hexane (20%) to provide the bright fluorescent product 4 (253 mg, 0.83 mmol, yield over two steps: 55%). ¹H NMR (500 MHz, CDCl₃) δ 7.99 – 7.95 (m, 1H), 7.90 (dd, J = 8.0, 1.7 Hz, 1H), 7.60 (d, J = 8.4 Hz, 1H), 7.57 (dd, J = 8.0, 0.6 Hz, 1H), 6.74 - 6.58 (m, 2H), 3.45 (q, J = 7.1 Hz, 4H), 2.63 (s, 3H), 1.49 (s, 6H), 1.23 (t, J = 7.1 Hz, 6H). TOF MS ES $^+$ (C₂₁H₂₅NO): Calc. [M+H] $^+$: 308.201; found: 308.202.

mmol, 1 equiv.), 1-bromo-3-chloropropane (0.6 mL), Na₂CO₃ (297 mg, 2.8 mmol, 4 equiv.) and 4 Å MS (50 mg) was added to a 50 mL flask and heated with vigorous stirring under argon atmosphere by gradual increase of temperature (70 °C/1 h, 100 °C /2 h, 160 °C/12 h). The resulting mixture was then cooled down to RT and dissolved in dichloromethane after distilling off excess 1-bromo-3-chloropropane. The crude solution in dichloromethane was extracted with water two times, dried with sodium sulphate, concentrated, and washed with hot MeOH three times. Pure product was obtained as a brown solid (50 mg, 0.14 mmol, yield 20%). Spectral data: ¹H NMR (500 MHz, CDCl₃) δ 7.40 (s, 1H), 7.33 (m, 2H), 7.15 (s, 1H), 3.20 (q, J = 6.5 Hz, 4H), 3.01 (t, J = 6.4 Hz, 2H), 2.83 (t, J = 6.5 Hz, 2H), 2.01 (dt, J = 18.1, 6.1 Hz, 4H), 1.55 (s, 6H). ¹³C NMR (125 MHz, CDCl₃) δ 155.67, 148.01, 143.19, 138.87, 129.73, 126.73, 125.26, 120.80, 119.28, 118.73, 118.50, 118.27, 50.79, 50.08, 48.21, 28.43, 25.12, 24.35, 22.12, 21.89. TOF MS ES⁺(C₂₁H₂₂BrN): Calc. [M+H]⁺: 368.101; found: 368.0974.

Synthesis of 1-(13,13-dimethyl-2,3,5,6,7,13-hexahydro-1*H*-indeno[2,1f]pyrido[3,2,1-*ij*]quinolin-11-yl)ethan-1-one (5): Compound 13 (500 mg,
1.4 mmol, 1 equiv) was dissolved in dry THF (5 mL) and the solution was cooled down to -78 °C
under argon atmosphere. *n*-Buli (2.5 M in hexane, 1.7 mL, 3 equiv) was added to the resulting
solution dropwise and stirred for 20 minutes at that temperature. Then water (1 mL) was added
dropwise at -78 °C and temperature was raised to RT. The organic layer was extracted with ethyl
acetate three times, dried over sodium sulphate and concentrated. The dried crude 14 was directly
used for the next reaction. Compound 14 (498 mg, 1.7 mmol, 1 equiv) was dissolved in dry CH₂Cl₂
(20 mL), and the solution was cooled to 0 °C under argon atmosphere. Then anhydrous aluminum
chloride (0.9 g, 6.9 mmol, 4 equiv) was added to at once, followed by dropwise addition of acetyl

chloride (0.18 mL, 2.6 mmol, 1.5 equiv) in 30 min. The reaction was run at 0 °C for 1 h and subsequently at RT for 3 h. The reaction mixture was then slowly poured into a saturated sodium bicarbonate solution (200 mL). After extraction with dichloromethane (100 mL × 2), the organic layer was dried with anhydrous Na₂SO₄. The crude product was purified by column chromatography on silica gel eluting with ethyl acetate/hexane (20%) to provide the bright fluorescent product **5** (232 mg, 0.7 mmol, yield over two steps: 50%). ¹H NMR (500 MHz, CDCl₃) δ 7.93 (s, 1H), 7.86 (dd, J = 8, 1.5 Hz, 1H), 7.49 (d, J = 8 Hz, 1H), 7.24 (s, 1H), 3.24 (dt, J = 8.4, 5.5 Hz, 4H), 3.03 (t, J = 6.4 Hz, 2H), 2.84 (t, J = 6.4 Hz, 2H), 2.62 (s, 3H), 2.01 (dt, J = 19.1, 5.9 Hz, 4H), 1.60 (s, 6H). ¹³C NMR (125 MHz, CDCl₃) δ : 197.83, 153.60, 149.89, 145.18, 143.99, 133.83, 128.55, 126.11, 121.54, 120.85, 119.73, 118.24, 117.27, 50.71, 50.02, 47.98, 28.44, 26.65, 25.01, 24.29, 21.95, 21.71. TOF MS ES⁺(C₂₃H₂₅NO): Calc. [M+H]⁺: 332.201; found: 332.203.

Synthesis of 3,3,9,9-tetramethyl-7-nitro-3,9-dihydrocyclopenta[b]fluoren-1(2H)-one (19): To a THF solution (4 mL) of 15 (200 mg, 0.74 mmol, 1.0 equiv) was slowly added n-BuLi in hexane (0.44 mL, 1.1 mmol, 1.5 equiv) at -78 °C. After the mixture was stirred at -78 °C for 1.5 h, TMEDA (0.17 mL, 1.1 mmol, 1.5 equiv) was added. The mixture was further stirred for 10 min at -78 °C, 3,3 dimethylbromobutanne (0.13 mL, 1.1 mmol, 1.5 equiv) was slowly added to the mixture at -78 °C. The mixture was allowed to warm to RT and was further stirred for 12 h. The reaction was quenched with H₂O and extracted with ethyl acetate. The combined organic layer was washed with saturated NaCl and dried over Na₂SO₄. The solvent was removed under reduced pressure to afford the crude product, 16. Without further purification, crude was used for next step. A mixture of the crude 16 and Amberlyst 15 (200mg) in methylcyclohexane (5 mL) was heated to reflux for 7 h.

The reaction mixture was cooled to room temperature and Amberlyst 15 was removed by filtration. The filtrate was evaporated under reduced pressure to afford crude product, 17. Without further purification, compound 17 was utilized for the next step. The crude was mixed with 2 mL of acetic acid and of acetic anhydride each and the mixture was cooled to -10 °C. Then HNO₃ (65%, 0.5 mL) was added in portions over 30 min and reaction were monitored afterward with TLC. After the reaction was completed (~30 min), it was quenched by addition of ice-cold water. The compound was extracted with ethyl acetate, dried over anhydrous Na₂SO₄ and concentrated under reduced pressure to give the crude product 18, which was directly used for next reaction. To a CH₂Cl₂ (2 mL) solution of crude, **18** (100 mg, 0.33 mmol) was added chromium (VI) oxide (17mg, 0.17 mmol, 0.5 equiv) at room temperature. To the mixture was added dropwise 70% aqueous tbutyl hydroperoxide solution (2.0 mL, 6.6 mmol, 20 equiv) at room temperature, and the mixture was further stirred for 1 d. The reaction was quenched with saturated Na₂SO₃ aqueous solution, and the mixture was further stirred for 30 min with saturated NaHCO3 aqueous solution. Solid was removed by filtration and the filtrate was extracted with CH₂Cl₂ twice. The combined organic layer was washed with saturated NaCl solution twice and dried over Na₂SO₄. The solvent was removed under reduced pressure to afford the crude product, compound 19 which was purified by silica-gel column chromatography (hexane: ethyl acetate = 4:1) to obtain as yellow powder (24 mg, 0.074 mmol, yield 10% over four steps). Spectral data: ¹H NMR (500 MHz, chloroform-d) δ 8.33 - 8.27 (m, 2H), 7.94 (d, J = 8.2 Hz, 1H), 7.89 (d, J = 0.9 Hz, 1H), 7.80 (d, J = 0.9 Hz, 1H), 2.69 (s, 2H),1.56 (s, 6H), 1.51 (s, 6H) ¹³C NMR (125 MHz, CDCl₃) δ 205.47, 163.98, 156.08, 154.66, 148.16, 144.07, 143.81, 136.12, 123.42, 121.43, 118.57, 117.75, 116.16, 53.47, 47.14, 38.58, 30.22, 26.86. TOF MS AP⁺(C₂₀H₁₉NO₃): Calc. [M+H]⁺: 322.144; found: 322.148.

Synthesis of 7-(diethylamino)-3,3,9,9-tetramethyl-3,9dihydrocyclopenta[b]fluoren-1(2H)-one (6): To a solution of 19 (50 mg, 0.16 mmol, 1 equiv) in 50% acetic acid (5 mL) and ethanol (3 mL) at 90 °C, iron powder (90 mg, 1.6 mmol, 10 equiv) was added and kept at that temperature for 1 h under inert atmosphere. TLC was checked after 3 h, which shows complete consumption of starting material. Reaction was neutralized with saturated aqueous solution of NaHCO₃ (30 mL) and extracted with CH₂Cl₂ twice. The combined organic layer was washed with saturated NaCl solution twice and dried over anhydrous Na₂SO₄. The solvent was removed under reduced pressure to afford the crude product 20, which was directly used for next reaction. A mixture of crude 20 (36 mg, 0.12 mmol), ethyl iodide (56 mg, 0.36 mmol, 3 equiv), potassium carbonate (50 mg, 0.48 mmol, 4 equiv), 4 Å MS (50 mg) in DMF (4 mL) was heated at 80 °C for 5 h under inert atmosphere. The resulting crude was poured into water and extracted with ethyl acetate. The organic phase was combined and dried and concentrated under reduced pressure. The crude was purified by flash chromatography with 20% ethyl acetate in hexane to afford a greenish-yellow solid as 6 (19 mg, 0.056 mmol, yield 35% over two steps). Spectral data: ¹H NMR (500 MHz, CDCl₃) δ 7.65 (d, J = 0.8 Hz, 1H), 7.64 (dd, J= 8.1, 0.9 Hz, 1H), 7.56 (d, J = 0.8 Hz, 1H), 6.68 (m, 2H), 3.46 (q, J = 7.1 Hz, 4H), 2.64 (s, 2H),1.48 (d, J = 1.7 Hz, 12H), 1.24 (t, J = 7.0 Hz, 6H). ¹³C NMR (125 MHz, CDCl₃) δ 205.46, 164.66, 157.49, 152.68, 149.03, 148.02, 132.35, 125.35, 122.41, 116.76, 112.07, 110.88, 105.12, 53.59, 46.20, 44.70, 38.33, 30.20, 27.52, 12.63. TOF MS ES⁺(C₂₄H₂₉NO): Calc. [M+H]⁺: 348.232; found: 348.236.

mmol, 5 mol%) and BINAP (87 mg, 0.14 mmol, 10 mol%) in dry toluene (10 mL) was stirred for 15 min under argon. Subsequently, **15** (380 mg, 1.39 mmol, 1 equiv) and the 1-methylpiperazine (170 mg, 1.7 mmol, 1.2 equiv) dissolved in toluene (1 mL) were added. The mixture was heated to 100 °C in an oil bath overnight. The reaction was monitored by TLC (10% ethylacetate in hexane) until complete conversion of starting material (12 h). The resulting mixture was cooled to room temperature, diluted with CH₂Cl₂ (20 mL) and filtered over a pad of Celite. The solvents were removed under reduced pressure to get a yellow solid (348 mg, 1.19 mmol, yield: 85%). ¹H NMR (500 MHz, CDCl₃) δ 7.65 – 7.56 (m, 2H), 7.43 – 7.36 (m, 1H), 7.31 (td, J = 7.4, 1.2 Hz, 1H), 7.24 (td, J = 7.4, 1.2 Hz, 1H), 7.03 (d, J = 2.3 Hz, 1H), 6.92 (dd, J = 8.3, 2.3 Hz, 1H), 3.37 – 3.20 (m, 4H), 2.68 – 2.50 (m, 4H), 2.39 (s, 3H), 1.49 (s, 6H). ¹³C NMR (125 MHz, CDCl₃) δ :154.98, 153.17, 151.22, 139.40, 131.34, 126.90, 125.88, 122.38, 120.59, 119.07, 114.85, 110.59, 55.25, 49.59, 46.83, 46.21, 27.44. TOF MS ES⁺(C₂₀H₂₄N₂): Calc. [M+H]⁺: 293.201; found: 293.201.

Synthesis of 1-(9,9-dimethyl-7-(4-methylpiperazin-1-yl)-9*H*-fluoren-2-yl)ethan-1-one (7): Compound 21 (250 mg, 0.86 mmol, 1 equiv.) was dissolved in of dry CH₂Cl₂ (5 mL) and the solution was cooled to 0 °C under argon atmosphere. Then anhydrous aluminum chloride (454 mg, 3.4 mmol, 4 equiv.) was added to at once, followed by dropwise addition of acetyl chloride (0.092 mL, 1.3 mmol, 1.5 equiv.) in 30 min. The reaction was run at 0 °C for 1 h and subsequently at RT for 3 h. The reaction mixture was then slowly poured into a saturated sodium bicarbonate solution (100 mL). After extracted twice with dichloromethane (50 mL × 2), the organic layer was dried with anhydrous Na₂SO₄. The crude product was purified by preparative TLC plate eluting with MeOH (2%) in CH₂Cl₂ with Et₃N

(0.1%) to provide bright fluorescent product (78 mg, 0.23 mmol, yield: 26%). ¹H NMR (500 MHz, Chloroform-d) δ 8.00 (d, J = 1.6 Hz, 1H), 7.93 (dd, J = 8.0, 1.6 Hz, 1H), 7.65 (dd, J = 8.1, 6.8 Hz, 2H), 7.00 (d, J = 2.3 Hz, 1H), 6.94 (dd, J = 8.5, 2.3 Hz, 1H), 3.33 (t, J = 5.0 Hz, 4H), 2.64 (s, 3H), 2.62 (t, J = 5.0 Hz, 4H), 2.38 (s, 3H), 1.49 (s, 6H). ¹³C NMR (125 MHz, CDCl₃) δ : 197.92, 156.49, 153.30, 152.15, 144.55, 134.70, 129.48, 128.50, 122.10, 121.79, 118.57, 114.82, 109.91, 55.10, 49.05, 46.93, 46.19, 27.21, 26.74. TOF MS ES⁺(C₂₂H₂₃NO): Calc. [M+H]⁺: 335.212; found: 335.210.

Synthesis of 22 and 23 was accomplished following Dr. Wei Sheng's thesis (page 253)

Synthesis ethyl N-(7-acetyl-9,9-dimethyl-9H-fluoren-2-yl)-Nethylglycinate (9): Compound 23 (290 mg, 0.92 mmol, 1 equiv) was dissolved in dry THF (5 mL) and the solution was cooled down to -78 °C under argon atmosphere. n-Buli (2.5 M in hexane, 1.5 mL, 4 equiv) was added to the resulting solution dropwise and stirred for 20 min at that temperature. Then water (1 mL) was added dropwise at -78 °C and temperature was raised to RT. The organic layer was extracted with ethyl acetate three times, dried over anhydrous sodium sulphate and concentrated. The dried crude 24 was directly used for the next reaction. Crude 24 (218 mg, 0.92 mmol, 1 equiv) was dissolved in dry DMF (5 mL) and added with potassium carbonate (381 mg, 2.76 mmol, 3 equiv) and ethyl 2bromoacetate (0.22 mL, 2 mmol, 2.2 equiv) and heated to 80 °C for 4 h. The organic layer was extracted with DCM, dried with anhydrous Na₂SO₄, concentrated to get crude 25 which was used for next step without any further purification. Crude 25 was used for acetylation following the same procedure as 4 and 5 to produce 9 (168.1 mg, 0.46 mmol, yield over three steps: 50%). Spectral data: ¹H NMR (500 MHz, CDCl₃) δ 7.97 (d, J = 1.6 Hz, 1H), 7.90 (dd, J = 7.9, 1.6 Hz, 1H), 7.60 (dd, J = 9.7, 8.2 Hz, 2H), 6.68 (d, J = 2.4 Hz, 1H), 6.64 (dd, J = 8.5, 2.4 Hz, 1H), 4.22 (d, J = 7.2 Hz, 2H), 4.10 (s, 2H), 3.56 (q, J = 7.2 Hz, 2H), 2.63 (s, 3H), 1.47 (s, 6H), 1.38 – 1.18 (m, 6H). ¹³C NMR (125 MHz, cdcl₃) δ 197.96, 171.09, 156.91, 152.93, 148.75, 144.96, 134.20, 128.56, 127.10, 122.12, 122.01, 118.06, 111.24, 105.88, 63.85, 61.71, 61.13, 52.65, 46.80, 46.58, 14.29, 14.08, 12.45. TOF MS ES⁺(C₂₃H₂₇NO₃): Calc. [M+H]⁺: 366.206; found: 366.207.

Synthesis of 13,13-dimethyl-2,3,5,6,7,13-hexahydro-1*H*-indeno[2,1f]pyrido[3,2,1-ij]quinoline-11-carbaldehyde (26): Compound 13 (500 mg, 1.4 mmol, 1 equiv) was dissolved in dry THF (30 mL) and the solution was cooled down to -78 °C under argon atmosphere. n-Buli (2.5 M in hexane, 2.2 mL, 4 equiv) was added to the resulting solution dropwise and stirred for 45 min at that temperature. Then dry DMF (2.7 mL, 25 equiv) was added, stirred for 2 h at -78 °C and at RT for another 12 h. The reaction was quenched with water (10 mL), extracted with ethyl acetate three times, organic layer was dried over sodium sulphate and concentrated. The resulting crude was washed with hot MeOH three times and finally dried to get pure compound 26 as yellow fluorescent solid. (222 mg, 0.7 mmol, yield 50%). Spectral data: ¹H NMR (500 MHz, CDCl₃) δ : 9.95 (s, 1H), 7.81 (d, J = 1.0 Hz, 1H), 7.73 (dd, J = 1.0 Hz, 1H), 7.75 (dd, J8Hz, 1.0 Hz, 1H), 7.56 (d, J = 8 Hz, 1H), 7.25 (s, 1H), 3.22-3.26 (m, 4H), 3.03 (t, J = 6.4 Hz, 2H), 2.84 (t, J = 6.5 Hz, 2H), 2.10 – 1.88 (m, 4H), 1.59 (s, 6H). ¹³C NMR (125 MHz, CDCl₃) δ : 192.01, 154.03, 150.13, 146.78, 144.29, 131.16, 126.99, 125.76, 122.00, 120.95, 119.97, 118.13, 117.67, 50.69, 50.00, 47.86, 28.43, 24.94, 24.24, 21.87, 21.62. TOF MS ES⁺(C₂₂H₂₃NO): Calc. [M+H]⁺: 318.185; found: 318.183.

Synthesis of 7-bromo-9,9-dimethyl-9*H*-fluorene-2-carbaldehyde (29):

Cl₂CHOCH₃ (35 mg, 0.3 mmol, 1.5 equiv) was added dropwise to a stirred solution of **15** (54 mg, 0.2 mmol, 1 equiv) and ZrCl₄ (70 mg, 0.3 mmol, 1.5 equiv) in dry CH₂Cl₂ (5 mL) at 0 °C under argon. The reaction mixture was stirred for 2 h at 0 °C and then and poured into an ice-water bath (15 mL). The phases were separated, and the aqueous phase was extracted thrice with CHCl₃ (3 x 5ml). The combined extracts were washed with water and saturated aq. NaHCO₃ solution, dried over anhydrous Na₂SO₄ and concentrated in vacuo. The crude product was purified by flash chromatography on silica gel eluted with a mixture of hexane and ethyl acetate (10%) to afford the product **29** (54 mg, 60%) as a bright-yellow solid. Spectral data: ¹H NMR (500 MHz, CDCl₃) δ 10.06 (s, 1H), 7.97 – 7.94 (m, 1H), 7.87 (dd, J = 7.8, 1.4 Hz, 1H), 7.83 (dd, J = 7.5, 0.5 Hz, 1H), 7.66 (d, J = 8.1 Hz, 1H), 7.62 (d, J = 1.7 Hz, 1H), 7.52 (dd, J = 8.0, 1.8 Hz, 1H), 1.52 (s, 6H). ¹³C NMR (125 MHz, CDCl₃) δ 192.04, 156.86, 153.92, 144.48, 136.66, 135.78, 130.67, 130.61, 126.51, 123.09, 122.54, 120.39, 47.23, 26.78. TOF MS AP⁺(C₆H₁₃BrO): Calc. [M+H]⁺: 301.023; found: 301.022.

Synthesis of 9,9-dimethyl-7-(4-methylpiperazin-1-yl)-9*H*-fluorene-2-carbaldehyde (27): A solution of 'BuONa (8.1 mg, 0.084 mmol, 1.2 equiv.), Pd(OAc)₂ (0.78 mg, 0.0035 mmol, 5 mol%) and BINAP (4.35 mg, 0.007 mmol, 10 mol%) in dry toluene (5 mL) was stirred for 15 min under argon. Subsequently, compound 29 (20 mg, 0.07 mmol, 1 equiv) and the 1-methylpiperazine (8.4 mg, 0.084 mmol, 1.2 equiv.) dissolved in toluene (1 mL) were added. The mixture was heated to 100 °C in an oil bath overnight (12h). The resulting mixture was cooled to room temperature, diluted with CH₂Cl₂ (20 mL) and filtered over

a pad of Celite. The solvents were removed under reduced pressure, and the residue was purified

by preparative TLC plate using MeOH (2%) in CH₂Cl₂ to give the desired product as bright yellow solid (13.4 mg, 0.042 mmol, yield: 50%). 1 H NMR (500 MHz, CDCl₃) δ 10.01 (s, 1H), 7.91 (d, J = 0.9 Hz, 1H), 7.82 (dd, J = 7.8, 1.5 Hz, 1H), 7.72 (dd, J = 7.7, 0.6 Hz, 1H), 7.68 (d, J = 8.4 Hz, 1H), 7.00 (d, J = 2.3 Hz, 1H), 6.95 (dd, J = 8.5, 2.3 Hz, 1H), 3.39 – 3.30 (m, 4H), 2.64 (t, J = 5.1 Hz, 4H), 2.40 (s, 3H), 1.50 (s, 6H). 13 C NMR (125 MHz, CDCl₃) δ 13 C NMR (125 MHz, CDCl₃) δ 192.12, 156.77, 153.79, 151.77, 145.85, 134.44, 130.98, 127.14, 122.69, 122.16, 119.20, 115.58, 110.34, 54.54, 48.26, 46.93, 45.26, 27.12. TOF MS ES⁺(C₂₁H₂₁N₂O): Calc. [M+H]⁺: 321.197; found: 321.193.

IV.8 NMR Spectrum

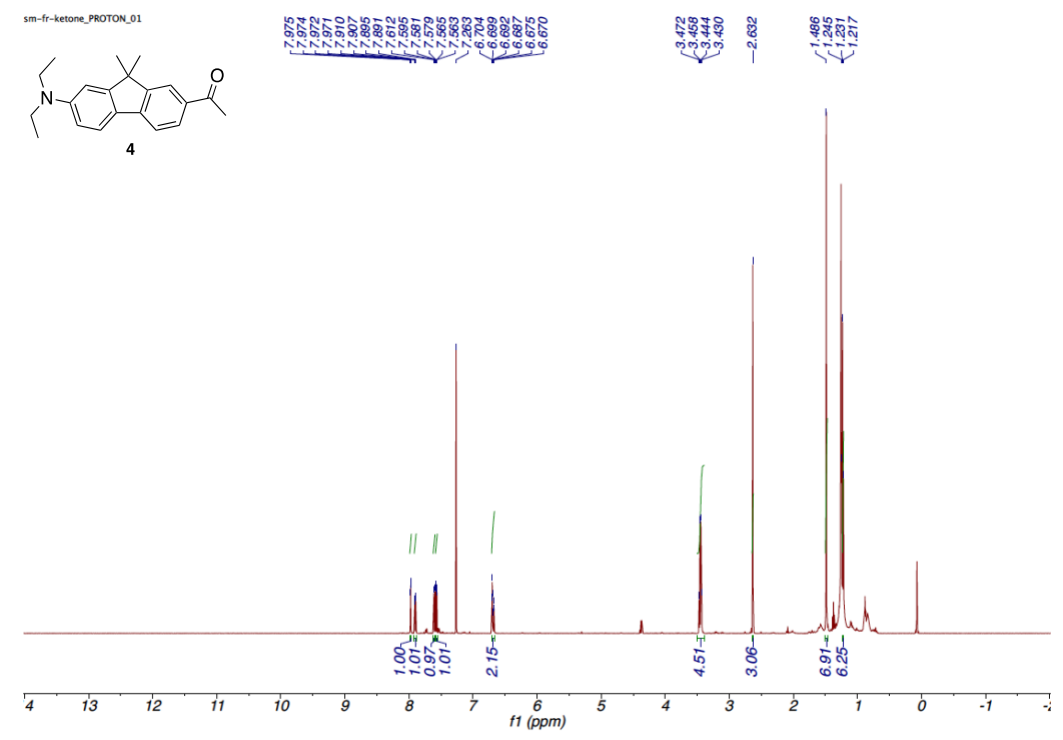


Figure 59. ¹H spectrum of compound 4.

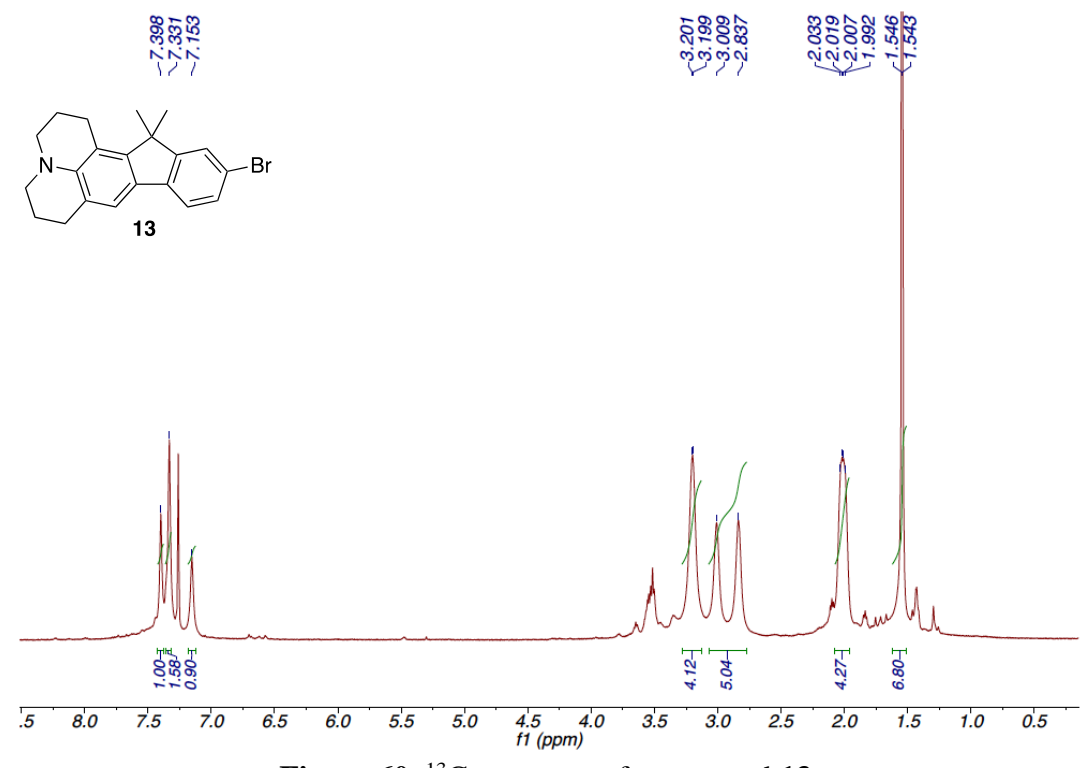


Figure 60. ¹³C spectrum of compound 13.

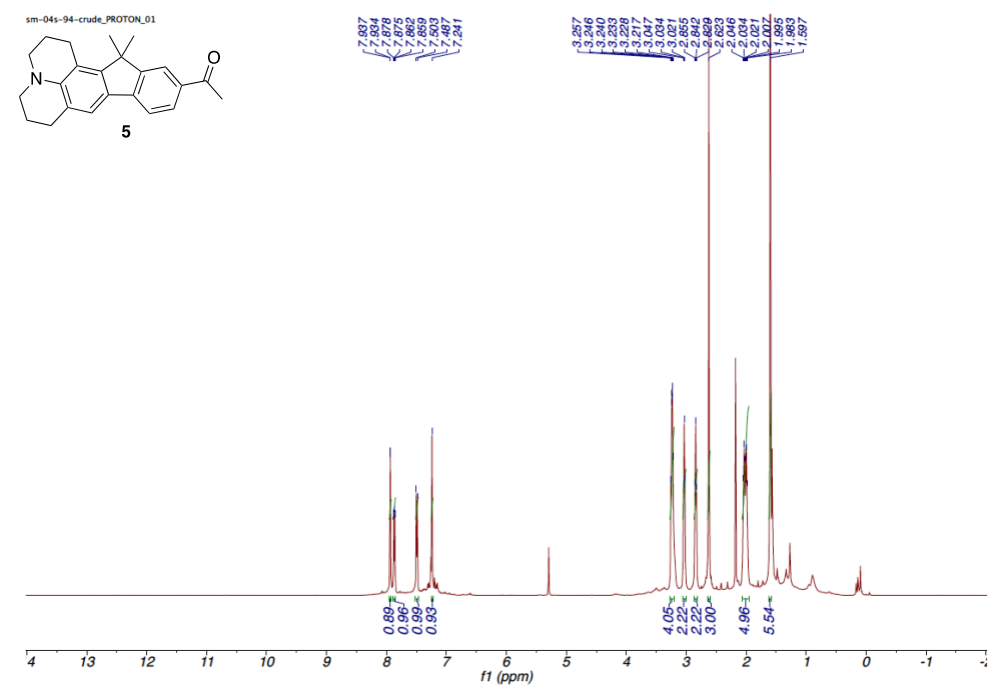


Figure 61. ¹H spectrum of compound **5**.

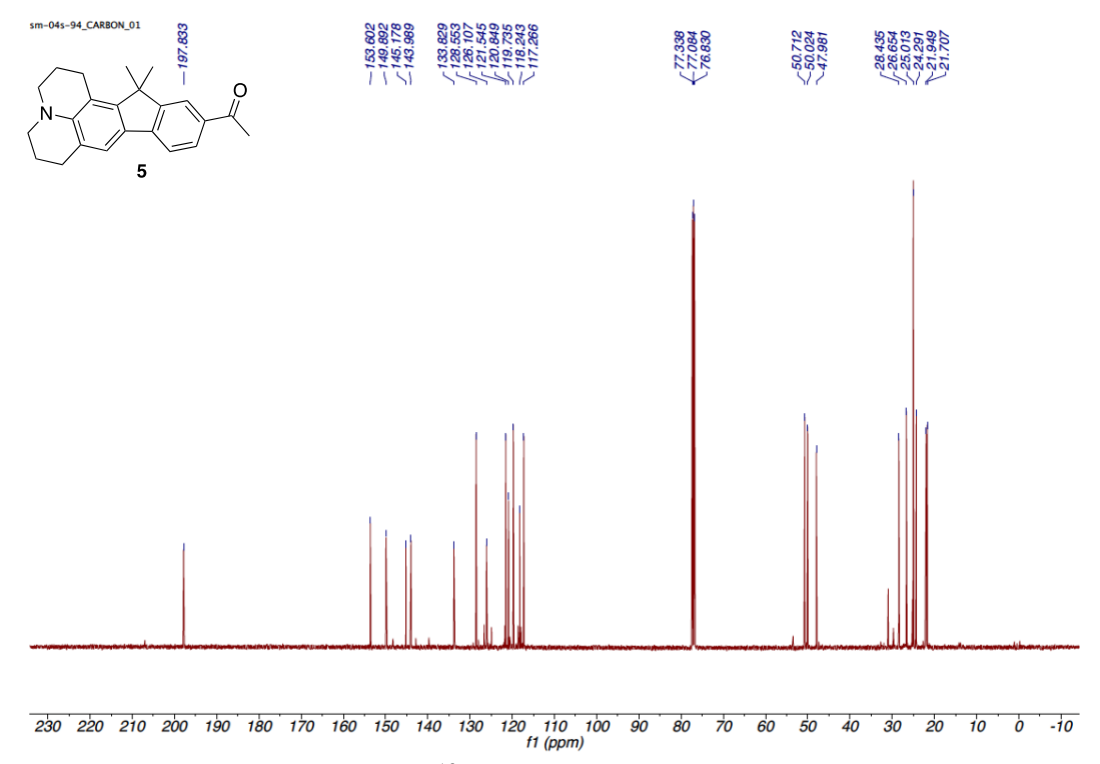


Figure 62. ¹³C spectrum of compound **5**.

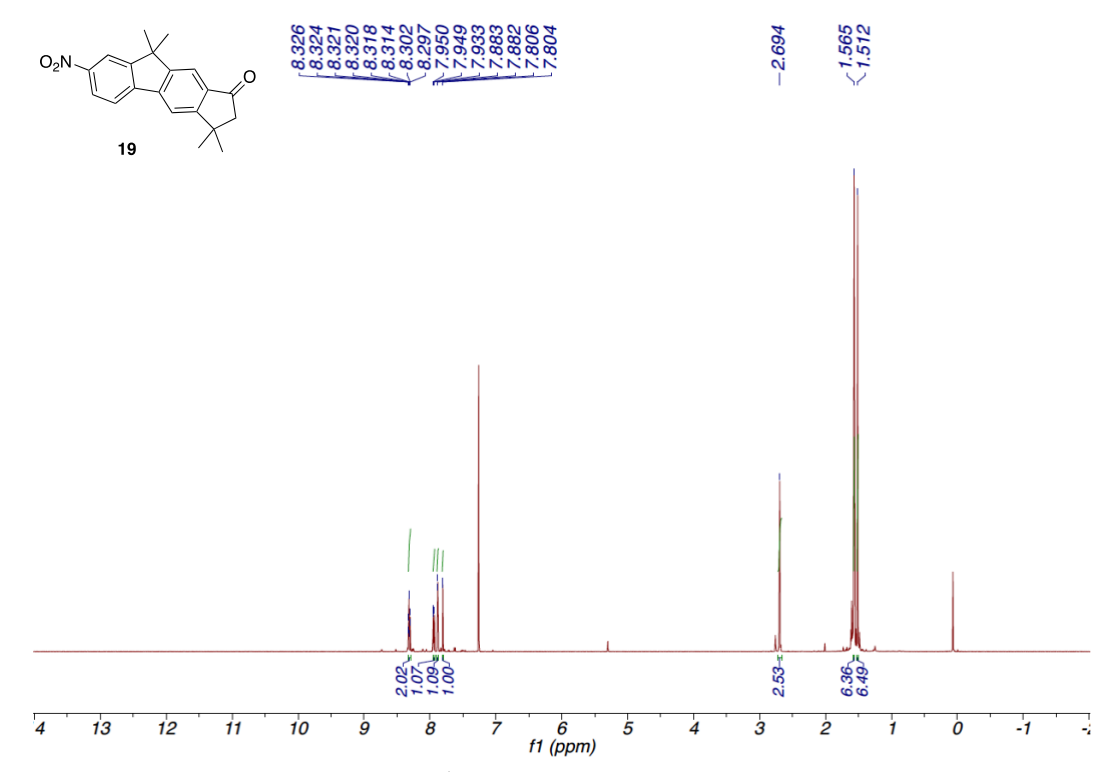


Figure 63. ¹H spectrum of compound 19.

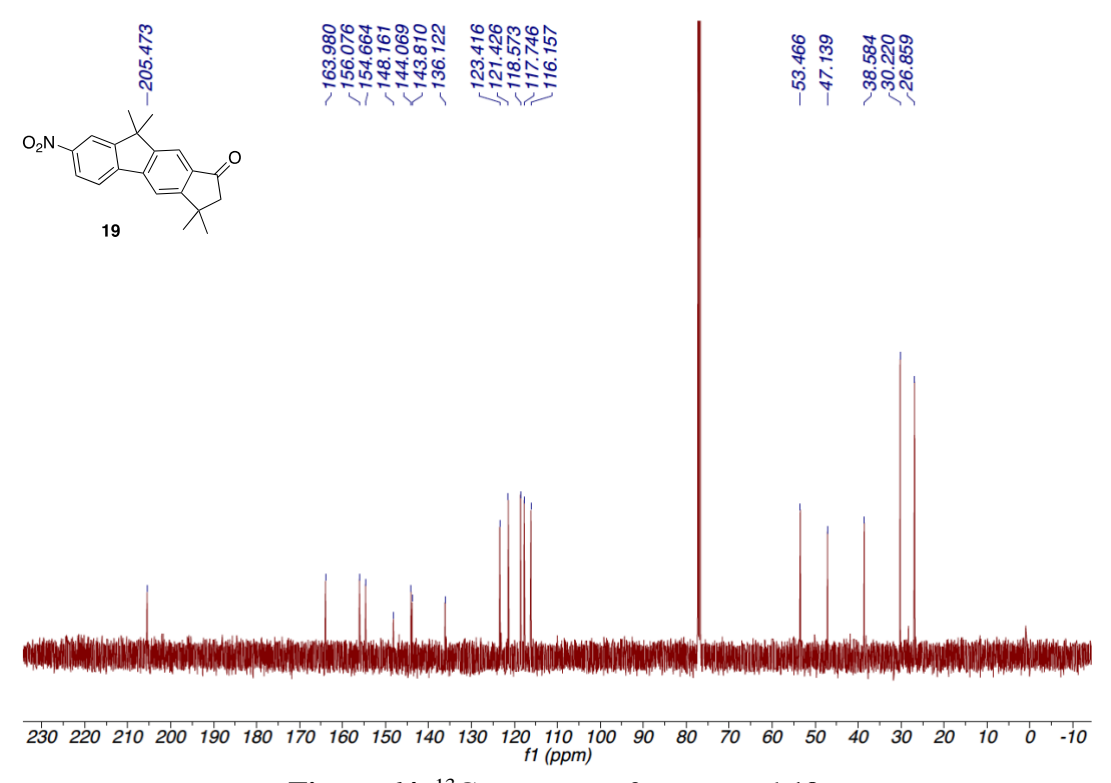


Figure 64. ¹³C spectrum of compound 19.

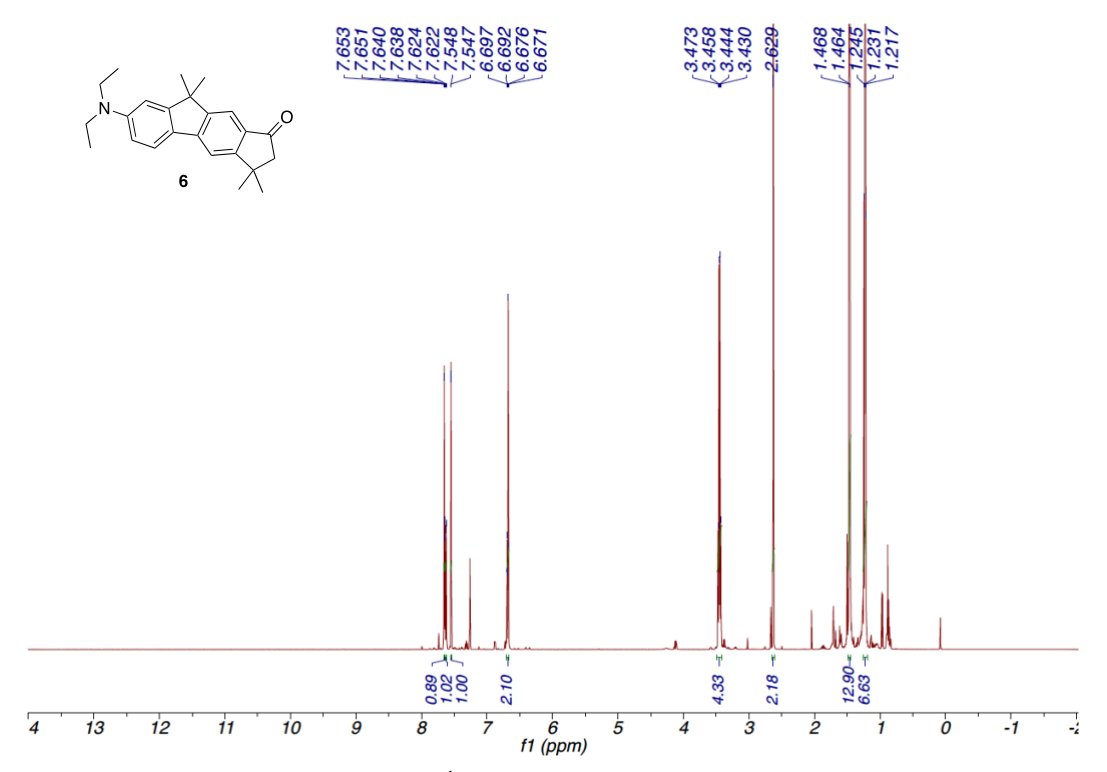


Figure 65. ¹H spectrum of compound 6.

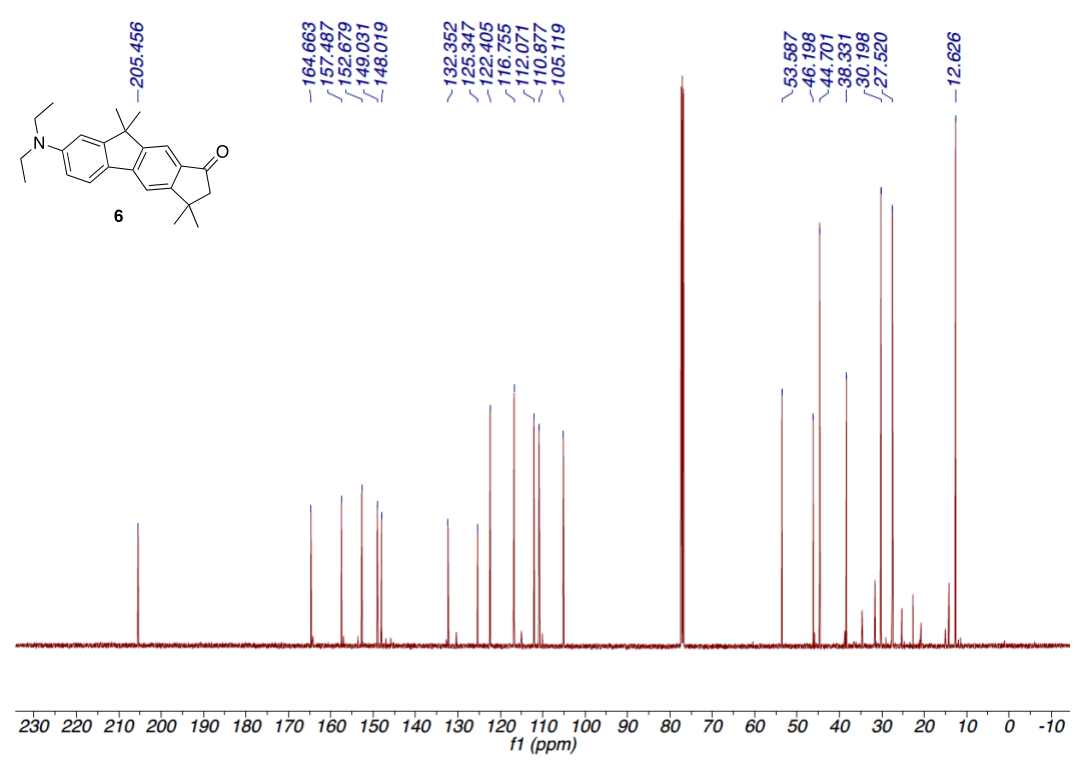


Figure 66. ¹³C spectrum of compound 6.

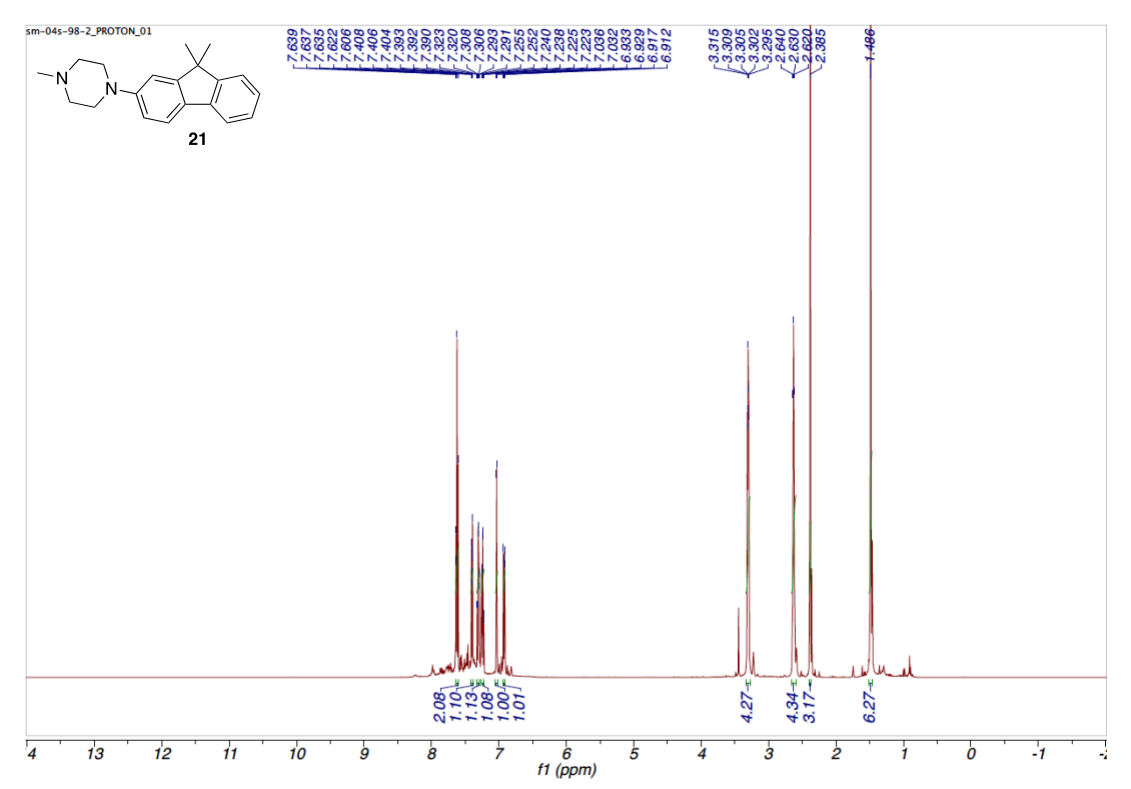


Figure 67. ¹H spectrum of compound 21.

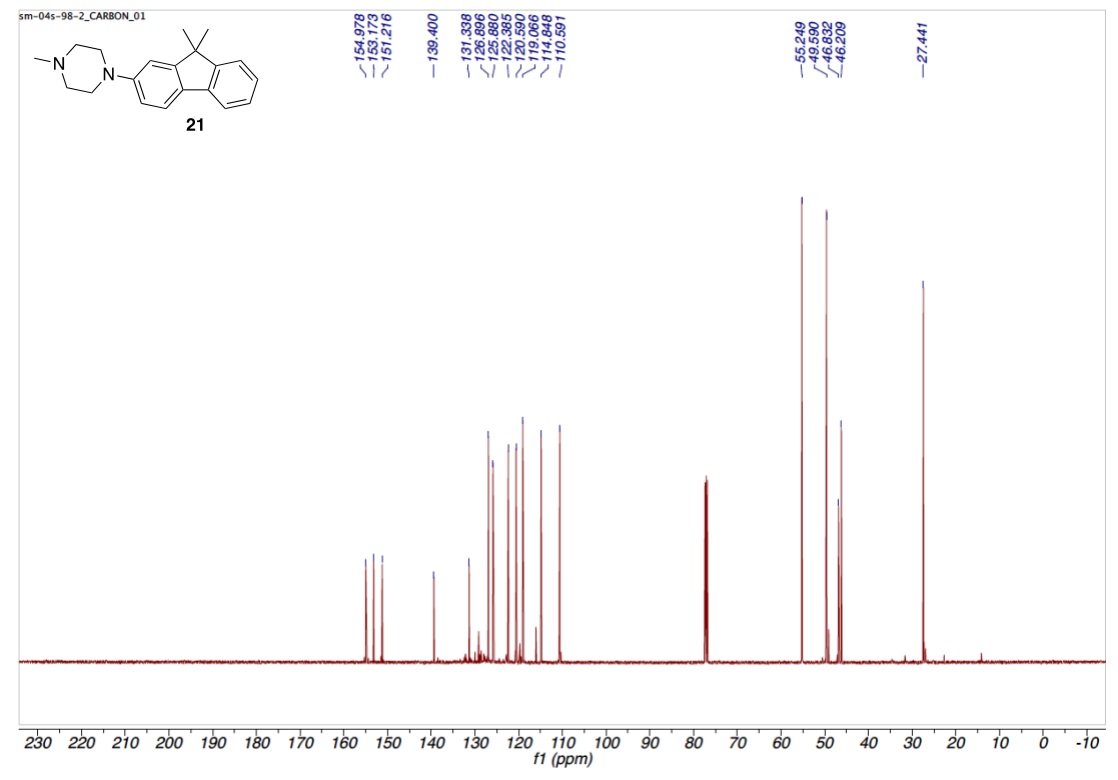


Figure 68. ¹³C spectrum of compound 21.

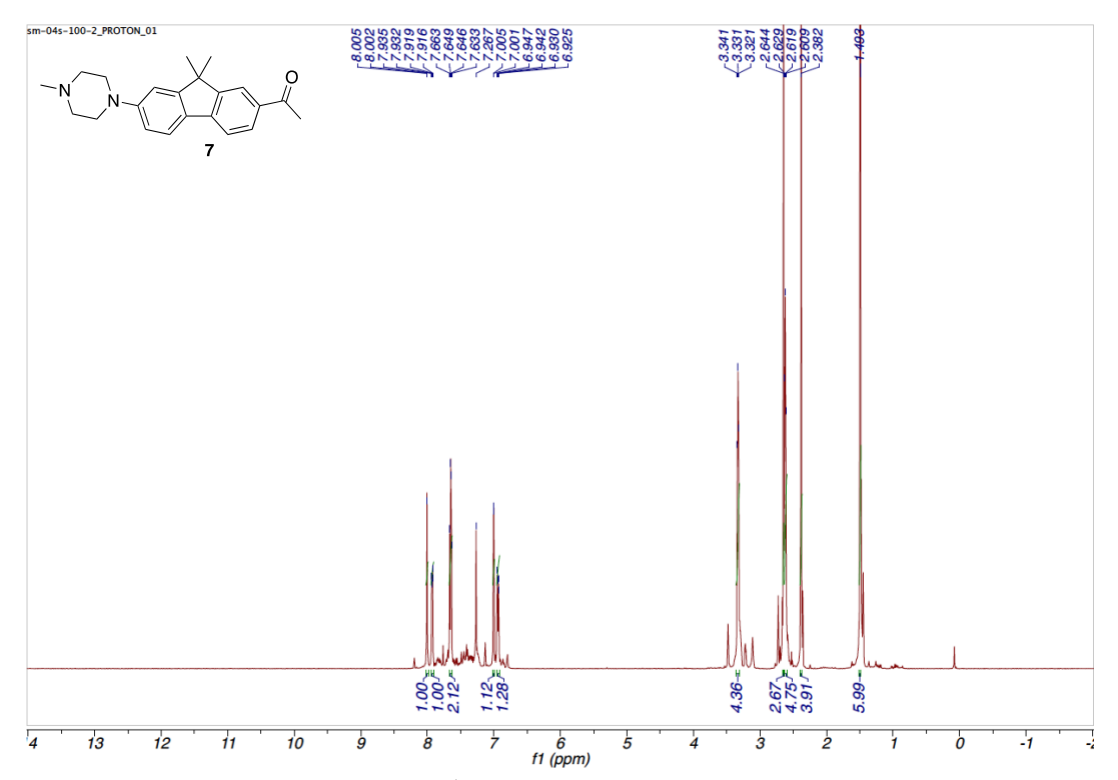


Figure 69. ¹H spectrum of compound 7.

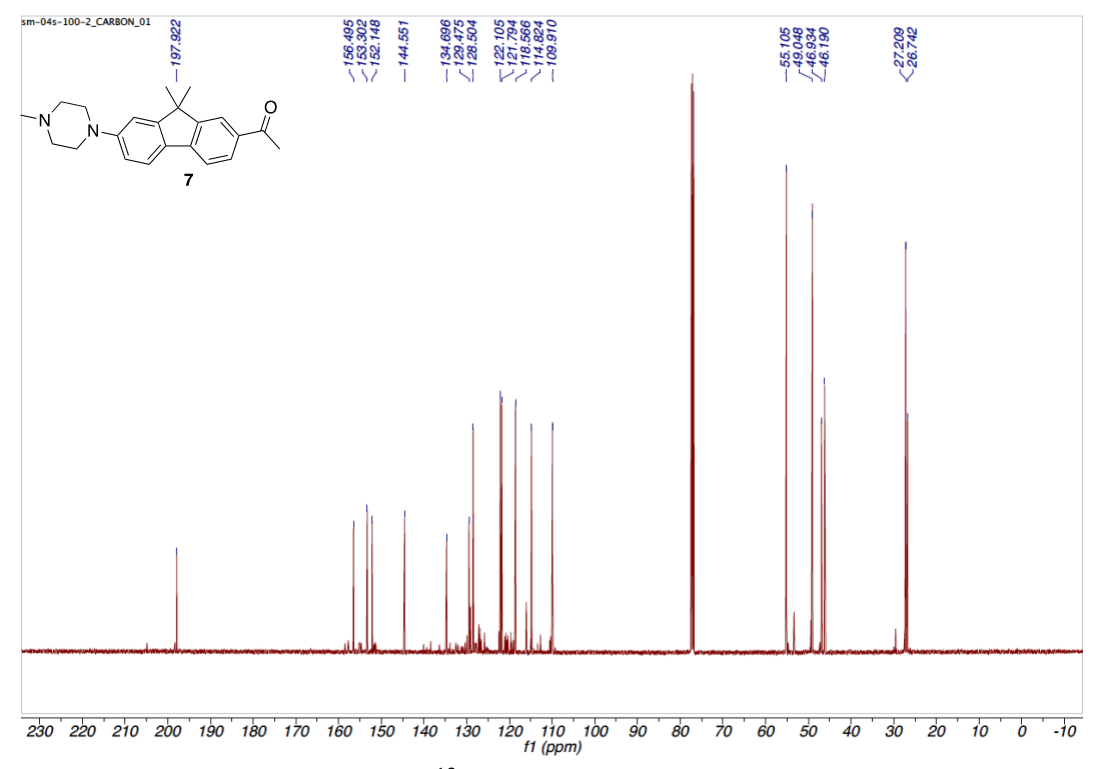


Figure 70. ¹³C spectrum of compound 7.

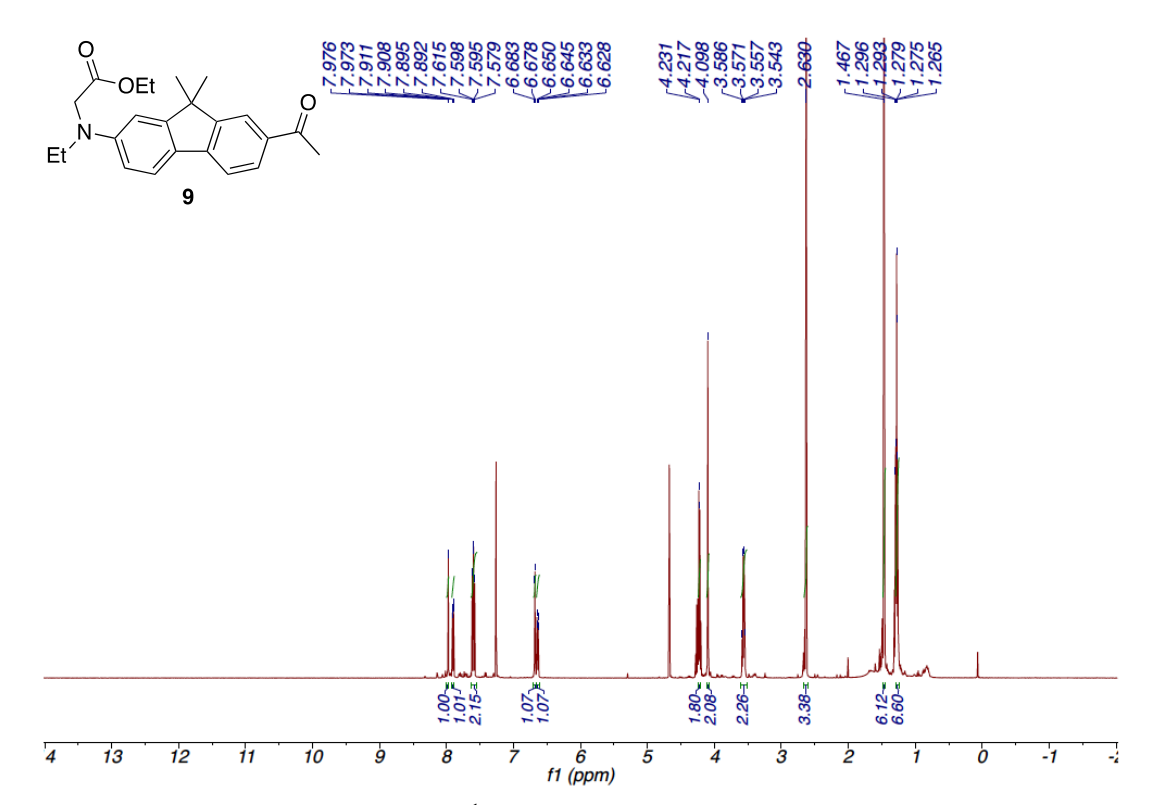


Figure 71. ¹H spectrum of compound 9.

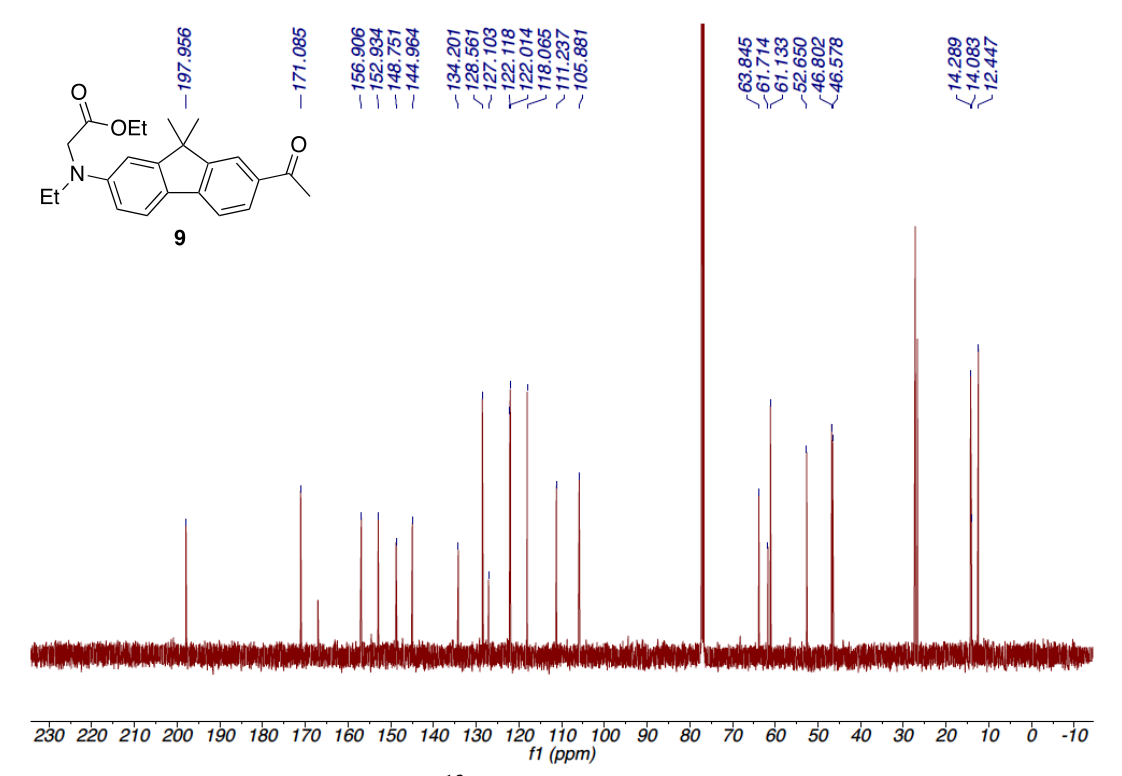


Figure 72. ¹³H spectrum of compound **9**.

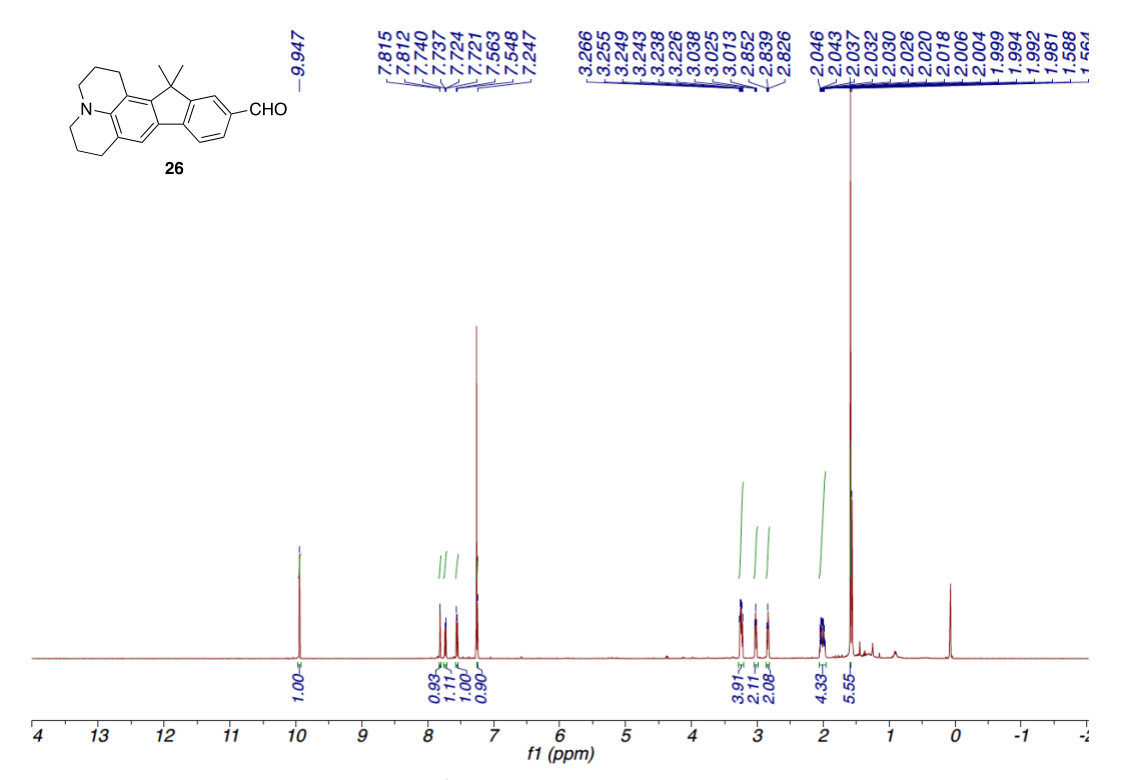


Figure 73. ¹H spectrum of compound 26.

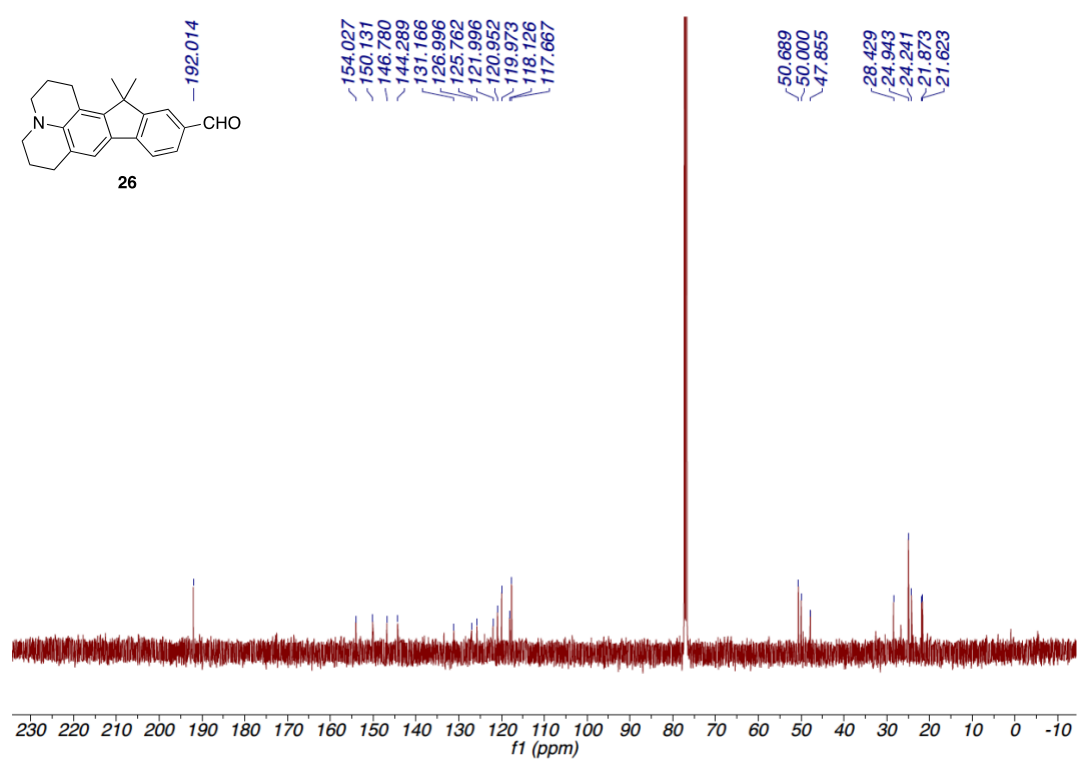


Figure 74. ¹³C spectrum of compound 26.

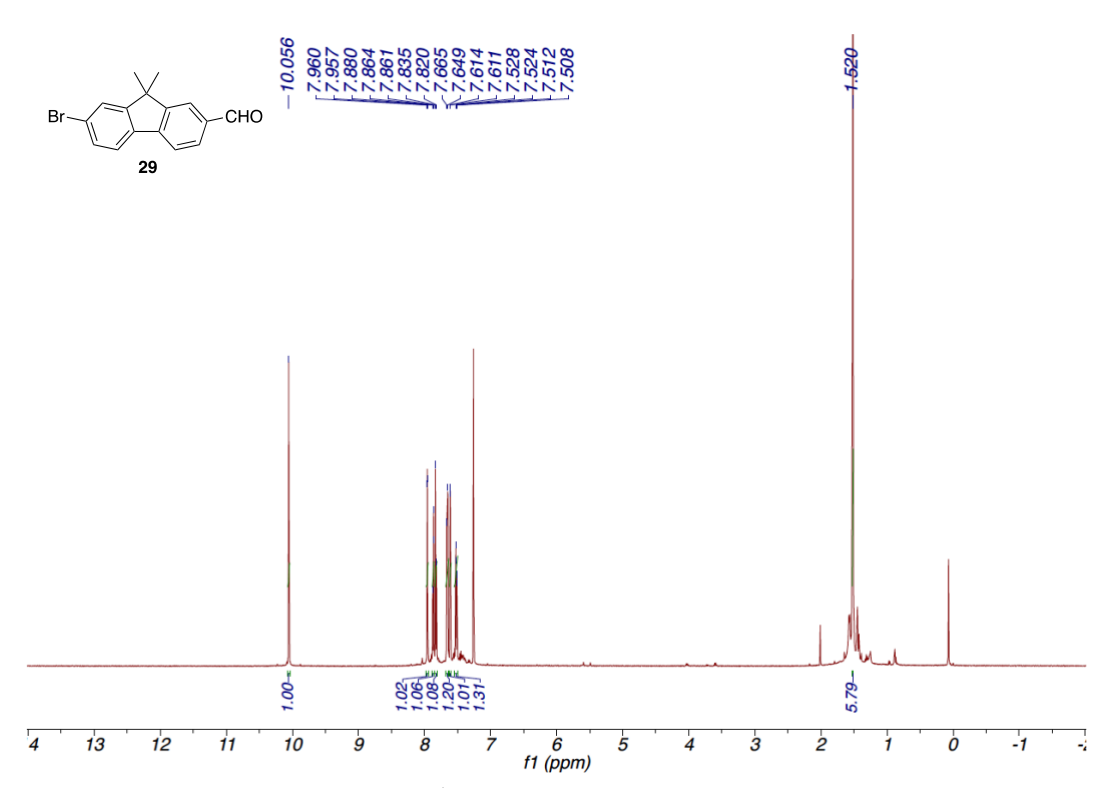


Figure 75. ¹H spectrum of compound **29**.

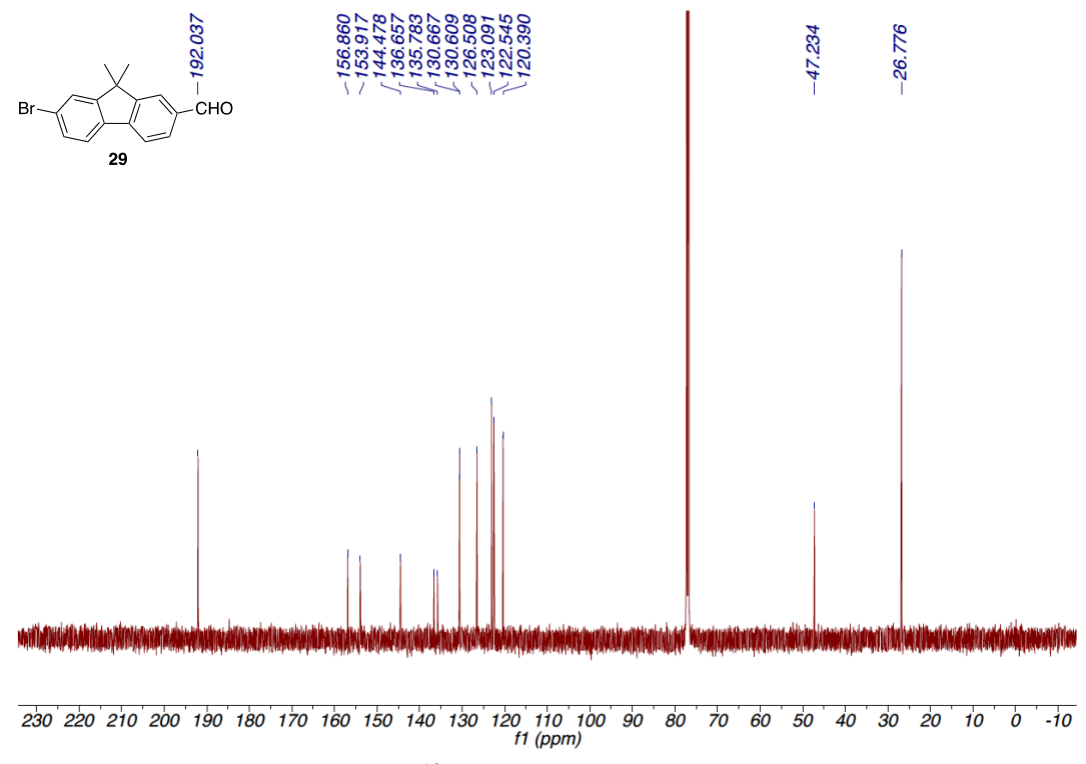


Figure 76. ¹³H spectrum of compound **29**.

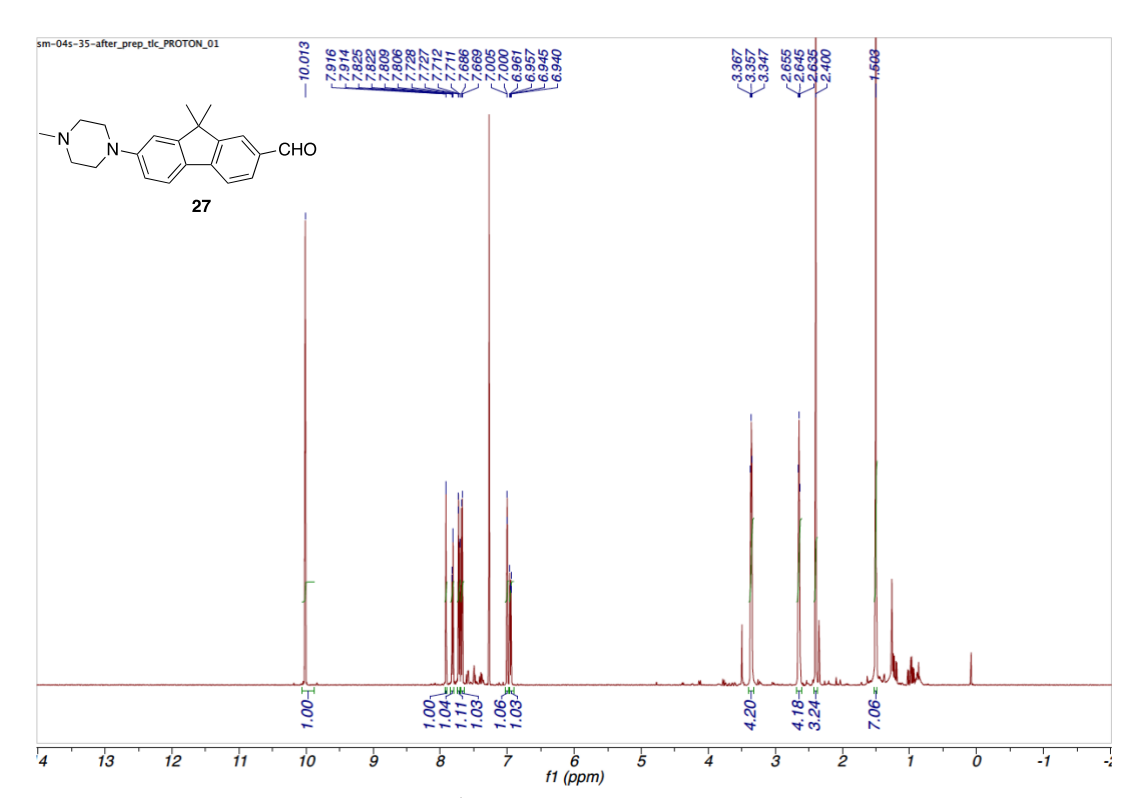


Figure 77. ¹H spectrum of compound 27.

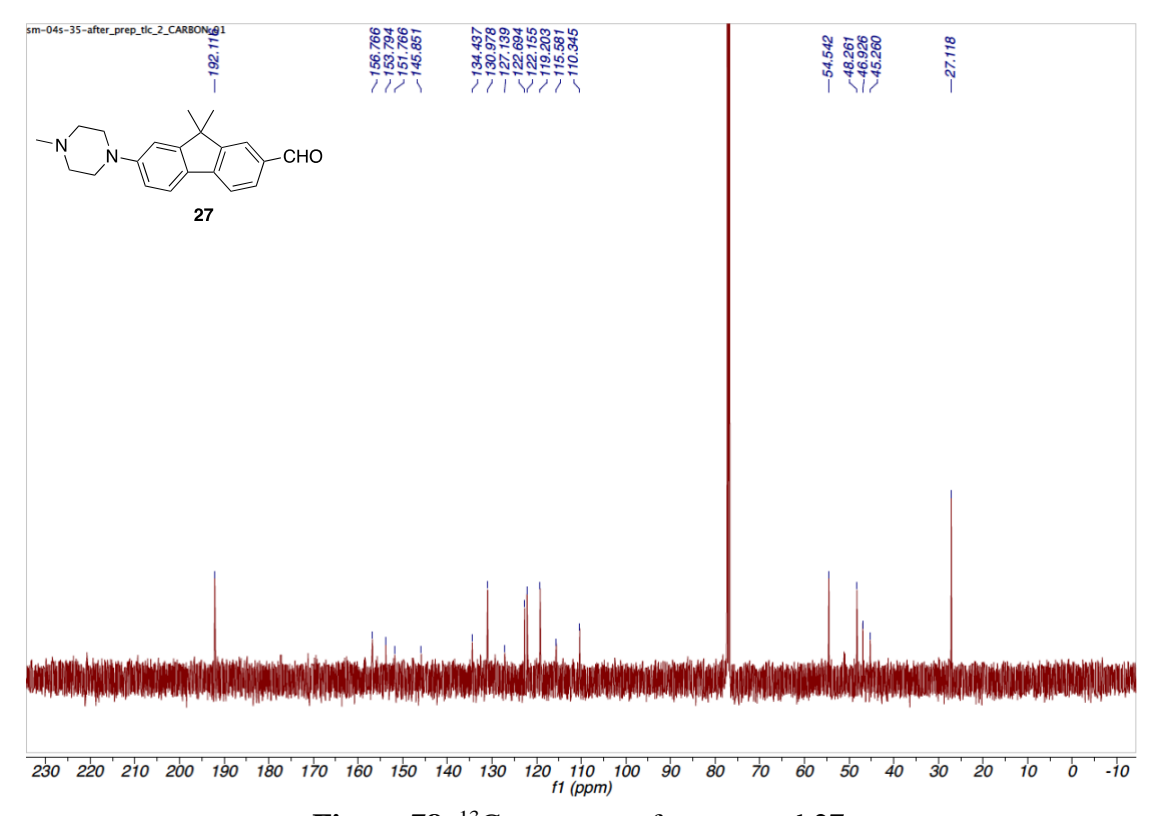


Figure 78. ¹³C spectrum of compound 27.

REFERENCES

- (1) Lavis, L. D.; Raines, R. T. Bright ideas for chemical biology. *ACS Chem. Biol.* **2008**, *3* (3), 142.
- (2) Johnson, I. Fluorescent probes for living cells. *Histochem J.* **1998,** *30* (3), 123.
- (3) Goddard, J. P.; Reymond, J. L. Enzyme assays for high-throughput screening. *Curr. Opin. Biotechnol.* **2004**, *15* (4), 314.
- (4) Johnsson, N.; Johnsson, K. Chemical tools for biomolecular imaging. *ACS Chem. Biol.* **2007,** *2* (1), 31.
- (5) Zhang, J.; Campbell, R. E.; Ting, A. Y.; Tsien, R. Y. Creating new fluorescent probes for cell biology. *Nat. Rev. Mol. Cell. Biol.* **2002**, *3* (12), 906.
- (6) Kivala, M.; Diederich, F. Conjugation and optoelectronic properties of acetylenic scaffolds and charge-transfer chromophores. *Pure Appl. Chem.* **2008**, *80* (3), 411.
- (7) Kato, S.; Diederich, F. Non-planar push-pull chromophores. *Chem. Commun (Camb)* **2010**, 46 (12), 1994.
- (8) Bureš, F. Fundamental aspects of property tuning in push–pull molecules. *RSC Adv.* **2014**, *4* (102), 58826.
- (9) Reichardt, C. Solvatochromic Dyes as Solvent Polarity Indicators. *Chem. Rev.* **1994,** *94* (8), 2319.
- (10) Marini, A.; Munoz-Losa, A.; Biancardi, A.; Mennucci, B. What is solvatochromism? *J. Phys. Chem. B* **2010**, *114* (51), 17128.
- (11) Klymchenko, A. S. Solvatochromic and Fluorogenic Dyes as Environment-Sensitive Probes: Design and Biological Applications. *Acc. Chem. Res.* **2017,** *50* (2), 366.
- (12) Bagatolli, L. A. To see or not to see: lateral organization of biological membranes and fluorescence microscopy. *Biochim. Biophys. Acta* **2006**, *1758* (10), 1541.
- (13) Demchenko, A. P.; Mely, Y.; Duportail, G.; Klymchenko, A. S. Monitoring biophysical properties of lipid membranes by environment-sensitive fluorescent probes. *Biophys. J.* **2009**, *96* (9), 3461.
- (14) Kim, H. M.; Choo, H. J.; Jung, S. Y.; Ko, Y. G.; Park, W. H.; Jeon, S. J.; Kim, C. H.; Joo, T.; Cho, B. R. A two-photon fluorescent probe for lipid raft imaging: C-laurdan. *Chembiochem* **2007**, *8* (5), 553.

- (15) Vazquez, M. E.; Blanco, J. B.; Imperiali, B. Photophysics and biological applications of the environment-sensitive fluorophore 6-N,N-dimethylamino-2,3-naphthalimide. *J. Am. Chem. Soc.* **2005**, *127* (4), 1300.
- (16) Song, X.; Johnson, A.; Foley, J. 7-Azabicyclo[2.2.1]heptane as a unique and effective dialkylamino auxochrome moiety: demonstration in a fluorescent rhodamine dye. *J. Am. Chem. Soc.* **2008**, *130* (52), 17652.
- (17) Chi, W.; Qiao, Q.; Lee, R.; Liu, W.; Teo, Y. S.; Gu, D.; Lang, M. J.; Chang, Y. T.; Xu, Z.; Liu, X. A Photoexcitation-Induced Twisted Intramolecular Charge Shuttle. *Angew. Chem. Int. Ed. Engl.* **2019**, *58* (21), 7073.
- (18) Zhao, G. J.; Han, K. L. Hydrogen bonding in the electronic excited state. *Acc. Chem. Res.* **2012**, *45* (3), 404.
- (19) Grabowski, Z. R.; Rotkiewicz, K.; Rettig, W. Structural changes accompanying intramolecular electron transfer: focus on twisted intramolecular charge-transfer states and structures. *Chem. Rev.* **2003**, *103* (10), 3899.
- (20) Mei, J.; Leung, N. L.; Kwok, R. T.; Lam, J. W.; Tang, B. Z. Aggregation-Induced Emission: Together We Shine, United We Soar! *Chem. Rev.* **2015**, *115* (21), 11718.
- (21) Vogel, M.; Rettig, W.; Sens, R.; Drexhage, K. H. Structural relaxation of rhodamine dyes with different N-substitution patterns: A study of fluorescence decay times and quantum yields. *Chem. Phys. Lett.* **1988**, *147* (5), 452.
- (22) Chang, T. L.; Borst, W. L. Effect of solvent polarity on a rotational isomerization mechanism of rhodamine-B in normal alcohols. *Chem. Phys.* **1990**, *93* (7), 4724.
- (23) Lv, X.; Gao, C.; Han, T.; Shi, H.; Guo, W. Improving the quantum yields of fluorophores by inhibiting twisted intramolecular charge transfer using electron-withdrawing group-functionalized piperidine auxochromes. *Chem. Commun (Camb)* **2020,** *56* (5), 715.
- (24) Beija, M.; Afonso, C. A.; Martinho, J. M. Synthesis and applications of Rhodamine derivatives as fluorescent probes. *Chem. Soc. Rev.* **2009**, *38* (8), 2410.
- (25) Grimm, J. B.; English, B. P.; Chen, J.; Slaughter, J. P.; Zhang, Z.; Revyakin, A.; Patel, R.; Macklin, J. J.; Normanno, D.; Singer, R. H.et al. A general method to improve fluorophores for live-cell and single-molecule microscopy. *Nat. Methods* **2015**, *12* (3), 244.
- (26) Liu, X.; Qiao, Q.; Tian, W.; Liu, W.; Chen, J.; Lang, M. J.; Xu, Z. Aziridinyl Fluorophores Demonstrate Bright Fluorescence and Superior Photostability by Effectively Inhibiting Twisted Intramolecular Charge Transfer. *J. Am. Chem. Soc.* **2016**, *138* (22), 6960.

- (27) Ye, Z.; Yang, W.; Wang, C.; Zheng, Y.; Chi, W.; Liu, X.; Huang, Z.; Li, X.; Xiao, Y. Quaternary Piperazine-Substituted Rhodamines with Enhanced Brightness for Super-Resolution Imaging. *J. Am. Chem. Soc.* **2019**, *141* (37), 14491.
- (28) Hoelzel, C. A.; Hu, H.; Wolstenholme, C. H.; Karim, B. A.; Munson, K. T.; Jung, K. H.; Zhang, H.; Liu, Y.; Yennawar, H. P.; Asbury, J. B. at al. A General Strategy to Enhance Donor-Acceptor Molecules Using Solvent-Excluding Substituents. *Angew. Chem. Int. Ed. Engl.* **2020**, *59* (12), 4785.
- (29) Lobo, B. C.; Abelt, C. J. Does PRODAN Possess a Planar or Twisted Charge-Transfer Excited State? Photophysical Properties of Two PRODAN Derivatives. *The Journal of Physical Chemistry A* **2003**, *107* (50), 10938.
- (30) Wang, C.; Qiao, Q.; Chi, W.; Chen, J.; Liu, W.; Tan, D.; McKechnie, S.; Lyu, D.; Jiang, X. F.; Zhou, W.et al. Quantitative Design of Bright Fluorophores and AIEgens by the Accurate Prediction of Twisted Intramolecular Charge Transfer (TICT). *Angew. Chem. Int. Ed. Engl.* **2020**, *59* (25), 10160.
- (31) Kucherak, O. A.; Didier, P.; Mély, Y.; Klymchenko, A. S. Fluorene Analogues of Prodan with Superior Fluorescence Brightness and Solvatochromism. *J. Phy. Chem. Lett.* **2010**, *1* (3), 616.
- (32) Shaya, J.; Fontaine-Vive, F.; Michel, B. Y.; Burger, A. Rational Design of Push-Pull Fluorene Dyes: Synthesis and Structure-Photophysics Relationship. *Chemistry* **2016**, 22 (30), 10627.
- (33) Wang, W.; Nossoni, Z.; Berbasova, T.; Watson, C. T.; Yapici, I.; Lee, K. S.; Vasileiou, C.; Geiger, J. H.; Borhan, B. Tuning the electronic absorption of protein-embedded all-trans-retinal. *Science* **2012**, *338* (6112), 1340.
- (34) Yapici, I.; Lee, K. S.; Berbasova, T.; Nosrati, M.; Jia, X.; Vasileiou, C.; Wang, W.; Santos, E. M.; Geiger, J. H.; Borhan, B. "Turn-on" protein fluorescence: in situ formation of cyanine dyes. *J. Am. Chem. Soc.* **2015**, *137* (3), 1073.
- (35) Sheng, W.; Nick, S. T.; Santos, E. M.; Ding, X.; Zhang, J.; Vasileiou, C.; Geiger, J. H.; Borhan, B. A Near-Infrared Photoswitchable Protein-Fluorophore Tag for No-Wash Live Cell Imaging. *Angew. Chem. Int. Ed. Engl.* **2018**, *57* (49), 16083.
- (36) Santos, E. M.; Sheng, W.; Esmatpour Salmani, R.; Tahmasebi Nick, S.; Ghanbarpour, A.; Gholami, H.; Vasileiou, C.; Geiger, J. H.; Borhan, B. Design of Large Stokes Shift Fluorescent Proteins Based on Excited State Proton Transfer of an Engineered Photobase. *J. Am. Chem. Soc.* **2021**, *143* (37), 15091.
- (37) Katayama, H.; Abe, E.; Kaneko, K. Synthesis of julolidines from anilines. *J. Heterocycl. Chem.* **1982**, *19* (4), 925.